BED-TO-SURFACE HEAT TRANSFER IN CONICAL SPOUTED AND SPOUT-FLUID BEDS

A THESIS SUBMITTED TO
THE GRADUTE SCHOOL OF NATURAL AND APPLIED SCIENCES
OF
MIDDLE EAST TECHNICAL UNIVERSITY

BY

ONUR YAMAN

IN PARTIAL FULFILLMENT OF THE REQUIREMENTS
FOR
THE DEGREE OF MASTER OF SCIENCE
IN
CHEMICAL ENGINEERING

JULY 2017

Approval of the Thesis:

BED-TO-SURFACE HEAT TRANSFER IN CONICAL SPOUTED AND SPOUT-FLUID BEDS

submitted by **ONUR YAMAN** in partial fulfillment of the requirements for the degree of **Master of Sciences in Chemical Engineering Department, Middle East Technical University** by,

Prof. Dr. Gülbin Dural Ünver
Dean, Graduate School of **Natural and Applied Sciences** _____

Prof. Dr. Halil Kalıpçılar
Head of the Department, **Chemical Engineering** _____

Assoc. Prof. Dr. Görkem Külah
Supervisor, **Chemical Engineering Dept., METU** _____

Examining Committee Members:

Prof. Dr. Murat Köksal
Mechanical Engineering Dept., Hacettepe University _____

Assoc. Prof. Dr. Görkem Külah
Chemical Engineering Dept., METU _____

Asst. Prof. Dr. Özgür Ekici
Mechanical Engineering Dept., Hacettepe University _____

Assoc. Prof. Dr. Şule Ergün
Nuclear Engineering Dept., Hacettepe University _____

Asst. Prof. Dr. İnci Ayrancı
Chemical Engineering Dept., METU _____

Date: 20.07.2017

I hereby declare that all information in this document has been obtained and presented in accordance with academic rules and ethical conduct. I also declare that, as required by these rules and conduct, I have fully cited and referenced all material and results that are not original to this work.

Name, Last name : ONUR YAMAN

Signature:

ABSTRACT

BED-TO-SURFACE HEAT TRANSFER IN CONICAL SPOUTED AND SPOUT-FLUID BEDS

Yaman, Onur
M.S., Department of Chemical Engineering
Supervisor: Assoc. Prof. Dr. Görkem Külah

JULY 2017, 102 pages

Bed-to-surface heat transfer investigation from a vertically immersed cylindrical surface was conducted in large laboratory scale conical spouted and spout-fluid beds in this study. In order to design a high performance spouted and spout-fluid beds, the effects of bed design parameters (such as conical angle, inlet diameter of spouting gas entrance) and operating conditions (such as static bed height, particle size and density and spouting and fluidization gas flow rates) on the heat transfer characteristics were investigated in detail. An empirical heat transfer correlation of the average heat transfer coefficients in the annulus section for high-density particles ($2500 \leq \rho_p \leq 6000$ kg/m^3) was also proposed for the practical use in industrial applications.

The heat transfer coefficients were found to depend on the density and size of the particles. The denser and larger particles had higher minimum stable spouting velocities, which in turn lead to higher operational spouting velocities resulting in higher heat transfer coefficient values. The effect of particle diameter was more pronounced in the spout and spout-annulus interface whereas its effect diminished in the annulus region. The conical angle had a significant effect on the gas flow distribution and particle-probe contact dynamics in the

spouted bed and it was observed that the heat transfer values in the annulus decreased with the increase in conical angle due to lowered particle circulation. Benefits of the spout-fluid operation on the heat transfer coefficients were found fairly minor considering maximum of 7 and 3 % increase in heat transfer coefficient observed during spout-fluid operation for 31º and 66º conical angle conical spout-fluid beds, respectively, since the fluidizing gas (G_f) was not able to penetrate sufficiently inside the annulus to maintain an effective gas flow on the heat transfer surface. Therefore, from the heat transfer point of view, given the required flow rates for spout-fluid bed operation, spouted beds were found to be more feasible compared to spout-fluid beds.

Keywords: conical spouted bed, spout-fluid bed, bed-to-surface heat transfer, immersed heat transfer surfaces.

ÖZ

TAŞKIN VE TAŞKIN-AKIŞKAN KONİK YATAKLARDA YATAK-YÜZEY ISI TRANSFERİ

Yaman, Onur
Yüksek Lisans, Kimya Mühendisliği Bölümü
Tez yöneticisi: Doç. Dr. Görkem Külah

TEMMUZ 2017, 102 sayfa

Bu çalışmada büyük ölçekli taşkın ve taşkın-akışkan yataklarda, yatağa diklemesine daldırılmış silindirik yüzeyden yatağa olan ısı transferi çalışması gerçekleştirilmiştir. Yüksek performansa sahip taşkın ve taşkın-akışkan yatakların tasarlanabilmesi için, yatak tasarım parametrelerinin (konik açı, taşkınlaşma gazı giriş çapı) ve çalışma koşullarının (statik yatak yüksekliği, parçacık çapı ve özkütlesi, taşkınlaşma ve akışkanlaşma gaz akış debileri) ısı transferi üzerindeki etkileri detaylı bir biçimde incelenmiştir. Ayrıca, özellikle yüksek özkütleye sahip paçacıklarla çalışacak endüstriyel sistemlerde pratik tahminler yapmak için halka bölgesindeki ısı transferi katsayıları kullanılarak ampirik ısı transferi korelasyonu da çıkarılmıştır.

Bu çalışmada ısı transferi katsayılarının parçacık özkütle ve büyüklüğüne bağlı olduğu görülmüştür. Ağır ve büyük parçacıkların daha yüksek minimum kararlı taşkınlaşma hızına sahip olmaları, daha yüksek operasyon taşkınlaşma hızlarının kullanılmasına ve dolayısıyla daha yüksek ısı transferi katsayılarına neden olmuştur. Parçacık çapının ısı transferine olan etkisinin taşkın bölgede daha etkili olduğu ancak halka bölgesinde etkinin ortadan kalktığı gözlemlenmiştir. Yataklardaki konik açının gaz akış dağılımını ve parçacık-yüzey kontak dinamiğini önemli şekilde etkilediği

gözlemlenmiştir. Böylece artan konik açı ile halka bölgesinde düşen parçacık sirkülasyonu ısı transferi katsayılarını düşürmektedir. Taşkın-akışkan yatağın ısı transferine etkileri sırasıyla 31º ve 66º konik açılı yataklarda maksimum % 7 ve 3 olarak düşük bulunmuştur. Bunun başlıca sebebi, yapılan çalışmalar ışığında, akışkanlaşma gazının yeterince yatağa nüfus etmemesi olduğu düşünülmektedir. Dolayısıyla, ısı transferi açısından taşkın–akışkan yatak yerine taşkın yatağın kullanılmasının daha elverişli olduğu kararına varılmıştır.

Anahtar kelimeler: konik taşkın yatak, taşkın-akışkan yatak, yatak-yüzey ısı transferi, daldırılmış ısı transferi yüzeyleri

ACKNOWLEDGEMENT

I would like to thank sincerely to my supervisor Assoc. Prof. Dr. Görkem Külah and I would like to express my gratitude to Prof. Dr. Murat Köksal for their guidance, support, suggestions and more importantly, motivation throughout this study.

I would like to give my special thanks to our invaluable technician, Hasan Çelikli, for his aids, technical supports and friendship.

I extend my gratitude to my colleagues Vahid Nasiri, Chiya Savari, Shahab Golshan and Ali Yeniçeri for their advices and precious friendships in this study.

Lastly, I sincerely thank all members of my family, especially my parents for their encouragement, support and love throughout my thesis.

This study was supported by the Scientific and Technological Research Council of Turkey (TUBITAK) as project numbered '115M392'.

TABLE OF CONTENTS

LIST OF TABLES

TABLES

LIST OF FIGURES

FIGURES

LIST OF SYMBOLS

A	Heat transfer surface area, m^2
Ar	Arcimedes number, $gd_p^3(\rho_p-\rho_g)/\mu^2$
C_p	Particle heat capacity, J/kg.K
C_g	Gas heat capacity, J/kg.K
d_p	Particle diameter, m
do	Hole diameter of fluidizing gas, m
D_o	Gas inlet diameter, m
D_i	Spouted bed inlet diameter, m
D_c	Column diameter, m
G	Gas mass flow rate, $kg/m^2.s$
G_s	Spouting gas flow rate, m^3/s
G_F	Fluidizing gas flow rate, m^3/s
G_{ms}	Minimum spouting gas flow rate, m^3/s
$G_{ms,s}$	Minimum stable spouting gas flow rate, m^3/s
Gr	Grashof number, $gL^3\xi\Delta T/\nu^2$
g	Gravitational acceleration, m^2/s

H_c Height of the conical section, m

H_b Height of the static bed height, m

h Total time-average heat transfer coefficient, $W/m^2.K$

h_{rad} Radiative heat transfer coeffcient, $W/m^2.K$

h_g Gas convective heat transfer, $W/m^2.K$

h_{pa} Particle convective heat transfer, $W/m^2.K$

h_w Heat transfer coefficient from the wall, $W/m^2.K$

k_{eff} Effective thermal conductivity of particles on the heat transfer surface, W/m.K

k_g Gas thermal conductivity, W/m.K

k_p Particle thermal conductivity, W/m.K

L Characteristic length, m

L_j Horizontal jet penetration length, m

Nu Nusselt number, $h.d_p/k_g$

P Power, W

Pr Prandtl number, $C_p.\mu_g/k_g$

Re Reynolds number, $U_s.\rho_g.d_p/\mu_g$

r Radial position of the heat transfer probe, m

R Conical-spouted bed radius at the specified static bed height, m

R_p Thermal contact resistances of the particles, $W/m^2.K$

r/R Radial dimensionless position

T_b Bed temperature, ºC

T_s Surface temperature of the probe, ºC

U_s Spouting gas velocity based on D_o, m/s

U_o Superficial gas velocity based on D_c, m/s

U_{ms} Minimum spouting gas velocity based on D_o, m/s

$U_{ms,s}$ Minimum stable spouting gas velocity based on D_o, m/s

U_{msf} Minimum spout-fluidizing gas velocity, m/s

Z Axial position of the heat transfer probe, m

Z/H_b Longitudinal dimensionless position of the heat transfer probe

Greek Letters

ΔP Bed pressure drop, Pa

γ Angle of the conical section, degree

δ_d Fraction of particle coverage on the heat transfer surface

ε_b Bed void fraction

ε_w Average void fraction on the wall surface

μ_g Gas viscosity, $k_g/m.s$

ρ_g Gas density, k_g/m^3

ρ_p Particle density, kg/m^3

τ Residence time of the particle on the surface, s

τ_p Thermal time constant of particles, s

Φ Particle sphericity

α Thermal diffusivity, m^2/s

ξ Coefficient of expansion of fluid, K^{-1}

ν Kinematic viscosity of fluid, m^2/s

CHAPTER 1

INTRODUCTION

Many chemical and physical processes include gas-solid interactions such as drying of granular particles, particle coating, adsorption, coal gasification, catalytic cracking of hydrocarbons (Mathur & Epstein, 1974). Fluidized beds have become prominent and preferred systems in most of these applications due to their effective gas-solid interaction characteristic.

In a fluidized bed, a fluid passes a cylindrical vessel filled with solid particles and forms several solid-gas behaviours e.g. bubbling, turbulent and pneumatic beds. Thus, larger surface area of the solid particles in contact with gas stream are benefited in an excellent mixing condition so that high heat and mass transfer rates between the gas and particles and the uniformity in terms of temperature and particle concentration distribution can be accomplished (Kunii & Levenspiel, 1991). By this way, the heat management inside the reactor is easier due to rapid solid mixing. In addition, controlling the average contact time between the gas stream and solid particles by changing either solid feed rate or gas flow rate enables to have a broad operational flexibility. Nevertheless, fluidized bed technology has faced slugging problems to some extent for the coarse (Geldart type D) and dense particles. This leads to high bed pressure drop and requirements of high gas flow rates, and thereby uneconomical operation. In this situation, systematic particle agitation also cannot be easily met due to non-uniform residence time of particles.

To overcome these problems, spouted beds are proposed as gas-solid contact reactors for Group D particles according to Geldart classification shown in **Figure 1.1**.

Group D particles can have large diameter or high density. When they are fluidized in a conventional fluidized bed, large bubbles form and the size of these bubbles can reach the size of the column diameter. Large bubbles can interfere with gas-solid contact in chemical or physical process and this situation causes significant reduction in reactor performance. Consequently, spouted beds are substituted instead of fluidized beds considering the advantages of spouted beds, such as not requiring complex gas distributor plates, lower pressure drops than fluidized beds and effective mixing between the particles and the gas phase especially when working with large diameter or high density particles.

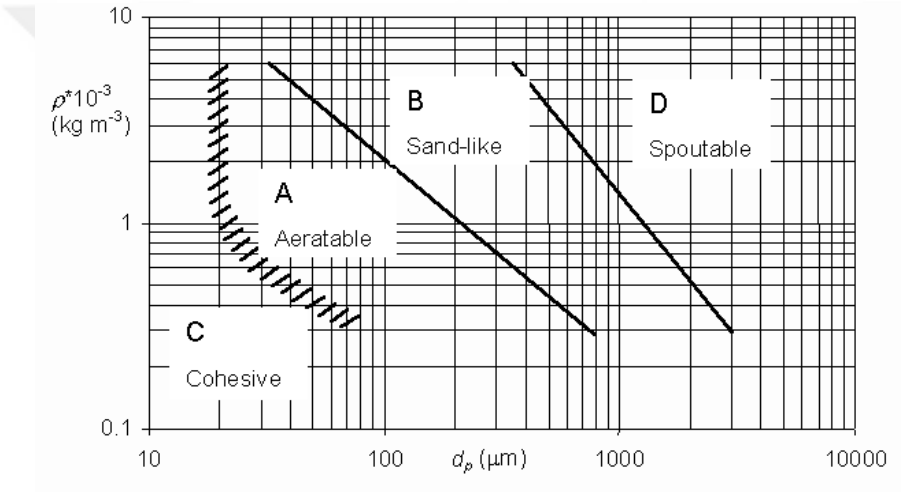

Figure 1.1 Classification of particles by Geldart (Kunii & Levenspiel, 1991)

1.1 Spouted and Spout-Fluid Beds

Spouted beds were first introduced by Mathur and Gishler (1954) to solve the aforementioned problems in fluidized beds operating with Group D particles. In the forthcoming years, use of spouted bed technique has broadened into gasification, pyrolysis, coating, granulation and catalytic reactions (Epstein & Grace, 2011).

In this technique, spouting is provided by a fluid passing axially through a centrally placed small nozzle at the bottom of a conical vessel as drawn in **Figure 1.2**.

By this way, fluid forms a jet stream – after enough flow rate supplied - at the core of the bed splitting the solid particles into three different characteristic regions; *spout*, *fountain* and *annulus*. Spout region is made of lean jet phase in which particle concentration is quite low (around 3-5 %). Upon getting through the spout area, particles reach fountain above the surface of the bed and then rain back to the annulus region. In the annulus, there is a counter current movement such that while the solid particles slowly travel down, gas flow goes in upward direction.

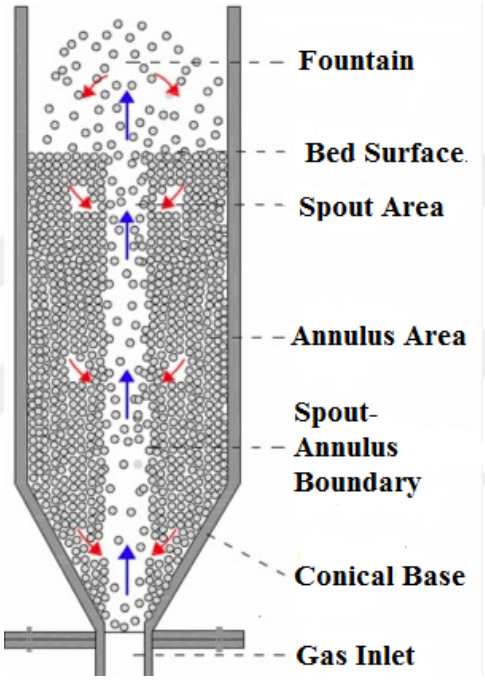

Figure 1.2 Conventional spouted bed

When the cylindrical section of the spouted beds is not filled with particles, and only the conical section is used, this type of bed is named as *conical spouted bed* shown in **Figure 1.3**. Compared to the conventional spouted beds, some essential advantages of conical spouted beds are (i) more satisfactory gas-solid contact due to less dead zone; (ii) short gas residence times with narrow distribution (Epstein & Grace, 2011). Successful applications of conical spouted beds include chemical vapour deposition, particle coating, drying and recently, biomass, waste plastic and scrap tire pyrolysis

(Olazar et al., 2011; Vahlas et al., 2002; Passos et al., 1997; Lopez et al., 2010).

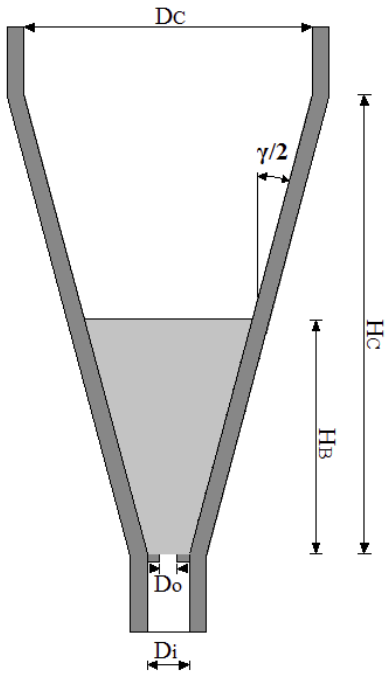

Figure 1.3 Conical spouted bed

During conical spouted bed operation, with the opening of the valve in the air supply line, a small gas void initially appears at the bottom of the bed. As the gas velocity is increased, the size of the gas void slightly increases. As illustrated in **Figure 1.4**, the bed pressure drop on the other hand increases almost linearly to its peak value since the bed is in the packed bed condition.

As the gas velocity is further increased, the gas suddenly rushes up to the bed surface and bursts. This point is designated as the *onset of internal spouting*. With further increase in gas velocity, the internal spout first collapses and then grows up again till second bursting takes place at the bed surface. This point is designated as the onset of external spouting and the corresponding gas velocity based on the gas inlet diameter, D_o, is accepted as the minimum spouting velocity (U_{ms}).

After this point, the spout can collapse momentarily and internal and external spouting can coexist intermittently. This behaviour can be characterized as unstable external spouting region. With further increase in gas velocity, stable spouting is observed which is designated by minimum stable spouting velocity ($U_{ms,s}$). Beyond this point, the spout and the fountain lose their corresponding salient features and the fluctuations of the bed pressure drop increase. This part is designated as jet spouting (dilute spouting) region.

In each conical spouted bed operation, the bed pressure drop should be firstly measured together with U_{ms} and $U_{ms,s}$. Based on those findings, economical and stable operating condition should be maintained.

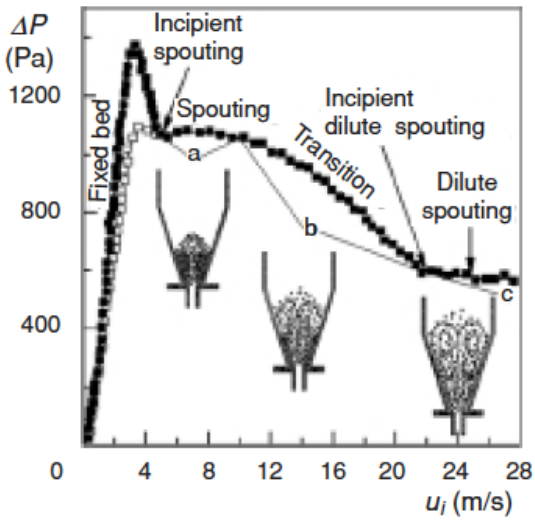

Figure 1.4 Evaluation of the flow regimes with pressure drop vs. spouting gas velocity graph in the conical spouted beds (Epstein & Grace, 2011)

Studies on investigation of hydrodynamics of conical spouted beds reveal that dead zone in the annulus section, particle agglomeration and adhesion problems have negative effects on the operation and creates serious disadvantages (Epstein & Grace, 2011). To alleviate these shortcomings, Chatterjee et al. (1970) proposed “hybrid” gas-solid contact reactors, called spout-fluid beds, which have the salient features of

both spouted and fluidized beds (Chatterjee et al., 1983). In a conical spout-fluid bed, as illustrated in **Figure 1.5,** the spouting gas enters the bed in the form of a jet from the bed bottom and the fluidizing gas is fed to the annulus region through the conical lateral surface. The fluidizing gas keeps the annulus region either at minimum fluidization or bubbling fluidization condition. This lateral gas introduction, which is unique to spout-fluid beds, increases the gas and particle mixing in the radial direction, decreases the agglomeration and sticking problems and enables the spout-fluid beds to process large particles using lower gas flow rates compared to fluidized and spouted beds.

Similar to spouted beds, a stable spouting state is first investigated following the same procedure explained above and the gas velocity at this condition is designated by *minimum spout-fluidizing gas velocity* (U_{msf}).

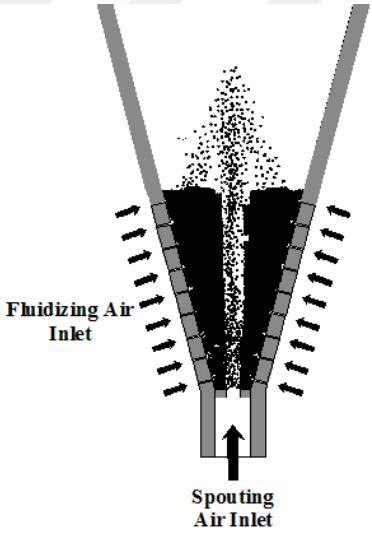

Figure 1.5 Conical spout-fluid beds

In order to design a high performance spout-fluid bed for a specific application, it is crucial that the effects of bed design parameters (such as conical angle, inlet diameter of spouting gas entrance) and operating conditions (such as static bed height, particle size and density and spouting and fluidizing gas flow rates) on gas-particle flow

dynamics and heat transfer characteristics in the bed are known. Especially in applications where drying, coating and chemical reactions take place, characterization of heat transfer in the system is of paramount importance. Although there are a lot of studies investigating heat transfer in fluidized beds, only one study exists on the bed-to-surface heat transfer in the spout-fluid beds conducted by Chatterjee et al. (1983). Absence of bed-to-surface heat transfer studies in the conical spouted and spout-fluid beds has led to the *objective of this study* which is the investigation of the effects of design parameters and operating conditions on the bed-to-surface heat transfer inside the spouted and spout-fluid beds.

CHAPTER 2

BED-TO-SURFACE HEAT TRANSFER IN SPOUTED AND SPOUT-FLUID BEDS

Two mechanisms of heat transfer are generally investigated in heat transfer studies conducted in gas-solid systems. *Gas-to-bed heat transfer* studies aim to figure out the heat transfer from hot or cold gas to the bed materials (particles and gas inside the bed). In *bed-to-surface heat transfer* studies, on the other hand, heat transfer either from the wall of the bed or from an immersed surface to the bed material are investigated. It is imperative to know the bed-to-surface heat transfer especially in applications where immersed heat exchange elements located in the annulus section of the spouted bed are utilized. Therefore, in this study, bed-to-surface heat transfer in spouted and spout-fluid beds is investigated.

For a gas-solid suspension near the surface, as illustrated in **Figure 2.1**, at any time, transitory particle-surface, particle-particle, particle-gas and gas-surface interactions all occur and are very significant for the exchange of heat from the surface. These individual interactions are created and destroyed by constant and sometimes irregular motions of particles and gas in contact with the surface hotter or colder than the bed. Simultaneous conductive and convective transport carries the heat between surface and the core of the bed (Mickley & Fairbanks, 1955).

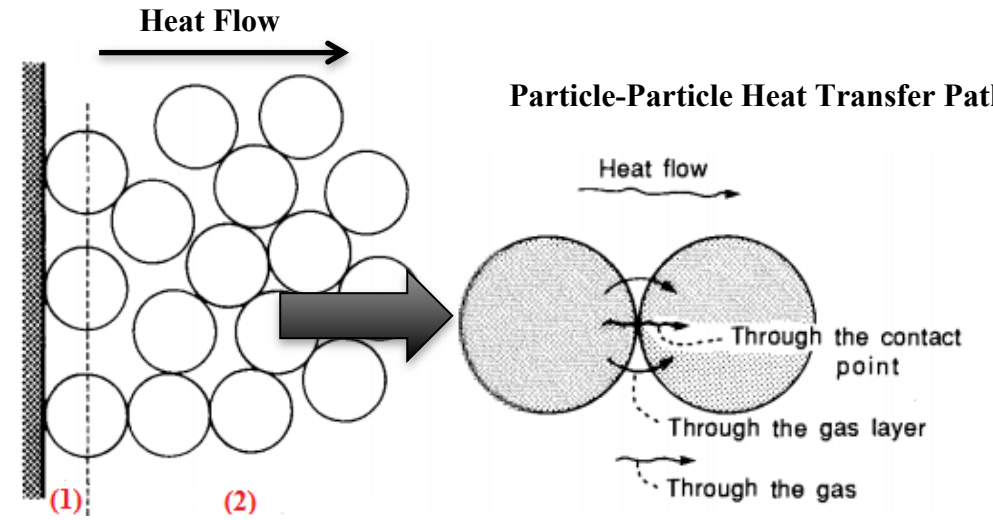

Figure 2.1 Heat transfer mechanism in the bed-to-surface approach (Kunii & Levenspiel, 1991)

The total bed-to-surface heat transfer coefficient in the dense phase can be usually defined as (Chen et al., 2005; Wong et al., 2014; Yao et al., 2014):

$$h = \delta_d h_{pa} + (1 - \delta_d) h_g + h_{rad} \tag{2.1}$$

where h_g is forced gas convection coefficient for gas passing the surface through the interstitial voids; h_{pa} is particle convection coefficient and h_{rad} is radiative heat transfer coefficient which can be neglected for systems operating under 500ºC. In **Equation 2.1**, δ_d indicates the fraction of particle coverage on the heat transfer surface.

Mickley and Fairbanks (1955) were the first researchers to characterize bed-to-surface heat transfer in fluidized bed systems. They developed the packet model for bubbling fluidized beds where they considered the heat transfer surface to be alternately contacted by gas bubbles and homogeneous packets of closely packed particles. They explained heat transfer by surface renewal theory where they assumed that heat transfer occurs primarily by transient conduction between the

particle packets and the surface during periods when the packets reside at the heat transfer surface.

Mickley and Fairbanks (1955) noted that radiation (h_{rad}) and gas convection (h_g) can be negligible at low operating temperatures and when the gas flow rate is very low, there is not much turbulence and particles near the wall move downward almost at a uniform speed. For these conditions, they proposed **Equation 2.2** to calculate the particle convection coefficient (for constant flux):

$$h_{pa} = 1.77\sqrt{\frac{k_{eff}\rho_p C_p(1-\varepsilon_p)}{\tau}} \tag{2.2}$$

where void fraction of packets (ε_p), residence time of packets on the surface (τ) and thermal properties of the packets (C_p and k_{eff}) constitutes the particle convection heat transfer (h_{pa}).

It should be noted that this model was proposed for fluidized beds operating with small particles. However, the studies with larger particles (>500 μm) showed some deviations, where the unsteady process turns into nearly a steady-state process (Chen et al., 2005). Thus, the contact characteristic between the surface and single particles becomes important, and thermal interaction contains mostly the first layer of the particles on the surface instead of packets (Gloski et al., 1983; Ozkaynak & Chen, 1980). Under this condition, thermal time constant (time for temperature change of a particle in contact with the heat transfer surface, τ_p) and contact resistance (R_p) of the particles should also be considered in the heat transfer mechanisms. Furthermore, for the case of gently descending particles under neglected gas convection (no bubbles) and radiation, total time-average heat transfer coefficient (h) can be defined as (Kunii & Levenspiel, 1991):

$$h = \frac{\delta_d}{1/h_{pa} + R_p} \tag{2.3}$$

where

$$R_p = \frac{d_p}{2k_{eff}} \tag{2.4}$$

$$\frac{k_{eff}}{k_g} = \frac{k^o_{eff}}{k_g} + (\alpha\beta)PrRe_p \tag{2.5}$$

$$k^o_{eff} = \varepsilon_w k_g + (1 - \varepsilon_w)k_s \left[\frac{1}{\varphi_w (k_s / k_g) + 1/3} \right] \tag{2.6}$$

In **Equations 2.6**, k^o_{eff} is specially proposed for bed-to-surface heat transfer applications with stagnant gas. ε_w is the average void fraction on the wall surface and φ_w can be read from **Figure 2.2**. Under fluid flow conditions, k_{eff} is defined in **Equation 2.5**, where $\alpha\beta$ constants is related with the particle size and packing configuration (Botteril et al., 1986; Yagi & Kunii, 1960).

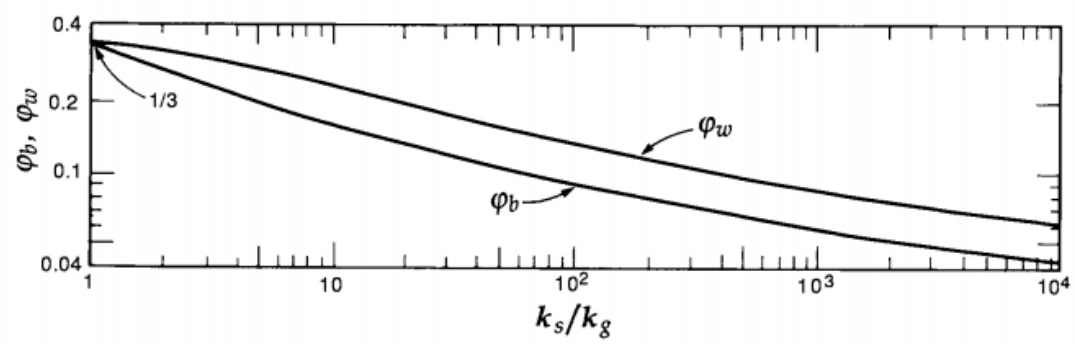

Figure 2.2 Ratio of effective thickness of gas layer around a contact surface to particle diameter (Botteril et al., 1986; Yagi & Kunii, 1960)

The surface renewal theory proposed by Mickley and Fairbanks (1955) for bubbling fluidized beds was adapted for the annulus region of spouted beds by Kakaç and Kılkış (1991) as they accepted the surface renewal theory as a suitable model for

spouted beds. In the annulus region of a spouted bed a close packing matrix of particles also named as dense phase exists. In this region, the particle convection dominates the total heat transfer rate.

Epstein and Mathur (1971) also proposed another theoretical model for the annulus section of spouted beds, based on the concept of a thermal boundary layer. In their approach, a two-dimensional penetration model was used instead of one-dimensional conduction equation used in the derivation of surface renewal theory. However, when the particles are assumed to move at a constant speed on the surface, the equations were simplified and the results of both models became identical.

Since the particles move quite slowly in the annulus section (~3-10 mm/s) in a spouted bed, bed-to-surface heat transfer coefficient can also be calculated by approximating the annulus section as a packed bed. In this respect, **Equations 2.7** and **2.8** developed by Yagi and Kunii (1960) using different particles (glass, lead and steel shots) can be used for the annulus section of a spouted bed.

$$Nu = \frac{h_w d_p}{k_g} = (\text{Heat transfer for stagnant gas}) + (\text{Heat transfer for gas flow}) \quad (2.7)$$

$$h_w = \frac{2k_{eff}}{d_p} + a_w (C_p \rho_p U_o) \quad (2.8)$$

where a_w is given as 0.05 in **Equation 2.8** based on the experimental findings and U_o is the superficial gas velocity, which is quite small in the annulus part of a spouted bed.

As discussed in Chapter 1, spouted beds are composed of two distinct regions: spout and annulus. Annulus region is made of a dense phase where the particles are close to loosely packed state and move slowly downwards. All of the models mentioned above can be used to calculate the heat transfer from the wall of the spouted bed to the bed material or from an immersed heat exchange element located in the annulus

section of the spouted bed to the bed material. Spout region, on the other hand, is made of lean jet phase in which particle concentration is quite low (around 3-5 %). The flow in this region is more or less similar to pneumatic transport in the fluidized beds, and the gas convection is the main heat transfer mechanism. Between these two regions, there is a slim transition region rather than a sharp boundary, where both gas and particle convections are effective on the total heat transfer rate. This thesis study focuses on the heat transfer between an immersed heat exchange element in the annulus section of the spouted bed and the bed material. Therefore, heat transfer in the annulus section will only be investigated. For this purpose, Mickley and Fairbanks' approach will be followed. Although this approach can be quite helpful to evaluate the heat transfer rates in spouted beds, the model parameters i.e. particle velocity, void fraction and effective thermal conductivity on the heat exchange surface are not easily available (Macchi et al, 1999) and should be obtained experimentally. In the following section, experimental studies conducted on bed-to-surface heat transfer in spouted and spout-fluid beds are summarized.

2.1 Literature Survey on Experimental Studies Conducted on Bed-to-Surface Heat Transfer in Spouted and Spout-Fluid Beds

Most of the heat transfer studies in the literature focused on gas-to-particle heat transfer in coating and drying of light particles such as grain, wheat and coal (Kucharski & Kmiec, 1989; Berghel, 2007; Makibar et al., 20011). However, bed-to-surface heat transfer investigations have drawn less attention and are quite scant in the literature. Klassen and Gishler (1958), Malek and Lu (1964), Uemaki and Kugo (1967) and Chatterjee et al. (1983) used the wall of the bed as a heat exchange surface and investigated heat transfer from the wall of the system to the bed. However, as a characteristic of spouted beds, there can be high temperature difference between spout and annulus section in thermal applications. This can lead to a sharp temperature jump from annulus to spout area since gas flow mainly passes from the spout section. Therefore, while one can control the temperature of spout by airflow rate, annulus section will be almost out of temperature control.

In this respect, the heat exchange by the wall of bed, especially in the large units, is insufficient and uninterruptedly long particle contact time with the bed wall lowers heat transfer coefficient. Therefore, for more effective control of the local bed temperature, submerged heat transfer surfaces provide higher heat transfer area per unit bed volume and help to meet fast heat transfer requirement. Bed-to-surface heat transfer studies, conducted using a submerged heat transfer surface in spouted beds, are summarized in **Table 2.1.**

Table 2.1 Summary of submerged bed-to-surface heat transfer studies in spouted beds

Author	Bed Type	Type of Particles	Measurement System	Heat Transfer Coefficient, W/m^2K
Zabrodsky and Mikhalik (1967)	Conical Spouted Bed (45º)	- Silica Gel (d_p = 2, 4 mm; ρ_p = 800 kg/m^3)	4 mm diameter and 35 mm long cylindrical probe	190-260
Klimenko et al. (1970)	Spouted Bed (90º)	- Aluminum Silicate (d_p = 2-2.8 mm; ρ_p = 1250 kg/m^3)	25 mm diameter spherical probe	45-208
Macchi et al. (1999)	Spouted Bed (60°)	- Nylon (d_p = 2.90 mm; ρ_p = 1120 kg/m^3) - Polyethleyne (d_p = 2.89, 3.07, 3.22 mm; ρ_p = 943 kg/m^3) - Glass Beads (d_p = 3, 1.6 mm; ρ_p = 2400 kg/m^3) - Activated Alumina (d_p = 3.75, 1.98 mm; ρ_p = 1300 kg/m^3)	12.7 mm diameter and 50.8 mm long cylindrical probe	95-230
Saldarriaga et al. (2015, 2016)	Conical Spouted Bed (28°)	- Sand (0.17 mm; ρ_p = 2650 kg/m^3) - Sawdust (0.76 mm; ρ_p = 496 kg/m^3)	22.2 mm diameter and 55 mm long cylindrical probe	25-505

Zabrodsky and Mikhalik (1967) published the pioneering paper on heat transfer conducted in a conical spouted bed with 45º conical angle using a submerged cylindrical heat transfer surface inserted both vertically and horizontally. They found out that heat transfer coefficients in the spout axis are 4-8 % smaller than that at the spout-annulus boundary and drops down sharply to the wall-side as depicted in **Figure 2.3 (a)**.

Klimenko et al. (1970) worked with a 25 mm spherical heat transfer surface in the 90º conical angle spouted bed. The measurements were taken from the cylindrical section of spouted bed. In this work, as shown in **Figure 2.3 (b),** no peak was detected in the spout-annulus boundary; on contrary, heat transfer coefficients between spherical surface and the bed gradually went down approaching to the bed wall.

Recently, Macchi et al. (1999) and Saldarriaga et al. (2015) investigated bed-to-surface heat transfer in spouted and conical spouted beds, respectively. Macchi et al. (1999) used a 50.7 mm long and 12.7 mm diameter cylindrical probe. Similar to Klimenko et al. (1970), Macchi et al. (1999) also inserted the probe in the cylindrical section of the spouted bed. The findings of Macchi et al. (1999) supported the ones obtained by Klimenko et.al. (1970) as can be observed in **Figure 2.3 (c)**. Saldarriaga et al. (2015) inserted vertically a 55 mm long and 22.2 mm diameter probe in a conical spouted bed and also detected the decline of heat transfer coefficient from the spout-annulus interface to the bed wall without entering the spout section. **Table 2.2** summarizes the effects of important operating and design parameters on bed-to-surface heat transfer coefficients observed in these studies.

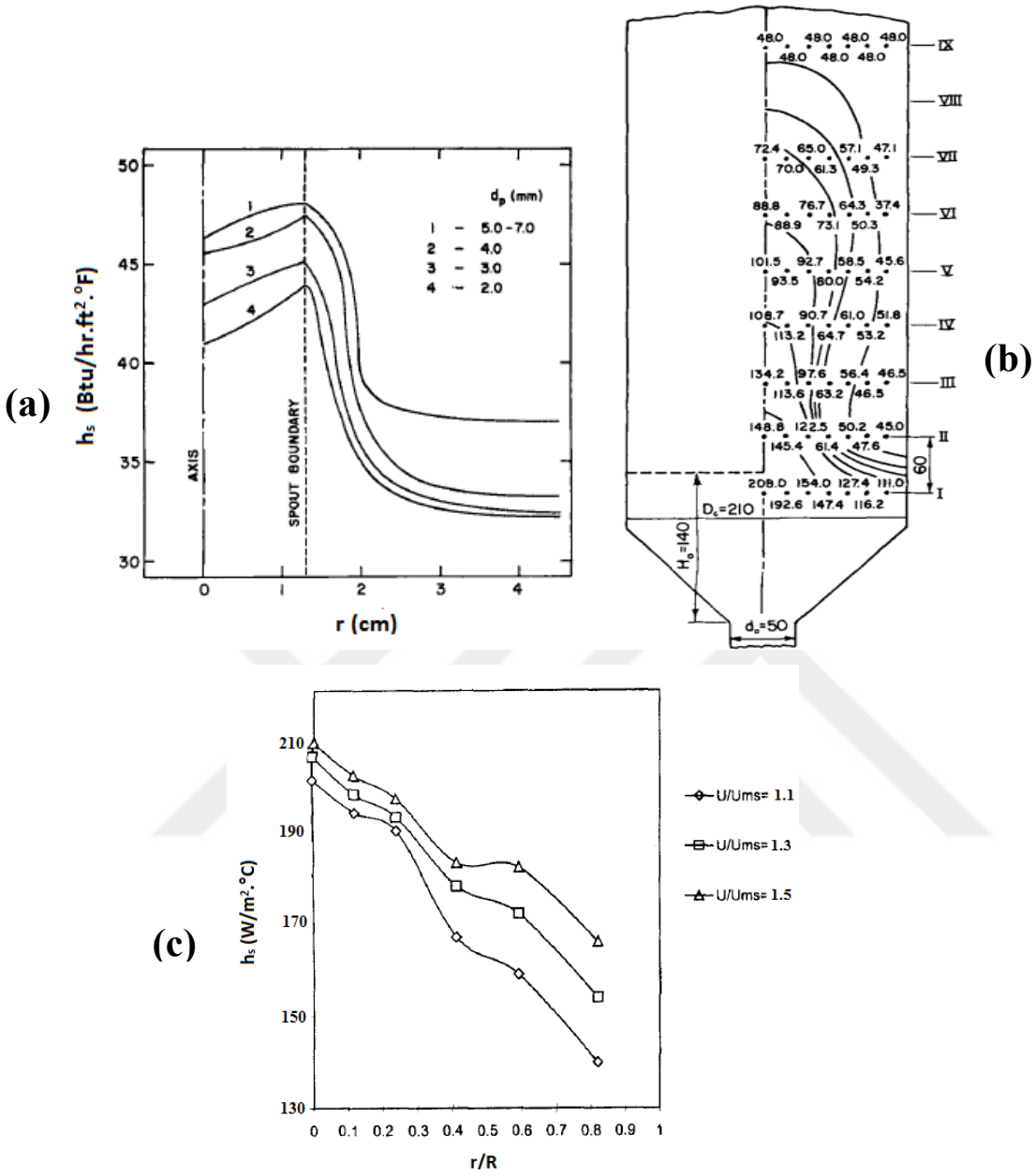

Figure 2.3 General trends in radial change of heat transfer coefficient measured by: **(a)** Zabrodsky and Mikhalik (1967) using silica gel particles (d_p = 2-7 mm); (b) Klimenko et al. (1970) using silica–aluminium catalyst particles (d_p = 2.4 mm); **(c)** Macchi et al. (1999) using glass particles (d_p = 1.6 mm)

Table 2.2 List of some important parameters and their effects on the submerged bed-to-surface heat transfer rates in the literature (Zabrdosky and Mikhalik, 1967; Macchi et al., 1999; Saldarriaga et al., 2015)

Parameters	Effects on h
Static Bed Height, H_b	Positive relation (h ↑ with H_b ↑)
Particle Diameter, d_p	Positive relation (h ↑ with d_p ↑)
Heat Capacity, C_p	Positive relation (h ↑ with C_p ↑)
Bed Contactor Angle, γ	Negative relation (h ↓ with γ ↑)
Spouting Air Flow Rate, U_s	Positive up to spouting, then remain constant
Spouting Air Inlet Diameter, D_o	No effect –

Looking at **Figure 2.3**, one can see a contradiction between the radial profiles of heat transfer coefficients obtained in the aforementioned studies. Heat transfer rate increases from the wall-side to spout axis and is maximum at the spout-annulus interface in Zabrodsky and Mikhalik's work. However, this peak was not detected by Klimenko et al. (1970) and Macchi et al. (1999). Therefore, further experiments should be conducted to clarify this contradiction. Moreover, as can be seen from **Table 2.1** all of the aforementioned studies were conducted with relatively light particles (< 2600 kg/m^3). Therefore, there is a lack of information for spouted beds operating with high-density particles.

All of the studies mentioned above were conducted in spouted beds. However, Chatterjee et al. (1983) showed that spout-fluid bed is the best option compared to the spouted and fluidized beds. As can be seen in **Figure 2.4** higher heat transfer coefficients are obtained in spout-fluid beds compared to other systems. Unfortunately, study conducted by Chatterjee and his co-workers is the only study in

the literature on bed-to-surface heat transfer in spout-fluid beds. Therefore, more detailed experiments have to be conducted to confirm their conclusion.

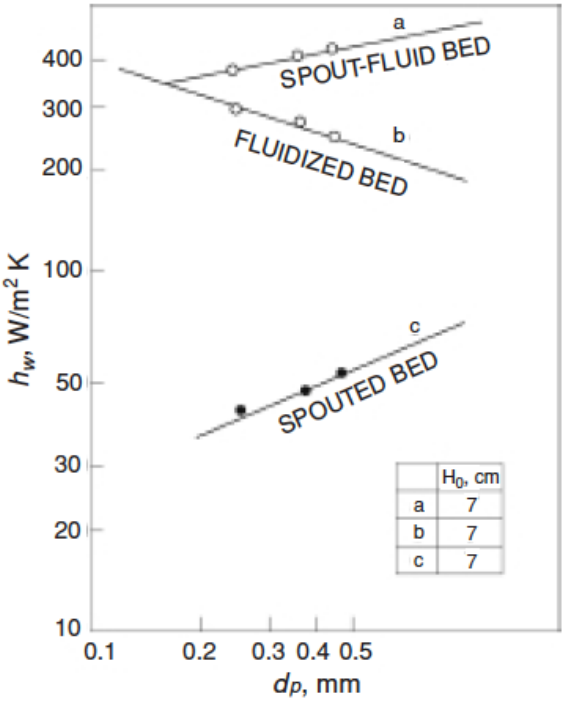

Figure 2.4 Comparison of heat transfer rates in different contactors (G = 0.19 kg/m^2.s, H_b = 70 mm) (Chatterjee et al., 1983)

In several of the heat transfer studies mentioned above, an empirical equation was also developed to estimate heat transfer coefficient under different operating and design conditions. These correlations are summarized in **Table 2.3**. The correlations developed by Malek and Lu (1964), Uemaki and Kugo (1967) and Chatterjee et al. (1983) were obtained by using the wall of the bed as a heat exchange surface. In these studies, Chatterjee et al. (1983) differs from others as it was conducted in a two-dimensional spout-fluid bed. The correlations developed by Macchi et al. (1999) and Saldarriaga et al. (2016), on the other hand, were obtained by using submerged cylindrical heat transfer surface. The correlation developed in Saldarriaga et al. (2016) took also into consideration the effect of radial and axial position of the immersed surface on the heat transfer coefficient. As can be seen from **Table 2.3**, all

of the correlations were developed for systems operating with relatively low density particles (< 2600 kg/m^3) and all of them were conducted in cylindrical systems rather than conical spouted or spout-fluid beds. Therefore, one of the aims of this study is to develop a correlation that can be used for the design and operation of conical spouted and spout-fluid beds operating with also heavy particles.

Table 2.3 Heat transfer correlations from wall or immersed vertical surface to spouted beds

Author	Bed Type	Heat Transfer Type	Correlation
Malek and Lu (1964)	Spouted Bed	Wall-to-Bed	$\mathbf{Nu} = \mathbf{0.54}\left(\frac{\mathbf{d_p}}{\mathbf{H_o}}\right)^{0.17}\left(\frac{\mathbf{d_p^3\rho_g g}}{\mathbf{\mu_g^2}}\right)^{0.52}\left(\frac{\mathbf{\rho_s C_{p,s}}}{\mathbf{\rho_g C_{p,g}}}\right)^{0.45}\left(\frac{\mathbf{\rho_g}}{\mathbf{\rho_s}}\right)^{0.08}$
Uemaki and Kugo (1967)	Spouted Bed	Wall-to-Bed	$\mathbf{Nu} = \mathbf{13}\left(\frac{\mathbf{d_p\rho_g U}}{\mathbf{\mu_g}}\right)^{0.1}\left(\frac{\mathbf{d_p^3\rho_g g}}{\mathbf{\mu_g^2}}\right)^{0.46}\left(\frac{\mathbf{\rho_s C_{p,s}}}{\mathbf{\rho_g C_{p,g}}}\right)^{-0.42}\left(\frac{\mathbf{D_o}}{\mathbf{d_p}}\right)^{0.2}(\mathbf{1}-\boldsymbol{\varepsilon})$
Chatterjee et al. (1983)	2D Spout-Fluid Bed	Wall-to-Bed	$\mathbf{Nu} = \mathbf{0.6}\left(\frac{\mathbf{D_p G}}{\mathbf{\mu}}\right)^{0.39}\left(\frac{\mathbf{C_g \mu}}{\mathbf{K_g}}\right)^{0.72}\left(\frac{\mathbf{\rho_{bC_s}}}{\mathbf{\rho_g C_g}}\right)^{0.12}$ $\mathbf{for\ Re_p} > 4.0$ $\mathbf{Nu} = \mathbf{0.42}\left(\frac{\mathbf{D_p G}}{\mathbf{\mu}}\right)^{1.16}\left(\frac{\mathbf{C_g}}{\mathbf{K_g}}\right)^{0.89}\left(\frac{\mathbf{\rho_{bC_s}}}{\mathbf{\rho_g C_g}}\right)^{0.24}\left(\frac{\mathbf{D_p}}{\mathbf{L}}\right)^{0.08}$ $\mathbf{for\ Re_p} < 4.0$
Macchi et al. (1999)	Spouted Bed	Immersed Surface-to-Bed	$\mathbf{Nu} = \mathbf{0.009\ Ar}^{0.35}\left(\frac{\mathbf{\rho_p(1-\varepsilon_b)C_p}}{\mathbf{\rho_g C_g}}\right)^{0.38}$ $\mathbf{for\ (r/R) = 0.59}$
Saldarriaga et al. (2016)	Conical Spouted Bed	Immersed Surface-to-Bed	$\mathbf{Nu} = \mathbf{17.11Re}^{0.516}\mathbf{Pr}^{0.333}\mathbf{Ar}^{0.033}\left(\tan\frac{\boldsymbol{\gamma}}{\mathbf{2}}\right)^{-2.331}\left(\frac{\mathbf{H_b}}{\mathbf{d_p}}\right)^{-1.334}\left(\frac{\mathbf{r}}{\mathbf{R}}\right)^{-0.51}\left(\frac{\mathbf{z}}{\mathbf{H_b}}\right)^{4.76}\boldsymbol{\varphi}^{2.102}$

CHAPTER 3

EXPERIMENTAL SET-UP

3.1 Design of Conical Spouted and Spout-Fluid Beds

The heat transfer experiments were performed in two separate units to see the effect of contactor angle on heat transfer. 31º and 66º conical spout-fluid beds are shown in **Figure 3.1-3.2** with photos and the axial measurement points, and the geometric dimensions of the units are summarized in **Table 3.1**. The system is composed of 3 parts basically; *upper transparent cylinder*, *bottom conical bed* and *bottom fluidizing cylinder*. These units are considered to be 'large scale' systems with their 250 mm cylindrical bed dimensions (D_c) according to the studies reported in the literature. The findings of this study, therefore, are crucial for the design of industrial scale systems.

Figure 3.1 Photographs of (a) 31º and (b) 66º conical spout-fluid beds

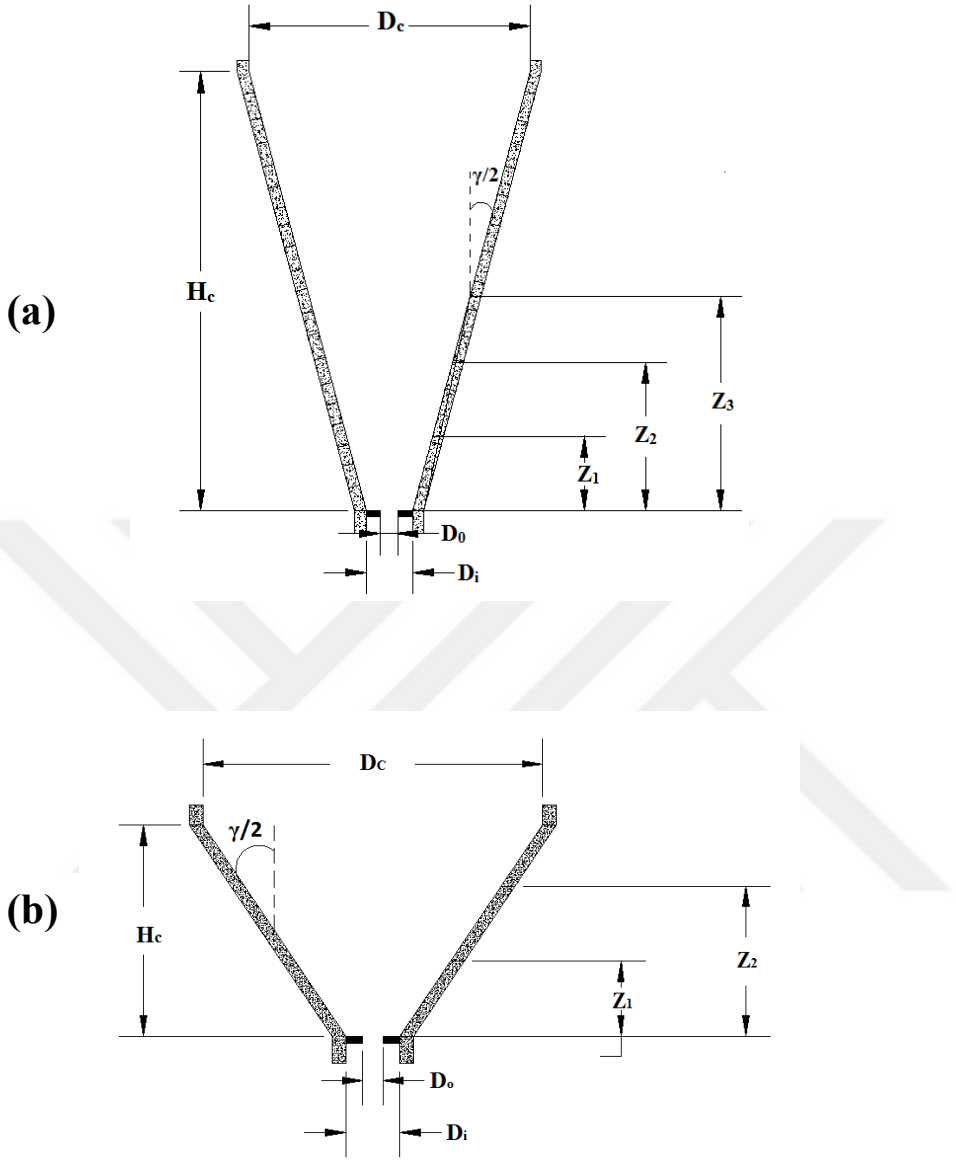

Figure 3.2 Geometric drawing of conical-spouted beds: **(a)** ϒ = 31° **(b)** ϒ = 66°

Table 3.1 Geometric dimensions of the 31º and 66º conical spout-fluid beds

Parameters	31º	66º
D_c (mm)	250	250
D_i (mm)	40	40
D_o (mm)	15, 19, 24	15, 19, 24
H_c (mm)	390	155
H_b (mm)	168, 235, 302	144
$Z_{1,2,3}$ (mm)	64, 128, 185	55, 110

For both of the units, construction material of bottom conical section was chosen as carbon steel because of its resistance to erosion and having almost no static electricity problem compared to polymeric materials. Considering especially the operation with high-density particles, this decision is quite beneficial in the long-term usage. Gas inlet diameters (D_o) shown in **Figure 3.3** were used to see the effect of inlet gas diameter on the operation. For the determination of inlet gas diameters, an important stability criterion, which underlines D_o/d_p ratio should be between 2 and 60, was also taken into consideration (Epstein & Grace, 2011). At the bottom of conical spouted bed, a thin mesh was used as in **Figure 3.3** to avoid the back flow of the particles into the spouting air inlet section. Moreover, a small hole was opened on the conical wall just above the gas inlet orifice for bed pressure drop measurements (ΔP). The other line of the pressure transducer was left open to atmosphere. The upper part of the conical beds was made of plexiglass (polymethylmethacrylate) to provide visual observation of particles' movement especially during the detection of the stable spouting velocity ($U_{ms,s}$).

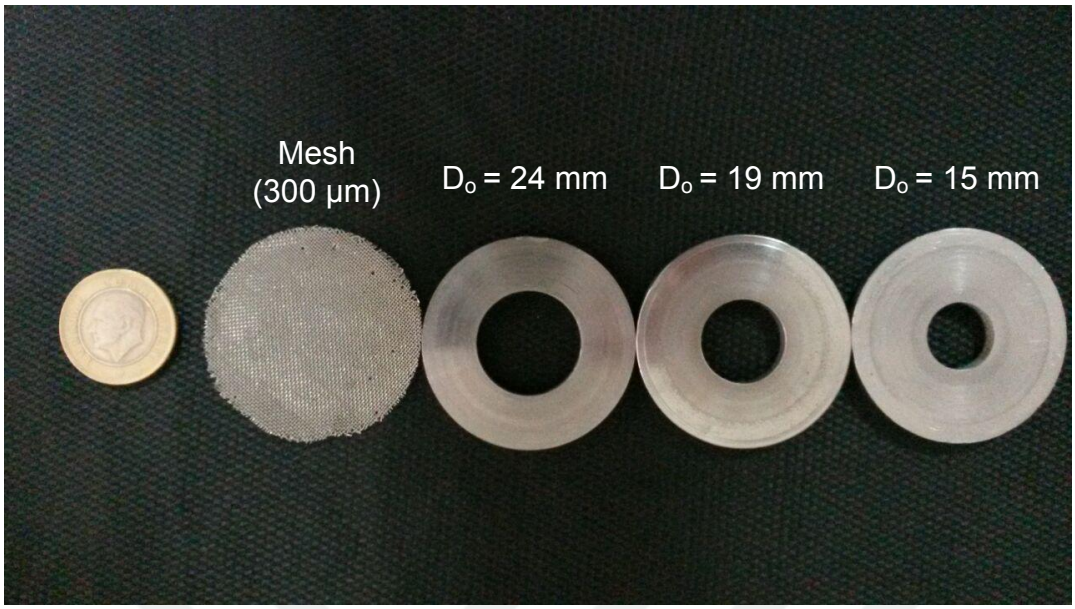

Figure 3.3 Metal orifice rings and mesh used for spouting air inlet

In order to operate the spouted beds under spout-fluid bed conditions, taking into consideration the diameters of the particles used in this study (1 and 2 mm), the holes with 1 mm diameter were uniformly drilled for the use of fluidizing gas flow on the lateral side of the conical beds as illustrated in **Figure 3.4**. The percentage of open area on the lateral surface was decided as 0.4 % based on the design criteria of distributor plate used in the fluidized beds and previous experiences in spout-fluid bed operations. Therefore, the pressure drop originated from those holes becomes quite small and air is dispersed evenly inside the bed. In order to introduce the fluidizing airflow, a bottom-fluidizing cylinder was constructed as a 'wind box'. Compressed air at ambient temperature was supplied from a screw type of compressor at 8 bar and maximum flow rate of 3 m^3/min. Before entering the bed, the main air line is divided into two; while the mass flow controller (Alicat MCR-1500SLPM-D/5M) arranges the spouting airflow rate, a rotameter (Dwyer RMC-123-SSV) regulates the fluidizing airflow rate with a maximum capacity of 0.85 m^3/min. The whole experimental set-up is sketched in **Figure 3.5**.

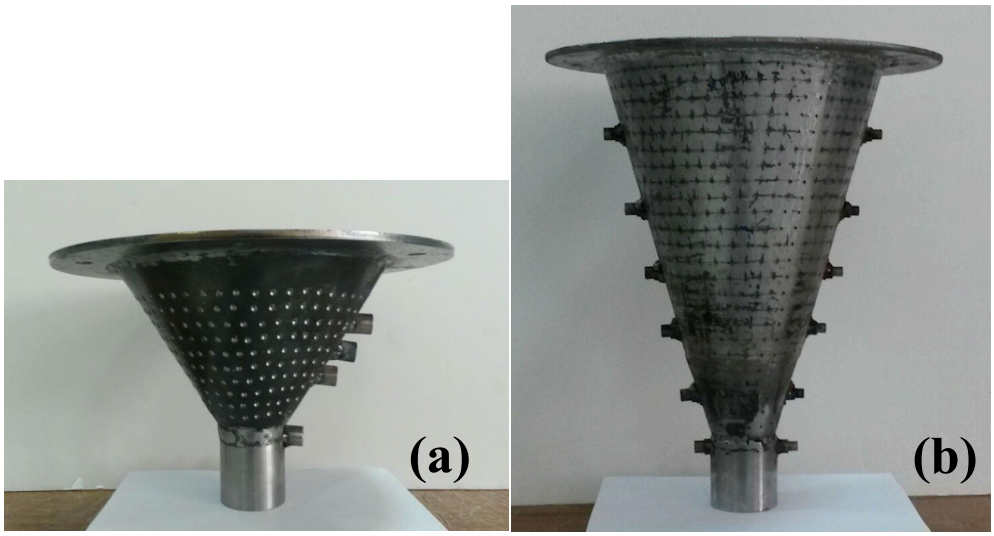

Figure 3.4 Photographs of conical spout-fluid beds with their holes on the lateral surfaces (a) 66° conical angle (b) 31° conical angle

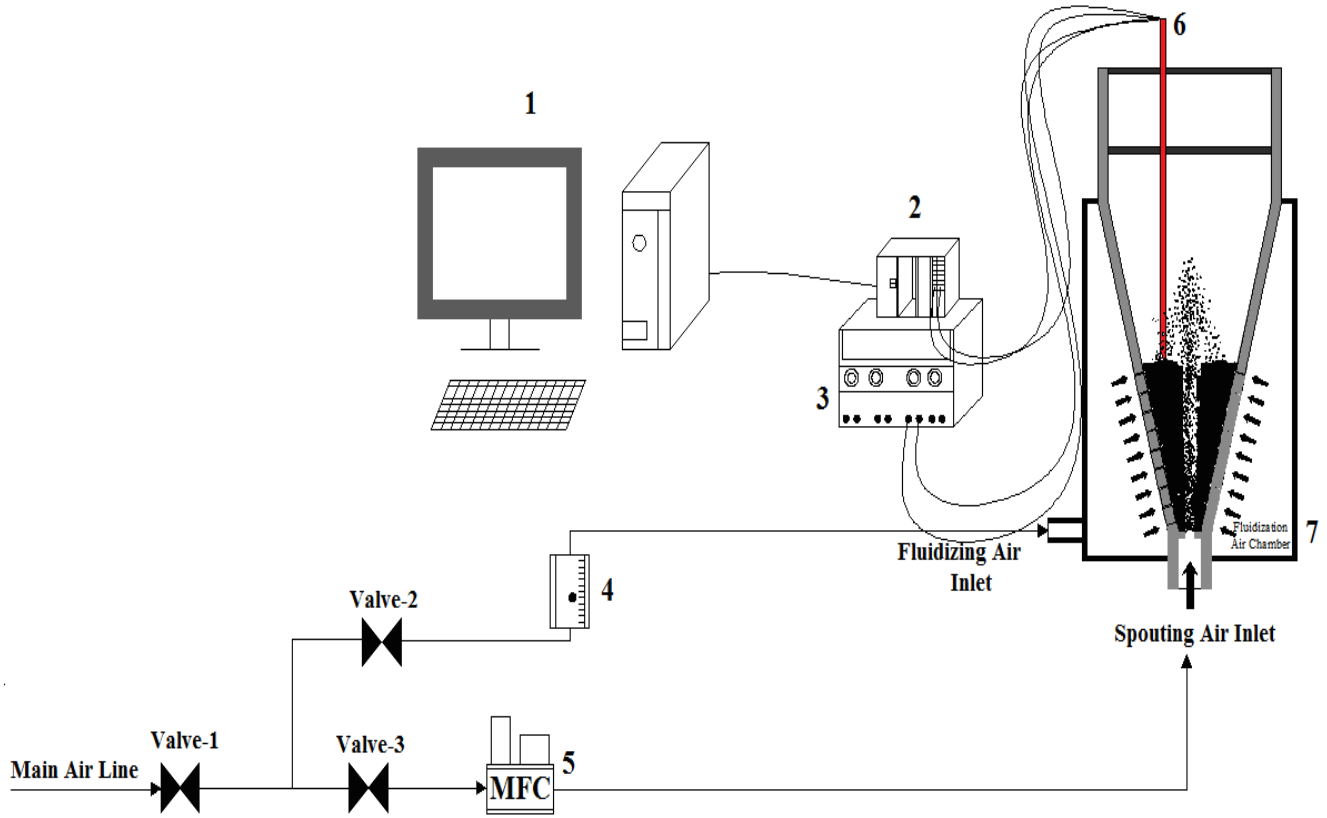

Figure 3.5 Experimental Set-up: (1) Computer, (2) Data Acquisition Card, (3) DC Power Supply, (4) Rotameter (5) Mass Flow Controller, (6) Heat Transfer Probe, (7) Spout-Fluid Bed

3.2 Design of Cylindrical Heat Transfer Probe

Two types of heat transfer probes, *conventional heat transfer probes* and *anemometers,* have generally been used in the area of fluidized and spouted beds. Conventional heat transfer probes are usually a cylindrical tube where a heater is embedded inside. They are mostly preferred in the fluidization area and used mainly for the characterization of bed-to-surface heat transfer. On the other hand, anemometers are composed of a thin wire or film used as a heater to be utilized both for air velocity and heat transfer measurements, especially in the turbulent flow conditions. Although choosing smaller size probes would be better for determining local heat transfer rates, a thin wire or film can be easily damaged by big particles (>1 mm). Therefore, conventional probes seem a better choice working with dense and coarse particles.

Table 3.2 summarizes the cylindrical probe dimensions used in the studies conducted in fluidized and spouted beds in the literature. As can be seen in this table, the probe designed in this study has the second smallest size after the one used in the study of Zabrodsky and Mikhailik (1967).

Table 3.2 Submerged cylindrical probe dimensions used in the literature

Author	Bed Type	Probe Length, mm	Probe Diameter, mm
Kim and Kim (2013)	Fluidized	80	25.4
Bacelos et al. (2011)	Fluidized	50	25
Zhang and Koksal (2006)	Fluidized	25.4	12.7
Brich et al. (1997)	Fluidized	85	24
Saldarriaga et al. (2015)	Conical Spouted	55	22
Macchi et al. (1999)	Spouted	50.8	12.7
Zabrodsky and Mikhailik (1967)	Conical Spouted	35	4
This investigation (2017)	Conical Spouted	26	7

The designed heat transfer probe is a 26 mm long and 7 mm diameter stainless steel tube, and a DC cartridge heater (Comstat MCH2-30W-001), which can supply 30 Watts at 24 Volts, was inserted as seen in **Figures 3.6-3.7**. The probe is composed of 5 parts; *30 mm long Teflon (PTFE) insulation tube*, *stainless steel (SS316) tube for the heat transmission*, *DC cartridge heater*, *silicon insulation (1 mm) pasted on the front section* and *brass tube to hold the probe*. The properties of probe's materials are given in **Table 3.3**. In order to measure the surface temperature of the probe, J-type thermocouples (Omega HJMQSS-10G-12) were placed inside the grooves of the probe from 2 sides with 180º angle.

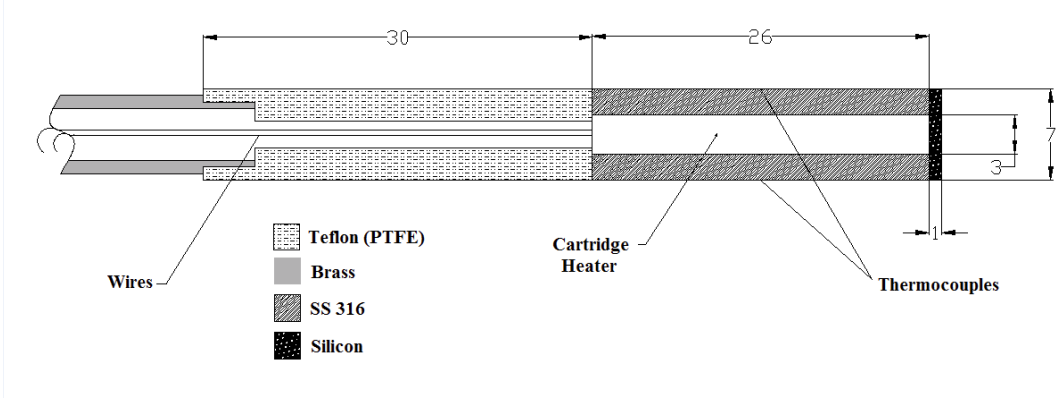

Figure 3.6 Front section of the heat transfer probe (All dimensions are in mm)

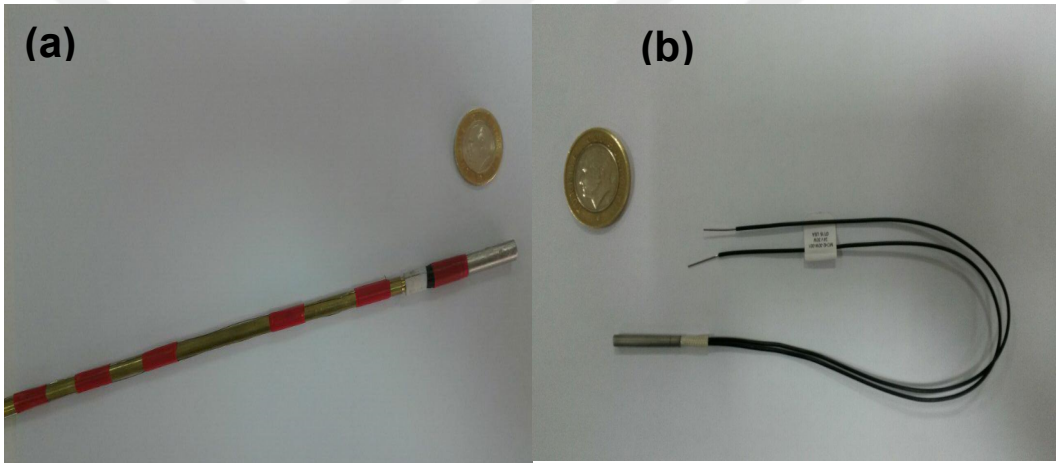

Figure 3.7 Photograph of the heat transfer probe (a) and DC cartridge heater (b)

Table 3.3 Properties of materials used in the heat transfer probe

Material	Conductivity, W/m.K	Heat Capacity, kJ/kg.K	Thermal Diffusivity, m^2/s
Teflon (PTFE)	0.25	1.4	0.124×10^{-6}
Stainless Steel	16	0.5	3.352×10^{-6}
Silicon	0.17	0.7	0.238×10^{-6}

The probe was always inserted vertically to the system during the experiments. Radial and axial probe locations are summarized in **Table 3.4-3.5** for 31º and 66º conical spouted beds, respectively. In order to keep the heat transfer probe fixed, two metal sheets were placed in the upper transparent cylinder and several radial holes were drilled on those metal sheets to fix the probe as shown in **Figure 3.8**.

Table 3.4 Radial and axial measurements locations in 31º conical spout-fluid bed

		Radial Locations, mm			
Axial Locations, mm		**Y_1 (r/R = 0)**	**Y_2 (boundary)**	**Y_3 (r/R = 0.5)**	**Y_4 (r/R = 0.8)**
Z_1	64	0	13	19	-
Z_2	128	0	17	28	41
Z_3	185	0	21	35	52

Table 3.5 Radial and axial measurements locations in 66º conical spout-fluid bed

		r/R					
Axial Locations, mm		**Y_1 (0 mm)**	**Y_2 (8 mm)**	**Y_3 (17.5 mm)**	**Y_4 (27.5 mm)**	**Y_5 (42.5 mm)**	**Y_6 (68 mm)**
Z_1	55	0	0.15	0.32	0.52	0.81	-
Z_2	110	0	0.09	0.20	0.32	0.50	0.80

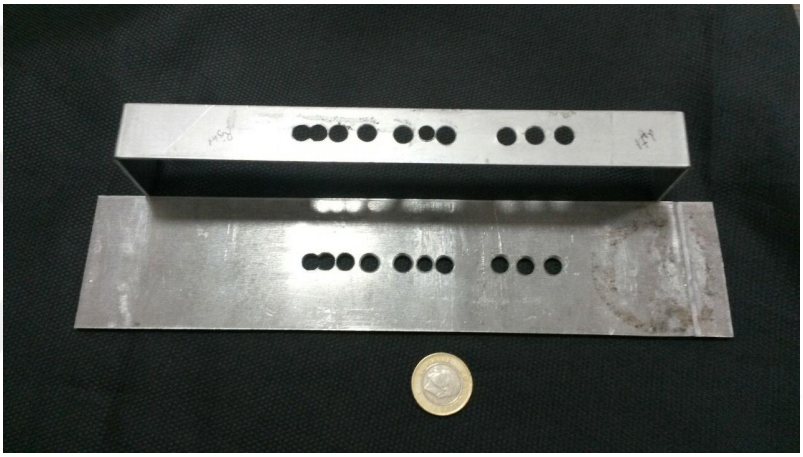

Figure 3.8 Drilled metal sheets to hold the heat transfer probe

For each experimental run, the bed-to-surface heat transfer coefficients (h) were calculated based on 30 s recorded temperature data by using the following equation:

$$h = \frac{P}{(T_S - T_b)A} \tag{3.1}$$

The surface temperature of the probe (T_s) was measured by the attached thermocouples inside the grooves. Additionally, the bed temperature (T_b) was recorded from the annulus area with J-type thermocouple (Tetcis TM08-J110-30-ME). During steady-state operation, it was determined that the electrical power (P) had almost no effect on heat transfer coefficient as indicated in **Figure 3.9** and thus,

3.5 Watts were provided during the experiments by a power supply (Gwinstek) in each experiment. The temperature signals were carried out by a data acquisition card (NI-PCI-6280) with a sampling frequency of 1000 Hz. The data was fed to a computer by a high-speed data acquisition board (National Instruments PCI-6280) and processed using LabVIEW version 8. Front panel (virtual interface) and block diagram of LabVIEW software is shown in **Figure 3.10-3.11**.

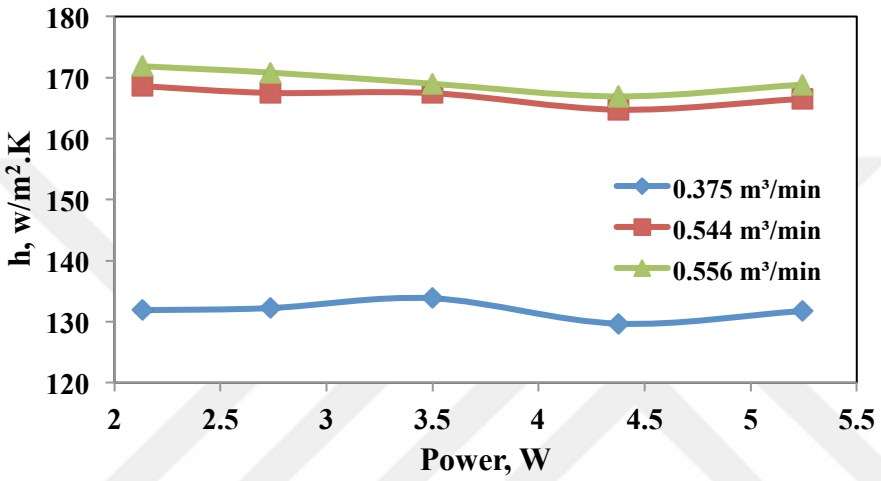

Figure 3.9 Sensitivity of the heat transfer probe to the electrical power with different flow rates in the empty bed (Z = 64 mm, r/R = 0, γ =31°)

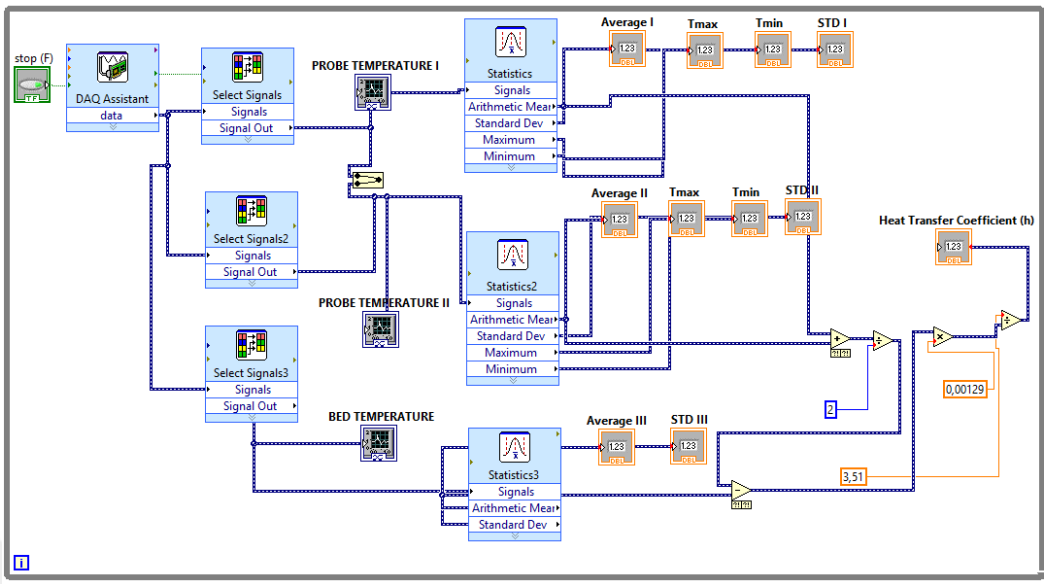

Figure 3.10 Block diagram of LabVIEW software for heat transfer measurements

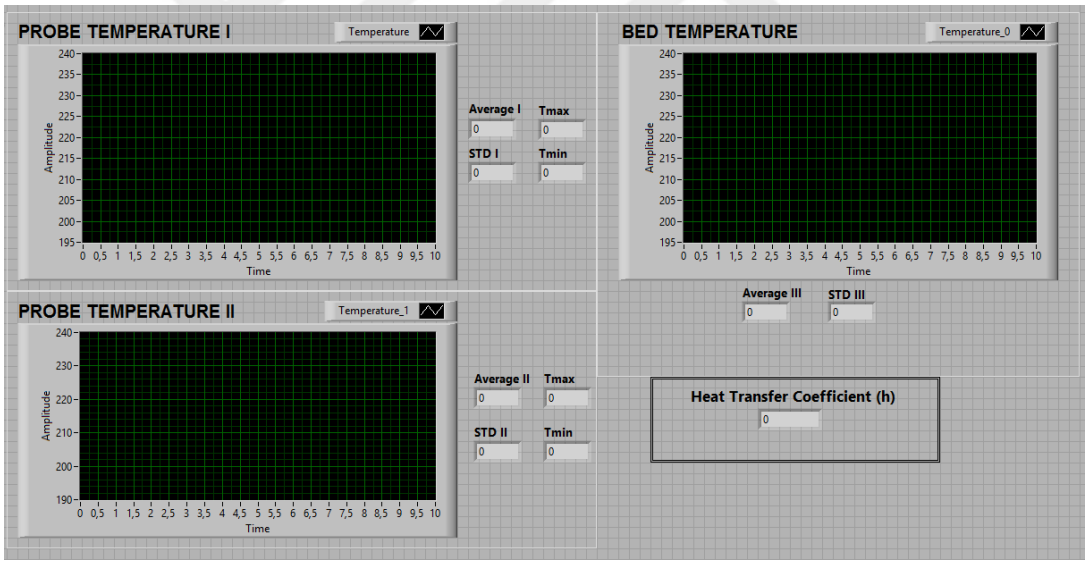

Figure 3.11 Front panel of LabVIEW software for heat transfer measurements

In order to check the reproducibility of the measurements, experiments were repeated 10 times in different days, the uncertainty of the measurements were found to be around 2.5 %. In addition, heat losses were also calculated from the ends of the probe

and found to be about 10 % (The details of these calculations are presented in Appendix A and B).

3.3 Properties of Solid Particles

In this study, glass, alumina (zirconia toughened) and yttra-stabilized zirconia particles as illustrated in **Figure 3.12** were used. The properties of these particles at 20ºC are presented in **Table 3.6**. These particles were especially chosen as they have different particle density and thermal properties. The particle humidity was also measured by a moisture analyser (Ohrus MB45) before and after each experiment and was found to be less than 1 wt. %.

Table 3.6 Properties of the particles at 20ºC

Particles	d_p (mm)	Φ	ρ_p (kg/m^3)	k_p (W/m.K)	C_p (kJ/kg. K)	α(m^2/s)	ε_b	Ar
Glass Beads	1	1	2500	0.94	0.800	4.70 x 10^{-7}	0.35	1.84 x 10^8
Glass Beads	2	1	2500	0.94	0.800	4.70 x 10^{-7}	0.36	14.72 x 10^8
Alumina (Zirconia toughened)	1	≥ 0.95	3700	22	0.650	9.15 x 10^{-6}	0.39	4.03 x 10^8
Alumina (Zirconia toughened)	2	≥ 0.95	3700	22	0.650	9.15 x 10^{-6}	0.4	32.25 x 10^8
Zirconia	1	≥ 0.95	6000	2	0.436	9.01 x 10^{-7}	0.37	7.63 x 10^8

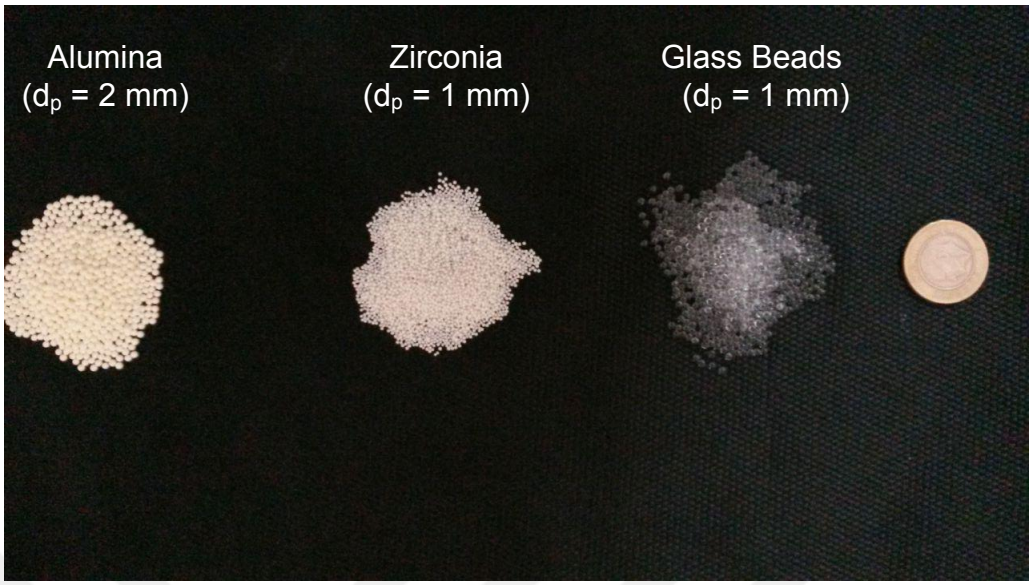

Figure 3.12 Photograph of the particles

CHAPTER 4

RESULTS AND DISCUSSION

This chapter presents the results of the experimental studies undertaken within the scope of this thesis. Firstly, the preliminary testing of the designed heat transfer probe was carried out in three different flow conditions to ensure the reliability of the heat transfer measurements. Secondly, operating conditions of the conical spout and spout-fluid beds (minimum spouting and fluidizing gas flow rates) were determined. Bed-to-surface heat transfer coefficients were determined for a wide range of operating conditions and design parameters. Lastly, based on the results of heat transfer measurements, an empirical correlation for the bed-to-surface heat transfer coefficient in conical spouted beds operated with high-density particles was proposed.

4.1 Preliminary Testing of Heat Transfer Probe

Designed and manufactured heat transfer probe had been tested in three different flow conditions before it was used in the spouted and spout-fluid beds. Within this scope, while natural and forced convection tests were done for one phase flow, the probe was also tested in the packed bed condition for two-phase flow. As a result of these tests, measured heat transfer coefficients were compared with the empirical correlations in the literature and the reliability of the probe was shown.

4.1.1 Natural Convection Tests

In order to test the probe under natural convection, the probe was placed in a piece of pipe (ID = 25 cm, L = 50 cm) as seen in **Figure 4.1** without exposing it to any air

stream. Many different correlations have been developed for the heat transfer between a cylinder surface and surrounding gas and also there have been numerous proposed analytical and numerical solutions. **Table 4.1** presents the major natural convection correlations available in the literature. The fluid properties are evaluated at the film temperature and the main assumptions are negligible end effects and sufficiently long cylinder.

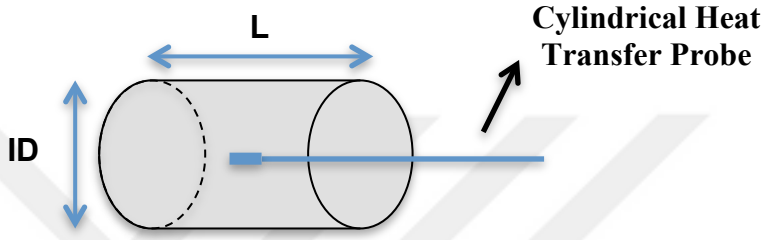

Figure 4.1 Natural convection test in a big cylinder tube (ID = 25 cm, L = 50 cm)

Table 4.1 Major natural convection heat transfer correlations for a cylindrical surface

Author	Correlation	Range
Churchill and Chu (1975)	$\mathrm{Nu_d}^{1/2} = 0.6 + 0.387\left(\frac{\mathrm{Gr_D Pr}}{[1+(0.559/\mathrm{Pr})^{9/16}]^{16/9}}\right)^{1/6}$	$10^{-11} \leq \mathrm{Gr_D Pr} \leq 10^{9}$
Kuehn and Goldstein (1976)	$\frac{2}{\mathrm{Nu_D}} = \ln\left[1 + \frac{2}{\left[\left\{0.518\mathrm{Ra_D}^{1/4}\left[1+\left(\frac{0.559}{\mathrm{Pr}}\right)^{3/5}\right]^{-5/12}\right\}^{15} + \left(0.1\mathrm{Ra_D}^{1/3}\right)^{15}\right]^{1/15}}\right]$	at any Rayleigh and Prandtl
Fand et al. (1977)	$\mathrm{Nu_D} = 0.474\mathrm{Ra_D}^{0.25}\mathrm{Pr}^{0.047}$	$(0.7 \leq \mathrm{Pr} \leq 3090)$ $(2.5\mathrm{x}10^2 \leq \mathrm{Gr_D Pr} \leq 2\mathrm{x}10^7)$
Fujii et al. (1979)	$\frac{2}{\mathrm{Nu_D}} = \ln\left[1 + \frac{3.3}{\mathrm{C(Pr)Ra_D^m}}\right]$ $\mathrm{m} = \frac{1}{4} + \frac{1}{10 + 5\mathrm{Ra_D}^{0.175}}$ $\mathrm{C(Pr)} = \frac{0.671}{[1+(0.492/\mathrm{Pr})^{9/16}]^{4/9}}$	$10^{-10} \leq \mathrm{Gr_D} \leq 10^{7}$

The experimental conditions and correlation results in natural convection tests are indicated in **Table 4.2** and **4.3**, respectively.

Table 4.2 Experimental conditions in natural convection test

Parameters	Values
Ambient temperature, $T_{ambient}$ (°C)	26.0
Probe surface temperature, T_{Prob} (°C)	74.9
Surface film temperature, T_{Film} (°C)	50.5
Surface area of the probe, (m^2)	0.00129
Power, (W)	0.70
Prandtl number	0.710
Grashof number	1470

Table 4.3 Natural convection heat transfer coefficients for the experimental conditions given in Table 4.2

Correlation	h (W / m^2.K)
Churchill and Chu (1975)	10.5
Kuehn and Goldstein (1976)	11.4
Fand et al. (1977)	10.6
Fujii et al. (1979)	11.7

For the conditions given in **Table 4.2**, the experimental heat transfer coefficient was found as **11.1 W/m^2.K**. In comparison with the correlations in **Table 4.3**, there is max. 6 % deviation. On the other side, if the average value of the results from all correlations (11. W/m^2.K) is used, the deviation becomes less than 1 %.

4.1.2 Forced Convection Tests

In the forced convection tests, the experiments were conducted in 3 different air velocities and inside a transparent tube with 32 mm internal diameter.

Air velocities were set as **6**, **8** and **10 m/s** during the experiments. Besides, the surface temperature was measured with a vertically inserted heat transfer probe at the middle of the tube as shown in **Figure 4.2**.

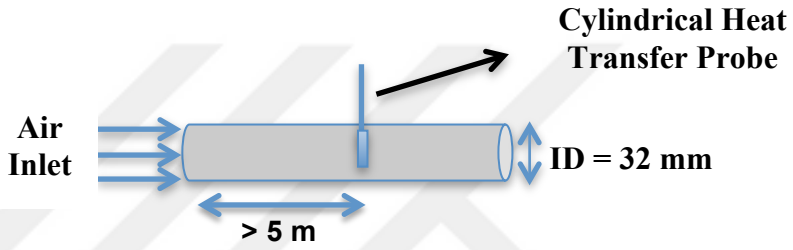

Figure 4.2 Heat transfer probe placed inside a tube with 32 mm internal diameter

The experimental conditions in forced convection tests are indicated in **Table 4.4**, and air properties in the film conditions are represented in **Table 4.5**.

Table 4.4 Forced convection experimental conditions

Parameters	Experiment 1	Experiment 2	Experiment 3
Ambient Temperature, $T_{ambient}$ (℃)	26.2	26.2	26.2
Probe Surface Temperature, T_{probe} (℃)	33.8	32.2	31
Film Temperature, T_{Film} (℃)	29.9	29.2	28.6
Surface Area of Probe, m^2	0.00129	0.00129	0.00129
Power, W	0.78	0.78	0.78
Air velocity, m/s	**6**	**8**	**10**
Reynolds number	2623.2	3510.3	4487.5
Prandtl number	0.714	0.714	0.715

Table 4.5 Air properties of the film temperatures for forced convection tests

Air properties	Experiment 1 (29.98 ºC)	Experiment 2 (29.18 ºC)	Experiment 3 (28.6 ºC)
Density, kg/m^3	1.165	1.168	1.170
Viscosity, $kg/m.s$	$1.868x10^{-5}$	$1.864x10^{-5}$	$1.861x10^{-5}$
Heat Capacity, $J/kg.K$	1006	1006	1006
Thermal Expansion Coefficient, $1/K$	$3.299x10^{-3}$	$3.308x10^{-3}$	$3.314x10^{-3}$
Conductivity, $W/m.K$	0.0263	0.0263	0.0262

Table 4.6 Major forced convection correlations for a cylindrical surface

Author	Correlation	Range
Kramers (1946)	$\mathrm{Nu} = 0.42\mathrm{Pr}^{0.2} + 0.57\mathrm{Re}^{0.5}\mathrm{Pr}^{0.31}$	$5 \leq \mathrm{Re} \leq 10^3$
Perkins and Leppert (1962)	$\mathrm{Nu}\left[\frac{\mu_w}{\mu_b}\right]^{0.25} = [0.3\mathrm{Re}^{0.5} + 0.1\mathrm{Re}^{0.67}]\mathrm{Pr}^{0.4}$	$40 \leq \mathrm{Re} \leq 10^5$ $1 \leq \mathrm{Pr} \leq 300$
Fand et al. (1965)	$\mathrm{Nu}_f = \left(0.35 + 0.34\mathrm{Re}_f^{0.5} + 0.15\mathrm{Re}_f^{0.58}\right)\mathrm{Pr}_f^{0.3}$	$0.1 \leq \mathrm{Re} \leq 10^5$
Zukauskas and Ziugzda (1985)	$\mathrm{Nu}\left[\frac{\mathrm{Pr}_w}{\mathrm{Pr}_b}\right]^{0.25} = [0.26\mathrm{Re}^{0.6}]\mathrm{Pr}^{0.37}$	$10^3 \leq \mathrm{Re} \leq 2\mathrm{x}10^5$
Whitaker (1972)	$\mathrm{Nu}\left[\frac{\mu_w}{\mu_b}\right]^{0.25} = \left[0.4\mathrm{Re}^{0.5} + 0.06\mathrm{Re}^{2/3}\right]\mathrm{Pr}^{0.4}$	$1 \leq \mathrm{Re} \leq 10^5$ $0.67 \leq \mathrm{Pr} \leq 300$
Churchill and Bernstein (1977)	$\mathrm{Nu} = 0.3 + \frac{0.62\mathrm{Re}^{1/2}\mathrm{Pr}^{1/3}}{[1+(0.4/\mathrm{Pr})^{2/3}]^{1/4}}\mathrm{x}\left[1 + \left(\frac{\mathrm{Re}}{282{,}000}\right)\right]^{4/5}$	$10^2 \leq \mathrm{Re} \leq 10^7$ $\mathrm{RePr} > 0.2$
Sanitjai and Goldstein (2004)	$\mathrm{Nu} = 0.446\mathrm{Re}^{0.5}\mathrm{Pr}^{0.35} + 0.528\left(\left(6.5\mathrm{e}^{\mathrm{Re}/5000}\right)\right)^{-5} + \left((0.031\mathrm{Re}^{0.8})^{-5}\right)^{-1/5}\mathrm{Pr}^{0.42}$	$2\mathrm{x}10^3 \leq \mathrm{Re} \leq 10^5$ $0.7 \leq \mathrm{Pr} \leq 176$

In **Table 4.6**, major forced convection correlations for a cylindrical surface are listed. It is known that fluid flow characteristics between the front and the rear section of a cylinder differ from each other. However, in most of the correlations, except that of Sanitija and Goldstein (2004), the angular effect is not taken into consideration. The

angular effect was not also taken into account in this thesis. The fluid properties are also evaluated at the film temperature and Reynolds numbers are calculated based on external flow on the probe surface in **Table 4.6**.

The calculated heat transfer coefficients for three different free stream velocities as well as the average values of all correlations are presented in **Table 4.7**. As can be seen from the table, there is as much as 30% discrepancy between different correlations. Therefore, the average value of the correlations was compared with the experimental results.

Table 4.7 Forced convection heat transfer coefficients from the given correlations for 6, 8 and 10 m/s air velocities

Correlations	**h (W / m^2.K) - 6 m/s**	**h (W / m^2.K) - 8 m/s**	**h (W / m^2.K) - 10 m/s**
Kramers (1946)	100.4	115.7	129.2
Perkins and Leppert (1962)	115.2	136.6	156.6
Fand et al. (1965)	109.4	127.5	143.7
Zukauskas and Ziugzda (1985)	94.8	118.2	135.7
Whitaker (1972)	71.4	82.6	92.6
Churchill and Bernstein (1977)	98.9	114.9	129.5
Sanitjai and Goldstein (2004)	94.8	110.3	125.2
Average value of the correlations (h_{ave})	**97.8**	**115.1**	**130.4**

In the wake of experimental tests, heat transfer coefficients for 6, 8 and 10 m/s air velocities were found as **80.2**, **101.9** and **126 W/m^2.K**, respectively. Especially as the velocity is increased, the results become more compatible with the average values of the correlations. **Figure 4.3** shows the variation of the correlation and experimental results with the air velocity. In conclusion, considering the inherent uncertainty of the forced convection correlations, discrepancy between the existing correlations and the difficulty in achieving a perfect flow over a cylinder condition experimentally, the performance the probe was found to be acceptable.

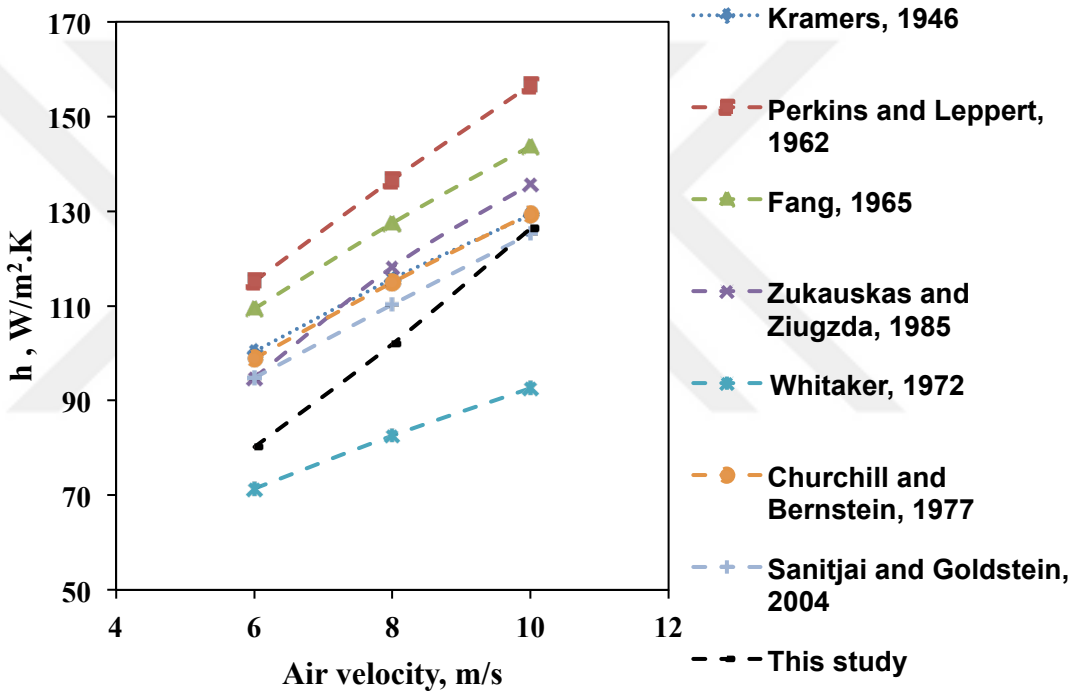

Figure 4.3 Comparison of forced convection heat transfer coefficients between the literature correlations and the experiments at different air velocities

4.1.3 Packed Bed Tests

In addition to natural and forced convection tests, the designed heat transfer probe was also tested in the packed bed condition. Gas flow in the packed bed condition

resembles the annulus section in the spouted and spout-fluid beds. Thereby, packed bed tests are quite important for the reliability of the probe together with the natural and forced convection tests. In this context, an experimental apparatus in **Figure 4.4** was set -up, and glass and alumina particles were used as packed bed materials. During the experiments, airflow rate was carefully arranged so that the particles were not fluidized.

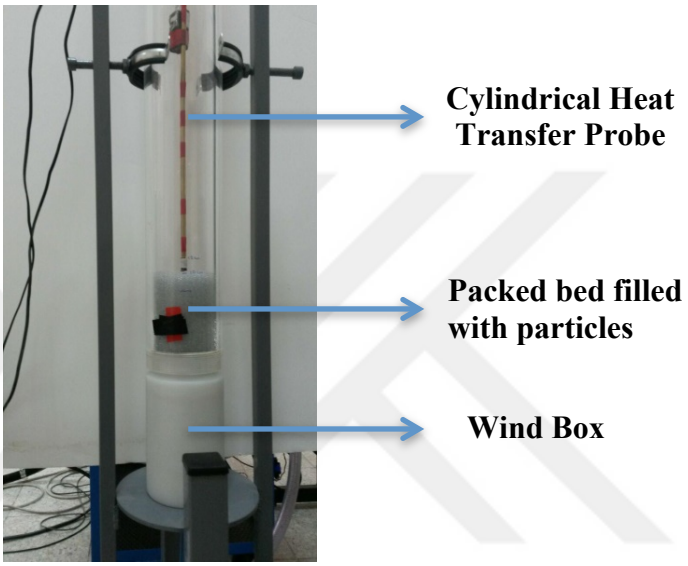

Figure 4.4 Packed bed apparatus for heat transfer tests (D = 10 cm, L = 100 cm, H_b = 10 cm)

In order to compare the experimental results, a known correlation proposed by Yagi and Wakao (1960) was chosen, and it is defined as follows;

$$h = 0.2\mathrm{Re}_p^{-0.2} C_g \left(\frac{G}{\mathrm{Pr}^{2/3}} \right) \tag{4.1}$$

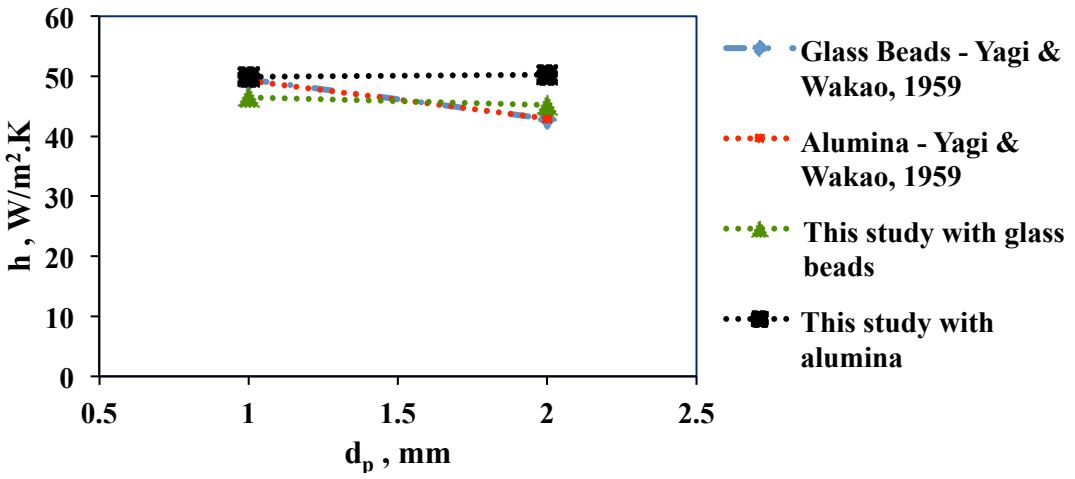

Figure 4.5 Comparison of heat transfer coefficients between the experimental data and Yagi and Wakao's correlation for different particle diameters in the packed bed (H_b = 10 cm, G = 0.35 kg/m^2.s, U_o = 0.3 m/s)

Based on the Yagi and Wakao's correlation, which is independent from the thermal properties of the particles, experimental and correlation results were compared in **Figure 4.5** for 1 and 2 mm glass and alumina particles. It is seen that the experimental results are compatible with the correlation results with a deviation less than 18%.

4.2 Hydrodynamic Tests and Determination of Minimum Spouting Velocities

Minimum stable spouting velocity ($U_{ms,s}$) is the most important operational parameter in spouted and spout-fluid beds. The bed must be operated at a superficial gas velocity higher than the minimum spouting velocity without the presence of any instability (such as pulsative spout flow, collapse of the spout, changing fountain height). On the other hand, the operational velocity should not be high enough to lead to jetting. Compared to conventional fluidized beds, the operational range – in terms of superficial gas velocity – of spouted and spout-fluid beds is quite limited, therefore, the determination of the minimum spouting velocity is critical.

The classical method to determine the minimum spouting velocity is to measure the bed pressure drop while increasing and/or decreasing the superficial gas velocity. The minimum spouting velocity lies in the region when the bed pressure drop levels off after the point of peak pressure, however, the exact point must be determined based on the visual observations. **Table 4.8** shows the effect of the various operating and geometric factors on $U_{ms,s}$ and $G_{ms,s}$ based on the available literature (Olazar et al., 1992; Choi & Meisen, 1992). In addition to $U_{ms,s}$, $G_{ms,s}$ shows the supplied total gas flow rate (m^3/min), which is very important in the economical evaluations of the beds. As can be seen from the **Table 4.9-4.10**, gas inlet diameter (D_o), static bed height (H_b), particle density (ρ_p) and size (d_p) are effective on the minimum stable spouting velocities or flow rates.

Table 4.8 Effect of operating and geometric factors on $U_{ms,s}$ and $G_{ms,s}$

Parameter	Effect
Gas Inlet diameter (D_o)	While $G_{ms,s}$ increases with increasing D_o, $U_{ms,s}$ decreases.
Static Bed Height (H_b)	$G_{ms,s}$ and $U_{ms,s}$ increase with increasing H_b
Particle Size (dp)	$G_{ms,s}$ and $U_{ms,s}$ increase with increasing d_p
Particle Density (ρ_p)	$G_{ms,s}$ and $U_{ms,s}$ increase with increasing ρ_p

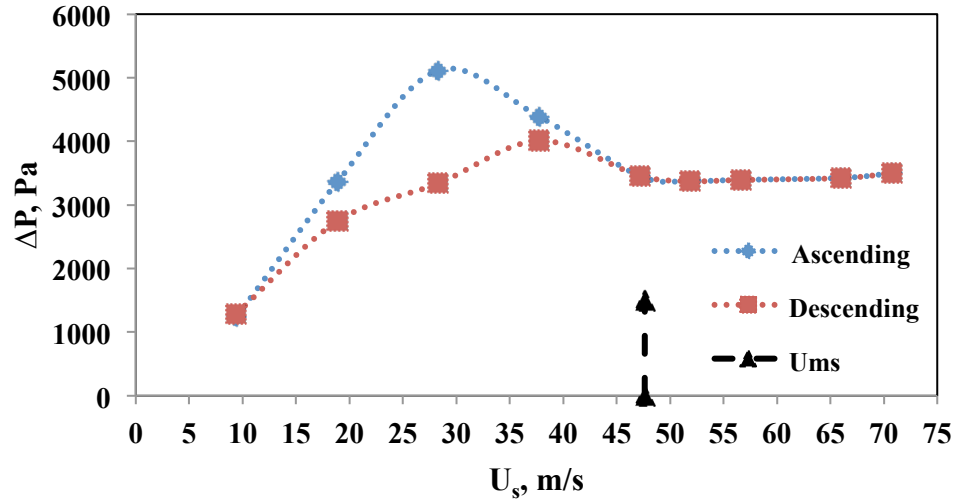

Figure 4.6 Time-averaged bed pressure drop for zirconia particles (H_b = 168 mm, γ = 31°, d_p = 1 mm)

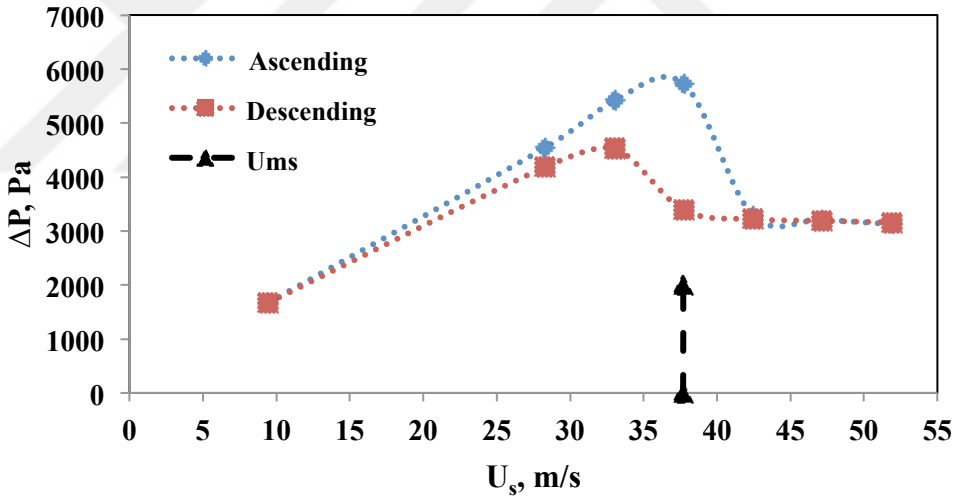

Figure 4.7 Time-averaged bed pressure drop for glass beads (H_b = 144 mm, γ = 66°, d_p = 1 mm)

Figure 4.6-4.7 show the typical variation of the time-averaged bed pressure drop with spouting gas velocity for zirconia and glass bead particles. It is seen that in the packed bed condition of both 31° and 66° conical angle conical spouted beds, the pressure drop rises from around 1000 Pa to 6000 Pa in general till the peak point,

where the onset of external spouting is first observed, and drops down significantly to about 3000 Pa in the operating section of bed. By means of ascending and descending, it is indicated when the spouting gas flow rate is increased and decreased during the operation, respectively. To eliminate the effect of unsteady operation, the bed was initially operated 15 minutes, and the measurements were taken afterwards. During the bed pressure drop measurements, the sampling frequency was set as 1000 Hz, and the sampling time was 10 s. $U_{ms,s}$ values were determined based on the decreasing air flow rate experiments. The point, just before stable spouting ceases, was noted as $U_{ms,s}$. **Table 4.9-4.10** present all $U_{ms,s}$ and $G_{ms,s}$ values as well as the corresponding operational conditions and design parameters.

Table 4.9 Minimum stable spouting velocities ($U_{ms,s}$) in 66º conical angle spouted bed

Particle	Angle, γ	d_p, mm	D_o, mm	D_c, mm	H_b, mm	$U_{ms,s}$, m/s	$G_{ms,s}$, m^3/min
Glass Beads	66	1	15	250	144	**37.7**	0.40
Glass Beads	66	1	19	250	144	**25.3**	0.43
Glass Beads	66	1	24	250	144	**17.3**	0.47
Glass Beads	66	2	15	250	144	**68.9**	0.73
Glass Beads	66	2	19	250	144	**47.6**	0.81
Glass Beads	66	2	24	250	144	**33.5**	0.91
Alumina	66	1	15	250	144	**47.2**	0.50
Alumina	66	1	19	250	144	**31.8**	0.54
Alumina	66	1	24	250	144	**23.5**	0.64
Alumina	66	2	15	250	144	**79.3**	0.84
Alumina	66	2	19	250	144	**55.9**	0.95
Alumina	66	2	24	250	144	**39.1**	1.06
Zirconia	66	1	15	250	144	**54.3**	0.58
Zirconia	66	1	19	250	144	**37.1**	0.63
Zirconia	66	1	24	250	144	**25.3**	0.69

Table 4.10 Minimum stable spouting velocities ($U_{ms,s}$) in 31° conical angle spouted bed

Particle	Angle, ϒ	d_p, mm	D_o, mm	D_c, mm	H_b, mm	$U_{ms,s}$, m/s	$G_{ms,s}$, m^3/min
Alumina	31	1	15	250	168	**41.9**	0.45
Alumina	31	1	15	250	235	**59.9**	0.64
Alumina	31	1	15	250	302	**77.8**	0.83
Alumina	31	2	15	250	168	**72.6**	0.77
Alumina	31	2	15	250	235	**92.9**	0.99
Alumina	31	2	15	250	302	**100.9**	1.07
Alumina	31	2	19	250	168	**47.2**	0.82
Alumina	31	2	19	250	235	**64.2**	1.07
Alumina	31	2	19	250	302	**79.5**	1.40
Alumina	31	2	24	250	168	**33.2**	0.90
Alumina	31	2	24	250	235	**44.0**	1.11
Alumina	31	2	24	250	302	**55.8**	1.53
Glass Beads	31	1	15	250	168	**28.3**	0.30
Glass Beads	31	1	15	250	235	**41.0**	0.44
Glass Beads	31	1	15	250	302	**57.1**	0.60
Glass Beads	31	1	19	250	168	**19.6**	0.34
Glass Beads	31	1	19	250	235	**26.8**	0.47
Glass Beads	31	1	19	250	302	**38.0**	0.66
Glass Beads	31	2	15	250	168	**60.4**	0.64
Glass Beads	31	2	15	250	235	**84.4**	0.87
Glass Beads	31	2	15	250	302	**101.4**	1.08
Glass Beads	31	2	19	250	168	**38.6**	0.67
Glass Beads	31	2	19	250	235	**53.6**	0.93

Table 4.10 Minimum stable spouting velocities ($U_{ms,s}$) in 31° conical angle spouted bed (Continued)

Particle	Angle, ϒ	d_p, mm	D_o, mm	D_c, mm	H_b, mm	$U_{ms,s}$, m/s	$G_{ms,s}$, m^3/min
Glass Beads	31	2	19	250	302	**67.7**	1.18
Zirconia	31	1	15	250	168	**47.6**	0.51
Zirconia	31	1	19	250	168	**29.9**	0.52

4.3 Local Bed-to-Surface Heat Transfer Measurements

The axial and radial variation of the local time averaged heat transfer coefficient (h) was determined for different operational conditions and design parameters. It should be noted that the spouting gas velocity (U_s) was kept at $1.1U_{ms,s}$ for all measurements. Majority of the results are presented and discussed in this section. The results of the experiments leading to similar discussions are given in Appendix C to avoid repetition.

4.3.1 Effect of Axial (z) and Radial Positions (r/R)

It is well known that the local hydrodynamics in conical spouted beds characterized by particle and gas velocities, and voidage is not homogeneous and vary significantly (San Jose et al., 2005a, 2005b; Kulah et al., 2016). As can be seen in **Figure 4.8**, solid movements based on solid flux (black arrows) in a conical spouted bed show the ordinary characteristics of solid particles in radial and axial locations.

In this direction, the bed-to-surface heat transfer coefficient, h, depends on the local hydrodynamics around the immersed surface. For this reason, the axial and radial variation of the heat transfer coefficient was investigated as shown in **Figure 4.9-4.11**. **Figure 4.9-4.10** show the heat transfer coefficient profiles of alumina and glass beads in 31° conical spouted bed at three axial measurement points (Z_1, Z_2 and Z_3)

while the radial distribution of heat transfer coefficient at two axial measurement points (Z_1 and Z_2) is given for alumina and zirconia particles in 66° conical spouted bed, in **Figure 4.11**.

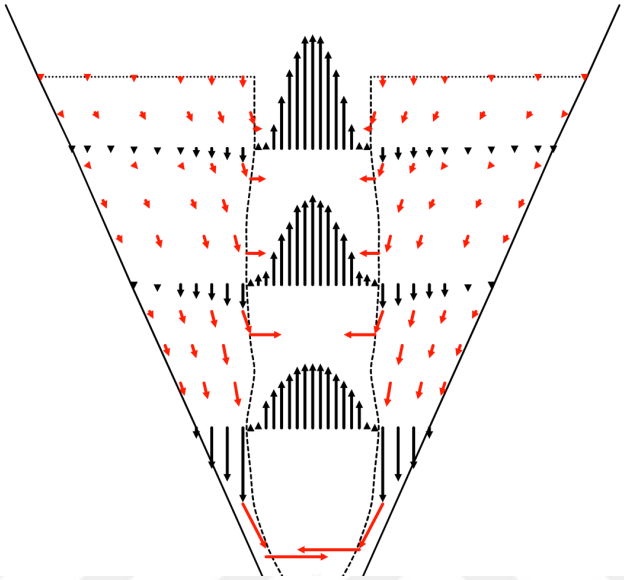

Figure 4.8 Conceptual diagram of solid flux in a conical spouted bed (Kulah et al., 2016)

As radially moving from the wall side to the spout axis in 31° conical spouted bed, heat transfer coefficient values increase until the spout-annulus interface and reaches to a peak point possibly by the virtue of increasing radial particle circulation and gas convection constitutively. On the other hand, there is a clear decline inside the spout zone. This type of heat transfer profiles was also reported by Zabrodsky and Mikhailik (1967) for 45º conical spouted beds with probe dimensions (35 mm long and 4 mm diameter) similar to this investigation. For 66º conical spouted bed, no peak was observed in the spout-annulus interface; instead, heat transfer coefficients decrease continuously from the spout axis to the wall-side. The difference between the trends inside the spout, probably originates from the hydrodynamic impact of the conical angle and the dimensional effect of the probe on the ascending gas and

particles' passage. Taking into account of the spout diameter, which is roughly $2D_o$, the probe occupies only around 5 % of the spout area in this research but a blockage of some particles is still inevitable. It should be also emphasized that insertion of the probe inside the spout results a decrease in the fountain height.

Analyzing the axial effect in 31º conical spouted bed; since the gas flow rate is the highest at the entrance and gradually decreases along the spout axis, the heat transfer coefficient in the spout has its maximum value in the lower section of the conical spouted bed. Although the solids hold-up is known to increase along the spout axis, which in turn is expected to augment the associated particle convection effect, the gas convection effect still dominates the heat transfer process in the spout (Sarı et al., 2012; Kulah et al., 2016).

On the other hand, the heat transfer coefficient values in the annulus part at Z_2 and Z_3 are fairly close to each other. This can be attributed to the counter-balancing effects of the particle and gas motions. While the particles descend, velocity in the annulus decreases with height more gas enters from the spout into the annulus section increasing the gas convection effect (Wang et al., 2009; Pianarosa et al., 2000; Mathur & Epstein, 1974). On the other hand, at the lowest position (Z_1) of the annulus region, the heat transfer coefficient is substantially higher than that in higher positions due to the increased local particle circulation.

Lifting up the position of the probe in 66º conical spouted bed, the heat transfer coefficient value increases both in the spout and annulus, which is consistent with 31° conical spouted bed results.

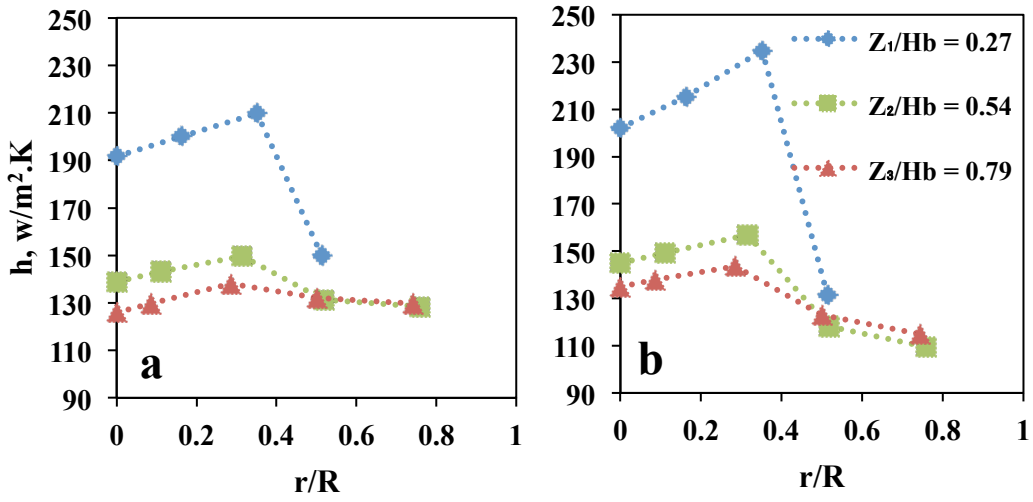

Figure 4.9 Effect of axial and radial positions on heat transfer coefficients for alumina particles (D_o = 15 mm, U_s/ $U_{ms,s}$ = 1.1, H_b = 235 mm, ϒ = 31°, (a) d_p = 1 mm, (b) d_p = 2 mm)

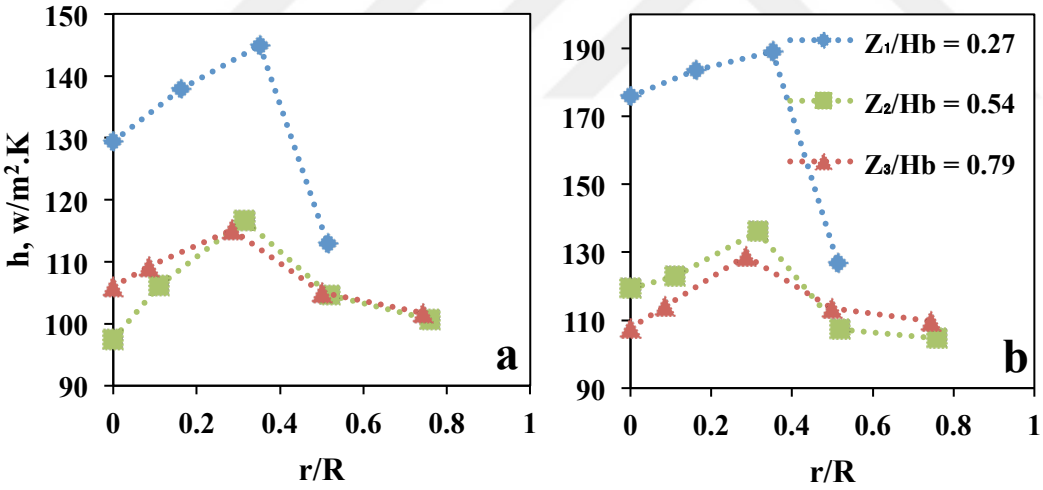

Figure 4.10 Effect of axial and radial positions on heat transfer coefficients for glass beads (D_o = 15 mm, $U_s/U_{ms,s}$ = 1.1, H_b = 235 mm, ϒ = 31°, (a) d_p = 1 mm, (b) d_p = 2 mm)

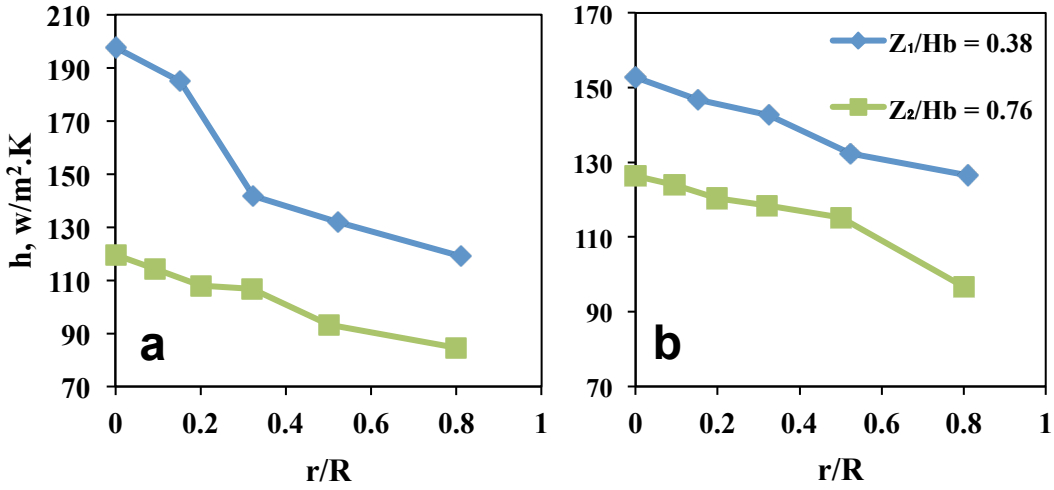

Figure 4.11 Effect of axial and radial positions on heat transfer coefficients (D_o = 15 mm, $U_s/U_{ms,s}$= 1.1, H_b = 144 mm, ϒ = 66º, (a) d_p = 2 mm, alumina particles (b) d_p = 1 mm, zirconia particles)

4.3.2 Effect of Static Bed Height (H_b)

Depending on the operational requirements, sometimes more materials need to be processed in the industrial applications. Loading more materials into the conical spouted beds basically needs higher gas flow rates due to increased minimum spouting velocity and causes higher bed pressure drop and relatively improved particle circulation rate till the conditions of maximum operational bed height (Mathur & Epstein, 1974; He et al., 2000; Spreutels et al., 2016; Kulah et al., 2016). **Figures 4.12** and **4.13** indicate that in the spout area, as the static bed height (H_b) increases the heat transfer coefficient rises considerably due to the dominant characteristics of gas flow rates over particle convection at the same measurement height. However, in the annulus section, heat transfer coefficients become closer to each other as seen in **Figures 4.12** and **4.13** since there is arguably no significant change in voidage, residence time of particles at the heater surface and gas velocity (Kulah et al., 2016; Senturk-Lule et al., 2015; San Jose et al., 2005a). Besides, Gbravcic et al. (1976) emphasizes that the variation of the gas velocities in the annulus is independent from H_b. One can also realize that alumina particles show

more salient trend than glass beads; an apparent increase can be observed as H_b goes up in **Figure 4.12**. This probably stems from the difference between particle circulation rates in each case at $1.1U_{ms,s}$ condition. In other words, the spouting quality marked by stability and particle circulation is more favourable for alumina particles at $1.1U_{ms,s}$.

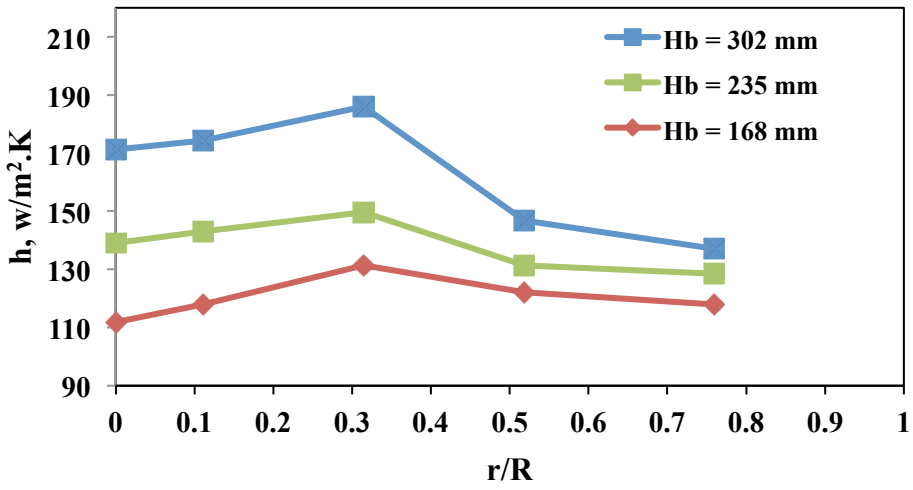

Figure 4.12 Effect of static bed height on radial profiles of h values for alumina particles (d_p = 1 mm, $U_s/U_{ms,s}$ = 1.1, D_o = 15 mm, Z_2 = 128 mm)

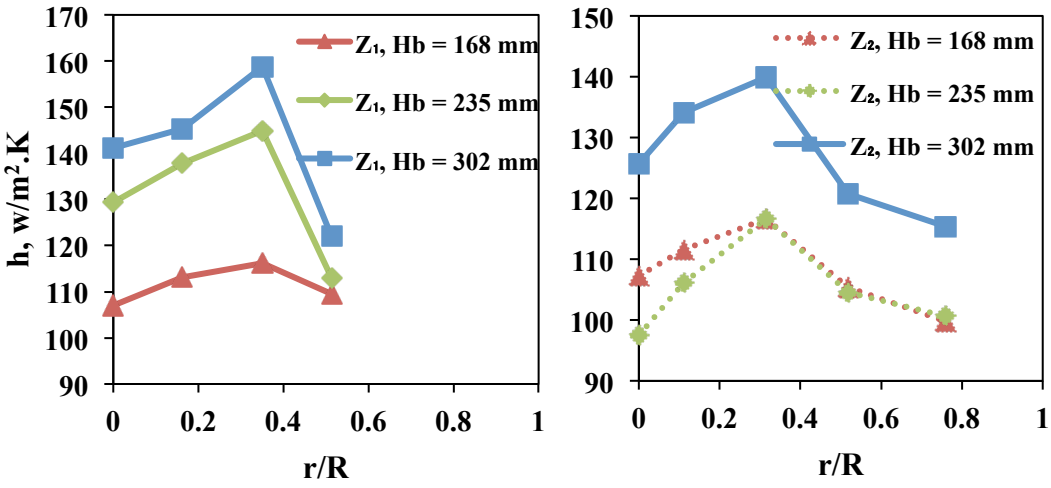

Figure 4.13 Effect of static bed height on radial profiles of h values for glass beads (d_p = 1 mm, $U_s/U_{ms,s}$= 1.1, D_o = 15 mm)

4.3.3 Effect of Inlet Diameter (D_o)

An increase in gas inlet diameter narrows down the annulus zone by enlarging the spout area and decreases the particle circulation rate (Spreutels et al, 2016; San Jose et al., 2005b). Three different inlet diameters (15, 19 and 24 mm) were used to investigate their effects on heat transfer coefficients for 66° conical spouted beds. The heat transfer coefficients in **Figure 4.14** for 66° conical spouted bed illustrate quite close heat transfer coefficients. Solely, the heat transfer coefficients with 15 mm inlet diameter are slightly separated from others. Macchi et al. (1999) also examined the effect of inlet diameter for 19, 26 and 38 mm inlet diameters in the cylindrical section of spouted bed and found that D_o does not affect heat transfer rates significantly. Furthermore, the average gas velocity and particle circulation rate does not change considerably for enlarged gas inlet diameters (Mathur & Epstein, 1974; Lim & Grace, 1987). Among the wall-to-bed heat transfer correlations, that of Uemaki and Kugo (1967) is the only one which considers the effect of D_o as Nu α $(D_o/d_p)^{0.2}$.

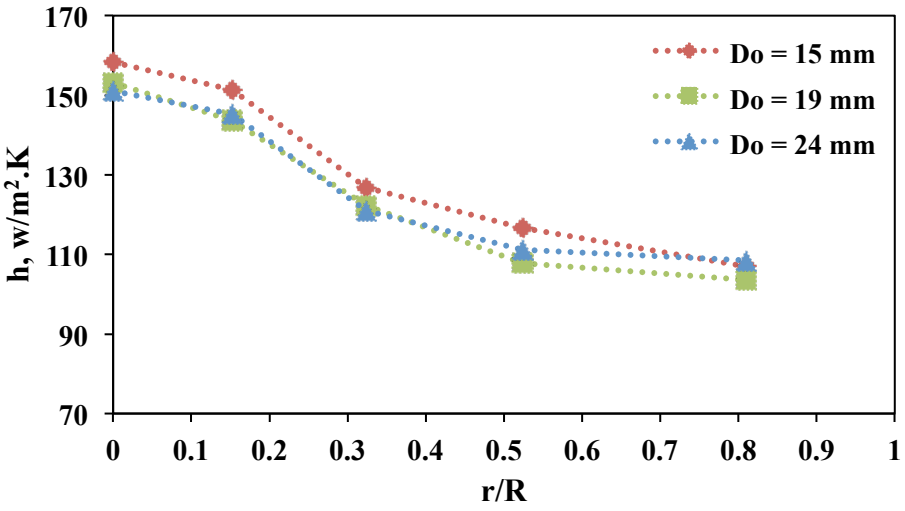

Figure 4.14 Effect of gas inlet diameter on radial profiles of h values for glass particles (d_p= 2 mm, $U_s/U_{ms,s}$= 1.1, Z_l/H_b = 0.38, H_b = 144 mm, Υ = 66º)

4.3.4 Effect of Spouting Gas Velocity (U_s)

The spouting gas velocity is the most important operating parameter for a spouted bed from hydrodynamics point of view. An increase in the supplied gas flow rate enhances the particle circulation rate and mixing but the average voidage in the annulus does not change considerably for a conventional cylindrical-conical spouted bed (Mathur & Epstein, 1974). From **Figures 4.15** and **4.16**, it can be seen that the heat transfer coefficient increases with gas velocity in the fixed bed regime due to increased gas convection effect and remains more or less constant after the point of minimum spouting both at the spout axis and in the annulus. To be in the safe side of the operation, the gas velocity below $1.1U_{ms,s}$ may entail a serious risk since the spouting action can break down easily for dense particles. Experimental observation has also supported this finding such that the immersed heater blocks some of the particles' passage inside the spout zone, especially in the lower part of the bed.

Beyond the minimum spouting velocity, change in the heat transfer coefficients is minimal both in the spout and annulus. The wall-to-bed heat transfer studies accept the superficial gas velocity as an ineffective parameter beyond U_{ms} as well (Klassen

& Gishler, 1958; Malek & Lu, 1964). On the other side, a close examination reveals that while heat transfer coefficients slightly drops down or remains almost stable in the spout area, it goes up slightly in the middle of annulus especially for alumina and glass bead particles. In the spout region, an increase in gas velocity is almost always accompanied by a decrease in solids-hold up, balancing the gas and particle convection effects. In the annulus, on the other hand, as the velocity is increased, gas passage from spout to annulus increases without significant change in the solids hold-up.

From **Figures 4.15** and **4.16**, it can also be deduced that the absolute value of the heat transfer coefficient is dependent on the particle density ($h_{ZIRCONIA}>h_{ALUMINA}>h_{GLASS}$) regardless of the particle thermal properties (k_p and C_p). Heavier particles have higher minimum spouting velocities, which lead to higher operating spouting gas flow rates (or velocities). Therefore, the gas convection effect is inherently more dominant in case of high-density particles.

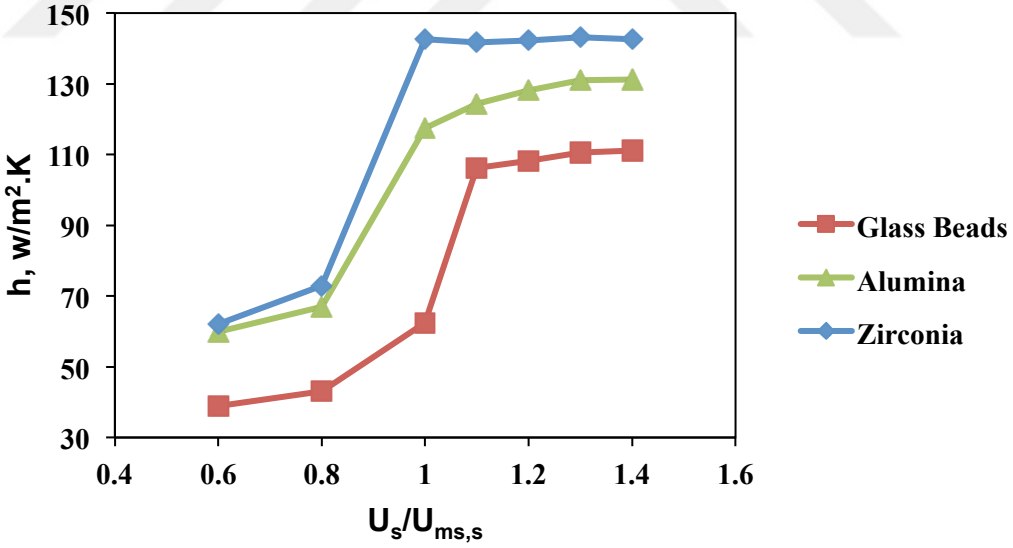

Figure 4.15 Effect of spouting gas velocity on heat transfer coefficients inside the annulus section (d_p = 1 mm, D_o = 15 mm, H_b = 168 mm, Z_2 = 128 mm, r/R = 0.5, Υ = 31°)

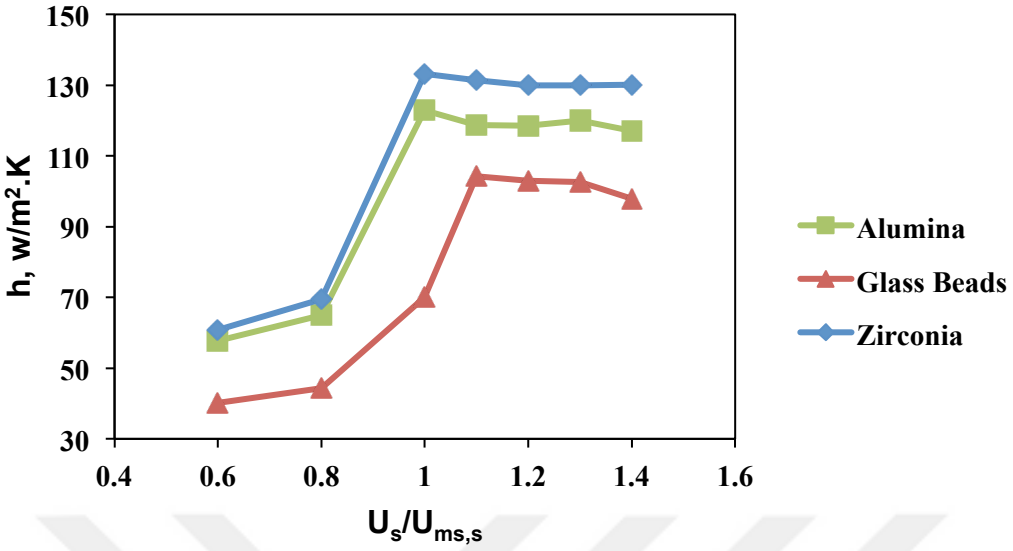

Figure 4.16 Effect of spouting gas velocity on heat transfer coefficients inside the spout section (d_p = 1 mm, D_o = 15 mm, H_b = 168 mm, Z_2 = 128 mm, r/R = 0, ϒ = 31°)

4.3.5 Effect of Particle Diameter (d_p)

In order to find out the effect of the particle diameter on the bed-to-surface heat transfer, experiments with 1 and 2 mm alumina and glass particles were carried out. **Figures 4.17** and **4.18** and **Table 4.11** collectively demonstrate that the heat transfer coefficient with 2 mm glass and alumina particles are always higher than that with 1 mm particles inside the spout region (defined as r/R = 0 - 0.2) regardless of the conical angle mainly due to higher gas flow rates used as the particle diameter increases at the same $U_s/U_{ms,s}$.

Going towards the wall-side, at the spout-annulus interface (defined as r/R = 0.3 - 0.35), heat transfer coefficient values for 1 and 2 mm particles follow the same trend as in the spout region as shown in **Table 4.12**. Thus, heat transfer coefficient values descend with decreasing d_p. The gas convection is thought to play a more dominant role in the heat transfer process.

Unlike to the spout and spout-annulus interface, 2 mm particles lose their advantage of higher gas flow rate in the annulus and particle convection becomes the main prevailing factor approaching to the wall-side. As far as the particle convection is concerned, a couple of important parameters can be quite important; thermal time constant (τ_p), particle velocity (v_p) and thermal contact resistance (R_p) created by particles on the heater surface. The calculated thermal time constants of the particles (based on Gloski et al., 1983) used in this work are quite close to each other with a same order of magnitude. Furthermore, it is also known that the particle velocities in the annulus region especially for high-density particles are very small (Kulah et al., 2016). Merely, one can underline the negative effect of particle contact resistance (R_p) on the heat transfer coefficient as the particle diameter enlarges (Baskakov et al., 1964; Botteril et al., 1986). Overall, no significant difference between the heat transfer coefficients for 1 mm and 2 mm particles was observed in the annulus region of both 31° and 66° conical spouted beds, especially at the higher axial locations as can be seen in **Table 4.13**.

The above findings are also consistent with the previous spouted bed studies, which indicate that as d_p decreases h also descends (Chatterjee et al., 1983; Zabrodsky & Mikhalik, 1967; Macchi et al, 1999; Klassen & Gishler, 1958; Malek & Lu, 1964). These studies assert that the larger particles create greater disturbances on the gas stream around the heater surface and have an improved particle circulation. On the other hand, for the bubbling fluidized bed applications, the dependency of the heat transfer coefficient on the particle diameter is just the opposite of the trend observed in spouted and conical spouted beds as suggested by Mickley and Fairbanks (1955).

Eventually, this issue cannot be resolved without the measurements of major heat transfer influences; void fraction (ε_w) and particle circulation rate over the heater surface and gas velocity distribution inside the annulus.

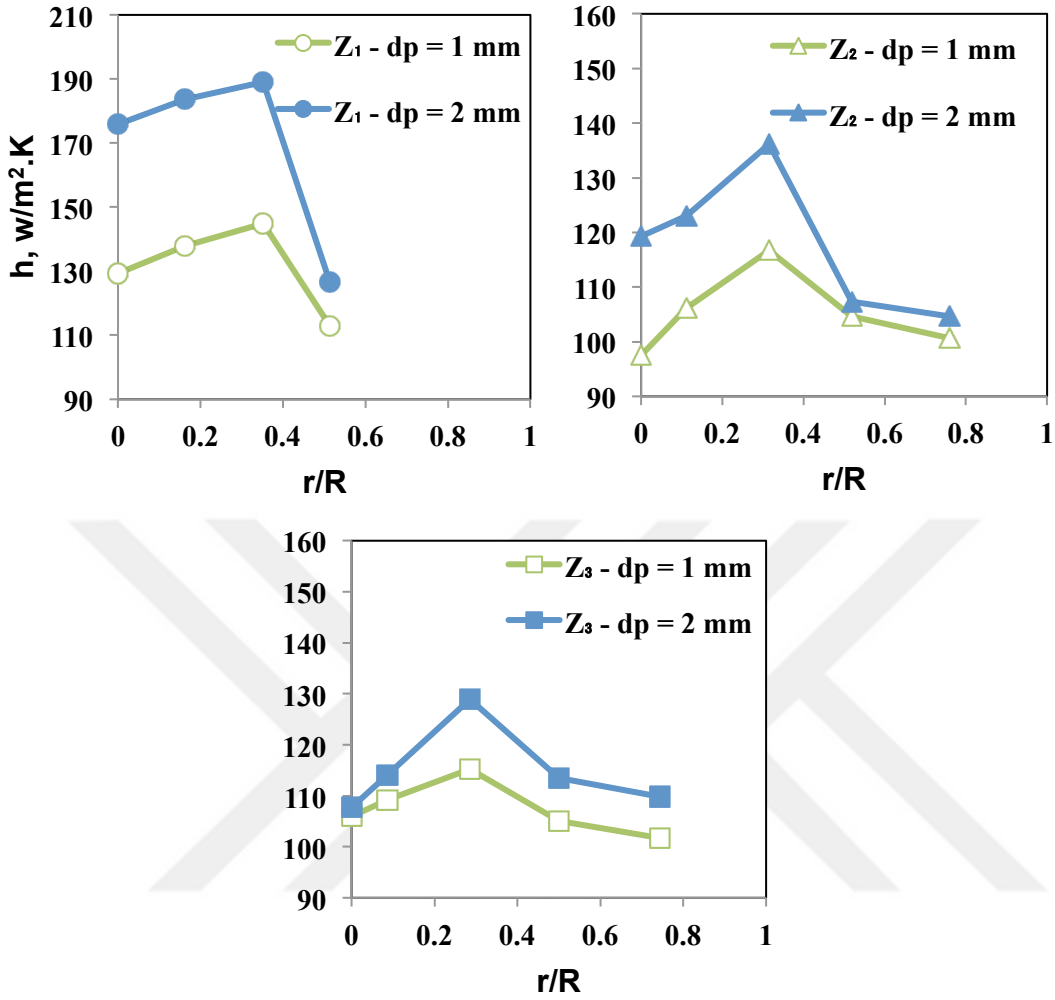

Figure 4.17 Effect of particle diameter on radial profiles of heat transfer coefficients for glass particles ($U_s/U_{ms,s}$ = 1.1, D_o = 15 mm, H_b = 235 mm, ϒ = 31°, $Z_{1,2,3}/H_b$ = 0.27, 0.54, 0.78)

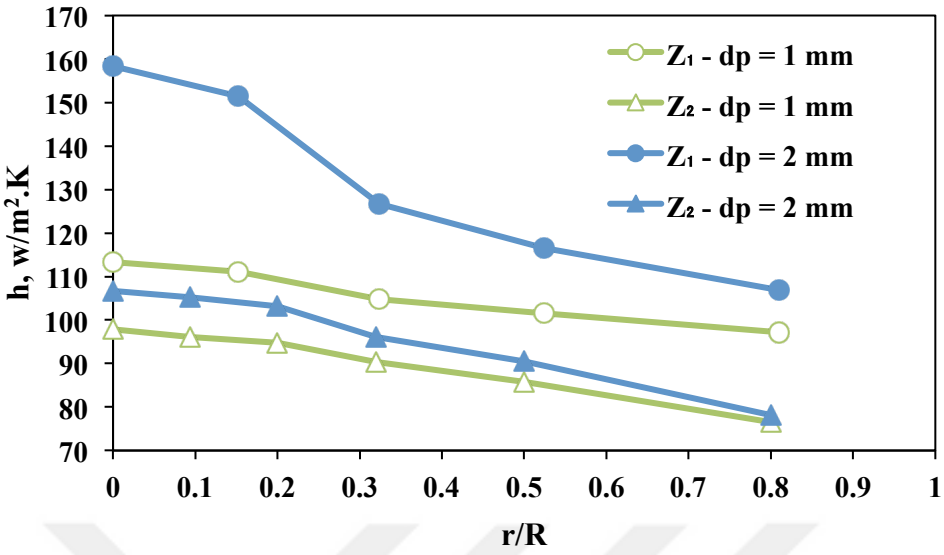

Figure 4.18 Effect of particle diameter on radial profiles of h values for glass particles ($U_s/U_{ms,s}$= 1.1, D_o = 15 mm, H_b = 144 mm, ϒ = 66º)

Table 4.11 Average heat transfer coefficients in the spout for 31º and 66º conical spouted beds ($H_{b,\,31^o}$ = 168 mm, $H_{b,\,66^o}$ = 144 mm)

			Heat transfer coefficients in the spout, W/m².K				
Axial Height	**H_b, mm**	**γ**	**Glass Beads (1 mm)**	**Glass Beads (2 mm)**	**Alumina (1 mm)**	**Alumina (2 mm)**	**Zirconia (1 mm)**
Z_1/H_b = 0.38	**168**	**31º**	110.1	131.7	130.1	145.9	154.0
	144	**66º**	108.0	154.9	146.4	191.3	149.8
Z_2/H_b = 0.76	**168**	**31º**	107.5	109.5	115.0	122.5	125.3
	144	**66º**	108.0	154.9	146.4	191.3	125.2

4.3.6 Effect of Conical Angle (γ)

In the conical spouted beds, the effect of conical angle (γ) can result in significant variations from a hydrodynamic aspect. Although they have similar performance in terms of minimum stable spouting gas flow rates ($G_{ms,s}$) and bed pressure drops (ΔP), especially dead zone problem in 66°, differences in gas distribution and particle velocities are some substantial points that should be urged upon. In the light of this information, **Figure 4.19** points out that while heat transfer coefficients go up monotonically starting from the wall side to the spout center in 66°, there is always a peak in the spout-annulus interface in 31° and a 5-15 % decline in heat transfer rates is beheld inside the spout areas. At this point, some distinctions should be revealed in 31° and 66° conical spouted beds; the effect of heat transfer probe over the gas distribution, cross-mixing behaviour of particles in the spout-annulus boundary and spout diameter. On the other hand, it is observed in **Table 4.11** that heat transfer coefficients in the annulus region of 31° conical spouted beds are greater than 66° conical spouted beds in general. Such a consequence can be more likely observed due to the higher particle circulation rate in 31° conical spouted beds. In the spout section, heat transfer coefficients are utterly dependent on spouting gas velocity (U_s) as can be investigated in **Table 4.11**.

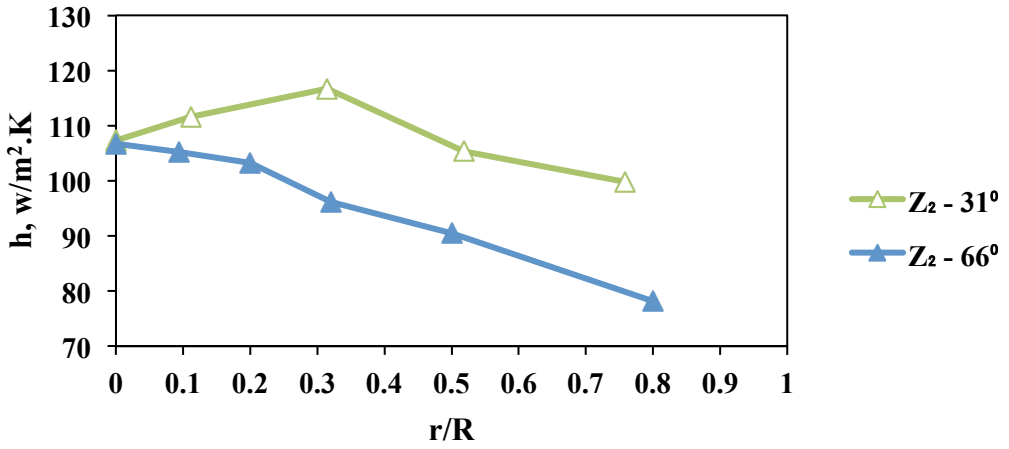

Figure 4.19 Effect of conical angle on radial profiles of heat transfer coefficients for glass particles (d_p = 2 mm, $U_s/U_{ms,s}$ = 1.1, D_o = 15 mm , Z_2/H_b = 0.76, $H_{b,\ 66^o}$ = 144 mm, $H_{b,\ 31^o}$ = 168 mm)

Table 4.12 Heat transfer coefficients in the spout-annulus interface for 31º and 66º conical spouted beds ($H_{b,\ 31^o}$ = 168 mm, $H_{b,\ 66^o}$ = 144 mm, * Jet Regime)

			Heat transfer coefficients in the spout-annulus boundary, W/m^2.K				
Axial Height	**H_b, mm**	**γ**	**Glass Beads (1 mm)**	**Glass Beads (2 mm)**	**Alumina (1 mm)**	**Alumina (2 mm)**	**Zirconia (1 mm)**
Z_1/H_b = 0.38	**168**	**31º**	116.1	139.0	139.9	158.0	187.9
	144	**66º**	104.8	126.7	130.6	141.8	142.6
Z_2/H_b = 0.76	**168**	**31º**	115.0	116.7	131.5	134.0	155.3
	144	**66º**	94.8	103.2	112.3	107.9*	120.4

Table 4.13 Average heat transfer coefficients in the annulus for 31º and 66º conical spouted beds ($H_{b,\,31^o}$ = 168 mm, $H_{b,\,66^o}$ = 144 mm, * Jet Regime)

			Average heat transfer coefficients in the annulus (r/R = 0.5 – 0.8), W/m^2.K				
Axial Height	**H_b, mm**	**γ**	**Glass Beads (1 mm)**	**Glass Beads (2 mm)**	**Alumina (1 mm)**	**Alumina (2 mm)**	**Zirconia (1 mm)**
Z_1/H_b = 0.38	**168**	**31º**	109.6	110.7	119.7	120.8	147.9
	144	**66º**	99.4	111.8	118.4	125.5	94.8
Z_2/H_b = 0.76	**168**	**31º**	101.1	102.6	120.1	112.9	132.7
	144	**66º**	84.2	88.2	99.6	94.8*	110.2

4.3.7 Effect of Fluidizing Gas Flow (G_f) – Spout-Fluid Operation

Effect of fluidizing gas (G_f) on the heat transfer characteristics in the conical spouted beds is one of the points, which is not investigated in the literature before. The introduction of the fluidization gas changes the reactor type from conical spouted bed to conical spout-fluid bed. It is mentioned that by the introduction of G_f through the conical walls, dead zones and agglomeration problems in reactor applications can be minimized, and better gas-solid contact can be potentially provided. Within this scope, the effect of G_f in the conical spouted beds was studied out by choosing two different gas flow rates and identifying them as “minimum” and “maximum”. In the spout-fluid bed operation, it is known that the introduction of the fluidizing gas decreases the minimum stable spouting velocities. In this context, the minimum fluidizing gas flow rate was decided as the first point at which G_f is lowered distinctly as the fluidization gas velocity is gradually increased. On the other side, the

maximum fluidizing gas flow rate was chosen based on a couple of criteria; spouting stability should not be affected, bubble formation in the annulus should not be observed, and G_f should be comparable to the spouting gas flow rate (G_T) ($G_f/G_T \approx 0.5$).

The hydrodynamic results in **Figure 4.20** show that the minimum stable spouting gas flow rate (G_{mss}) decreases as the fluidizing gas flow rate (G_f) increases, and additionally, the effect of G_f on the decrease of G_{mss} was found to be more significant for high density particles (alumina and zirconia) compared to glass beads, both in 31º and 66º conical spouted beds.

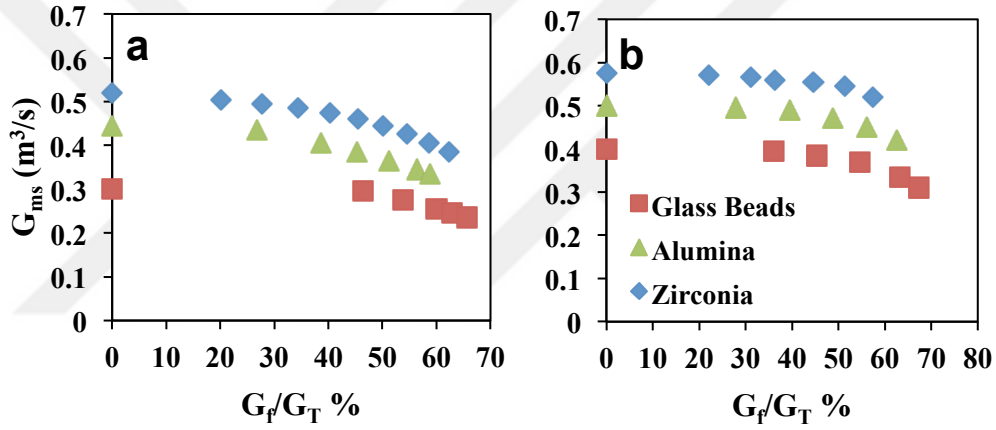

Figure 4.20 Effect of fluidizing gas (G_f) on the minimum stable spouting flow rates ($G_{ms,s}$) (d_p = 1 mm, D_o = 15 mm, (a) Υ = 31º, (b) Υ = 66º)

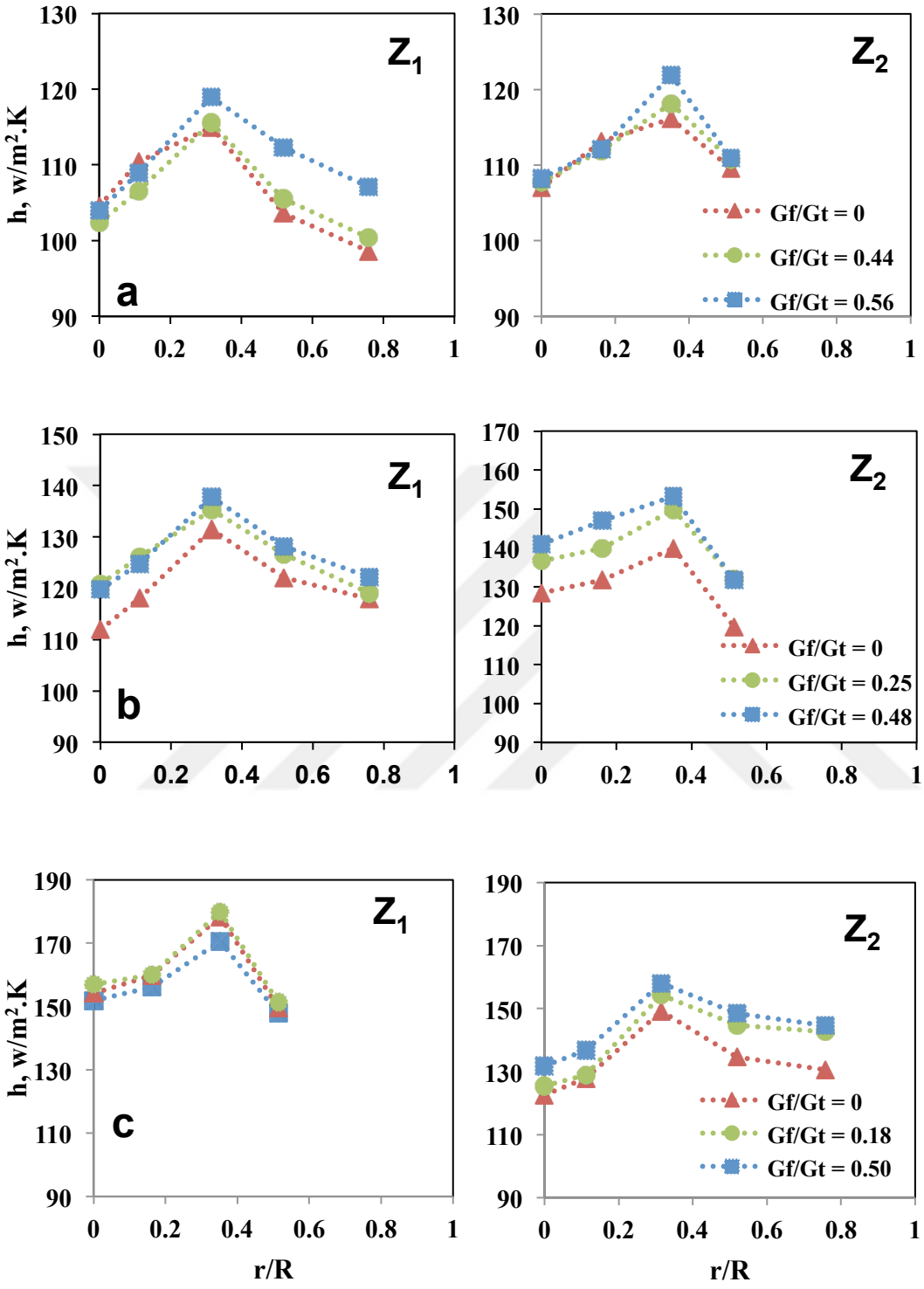

Figure 4.21 Effect of fluidizing gas (G_f) on the heat transfer coefficients (d_p = 1 mm, D_o = 15 mm, H_b = 168 mm, Υ = 31°, (a) glass (b) alumina (c) zirconia)

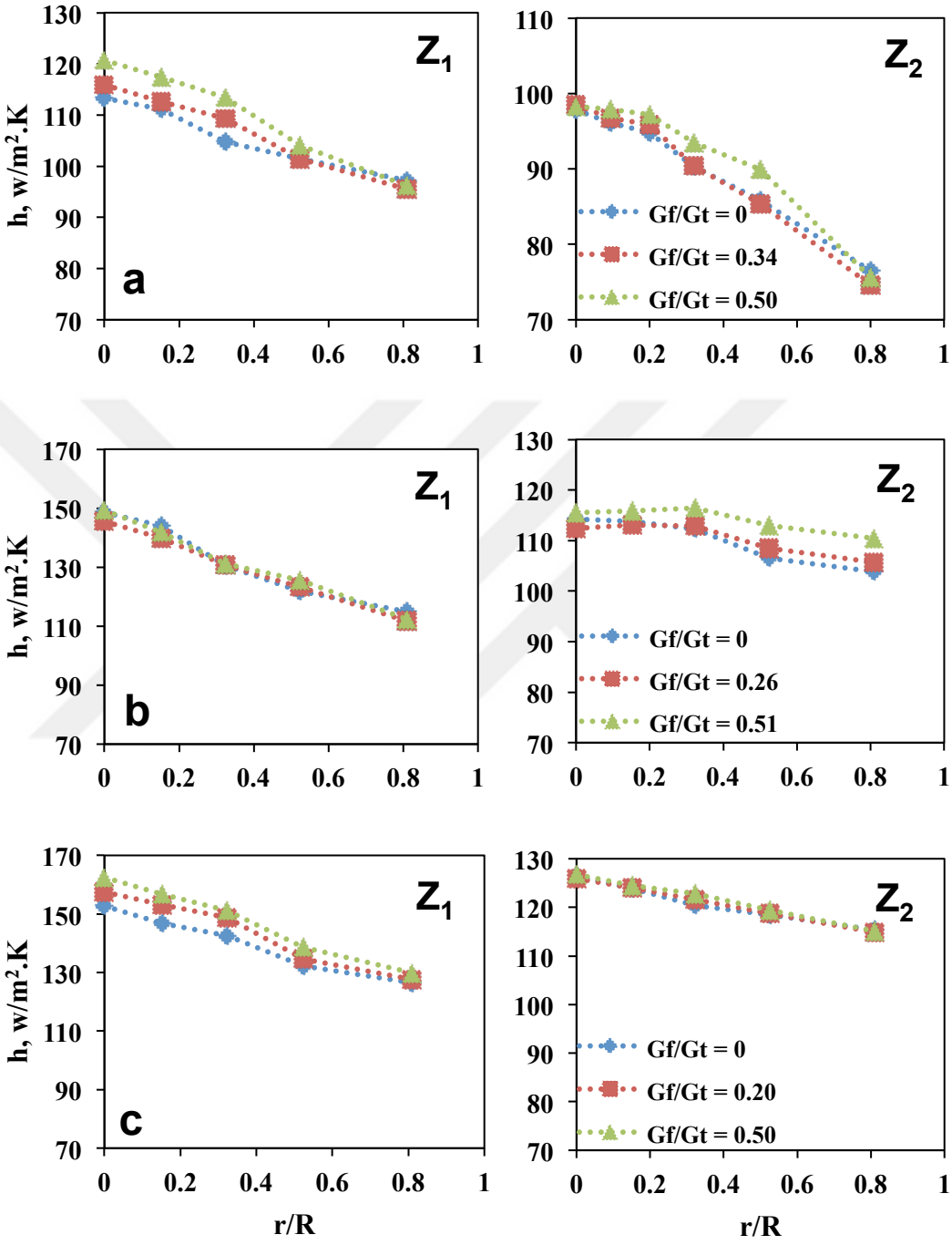

Figure 4.22 Effect of fluidizing gas (G_f) on the heat transfer coefficients (d_p = 1 mm, D_o = 15 mm, H_b = 144 mm, ϒ = 66º, (a) glass (b) alumina (c) zirconia)

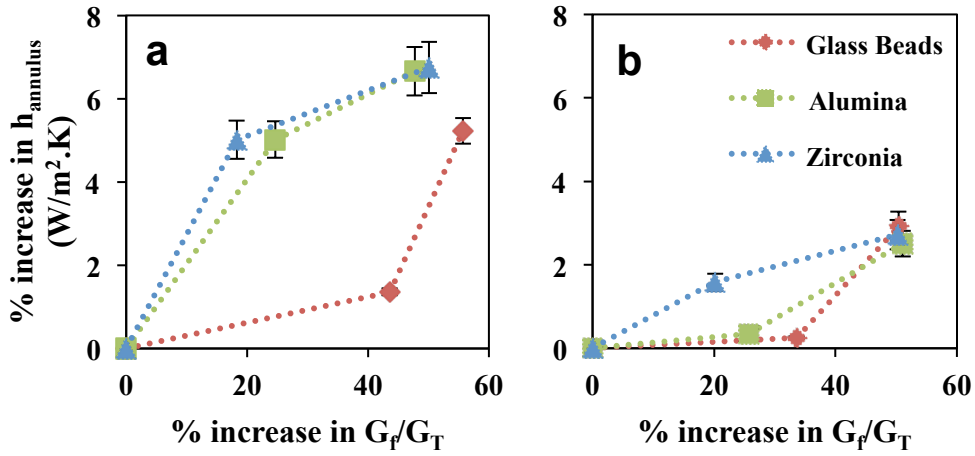

Figure 4.23 Effect of fluidizing gas (G_f) on the average heat transfer coefficients in the annulus (d_p = 1 mm, D_o = 15 mm, (a) Υ = 31º, (b) Υ = 66º)

From the heat transfer point of view, in **Figure 4.21-4.23**, benefits of the spout-fluid operation on the heat transfer in the whole annulus region were found fairly minor showing 7 and 3 % maximum increments for 31º and 66º conical angle conical spouted beds, respectively. One of the reasons for low heat transfer impact can be due to insufficient fluidizing gas penetrating through the annulus. In order to check this, horizontal jet penetration lengths were calculated using two correlations developed by Benjelloun (1991) and Yates et al. (1991). The details of these calculations are given in Appendix D. As can be seen in Appendix D the calculated horizontal jet penetration length is less than 15 mm. Furthermore, the effect of G_f on heat transfer is more dominant at the lower flow rates especially for high-density particles.

In **Figure 4.23**, it is seen that per cent increase in the average heat transfer coefficients in the annulus section of 31º and 66º conical angle conical spouted beds reach almost maximum values at around 50 % ($G_f \approx G_s$) for alumina and zirconia particles, whereas it seems that average heat transfer rate in the annulus section can be still improved for glass beads by introducing more G_f. Relative standard

deviations were also indicated as error bars, and increase with G_f/G_T ratio but their range is still small.

4.4 Overall Bed-to-Surface Heat Transfer Correlation

The heat transfer data obtained in this investigation was used in order to propose a new correlation for high-density particles for the annulus section. The annulus section is especially critical for the placement of the heat transfer surfaces in the actual reactor operation. By this means, wall or immersed vertical tube to spouted bed heat transfer correlations, summarized in **Table 2.3**, were evaluated. Since the previous correlations were not developed for high-density particles (> 2600 kg/m^3), there is a considerable deviation between the experimental results and correlation predictions as observed in **Figure 4.24**. Amongst all correlations, Uemaki and Kugo (1967) and Macchi et al. (1999) resulted in more accurate predictions. Therefore, it is decided that the original correlation proposed by Uemaki and Kugo (1967) be modified based on the experimental data obtained in this work. While the term with inlet diameter (D_o) used in the original correlation was omitted (since the effect of inlet diameter was found to be insignificant), the effect of conical angle was added to the new correlation. Other than these, no terms were changed; the modification is based only on altering the coefficients of the non-dimensional parameters used in the original correlation.

Utilizing a non-linear regression analysis, a new revised form of Uemaki and Kugo's empirical correlation is proposed as follows for the average Nusselt number in the annulus;

$$Nu = 0.0017\left(\frac{U_S d_p \rho_g}{\mu_g}\right)^{0.4134}\left(\frac{g d_p{}^3 \rho_g{}^2}{\mu_g{}^2}\right)^{0.0954}\left(\frac{\rho_p C_p}{\rho_g C_g}\right)^{0.5991}\left(\tan\frac{\gamma}{2}\right)^{-0.2136}\left(1-\varepsilon_p\right) \quad (4.2)$$

The proposed correlation is applicable for the whole annulus region as an average value, and has a very good fit with the experimental Nu values by less than 15 % deviation as shown in **Figure 4.24.**

Investigating the proposed correlation, it is seen that the leading parameters are composed of the volumetric heat capacity ($\rho_p C_p$) and Re_p. This implies that the spouting flow rate (G_{ms}) is, either directly by gas convection or indirectly by increasing the particle circulation rate, quite effective on the total heat transfer coefficients. On the other side, rather than the particle conductivity (k_p), the heat capacity of particle volume is more significant. This is basically due to higher contact resistances of spherical particles (R_p) in contact with surface. In addition, an increase of the conical angle negatively influences heat transfer coefficients in the annulus part.

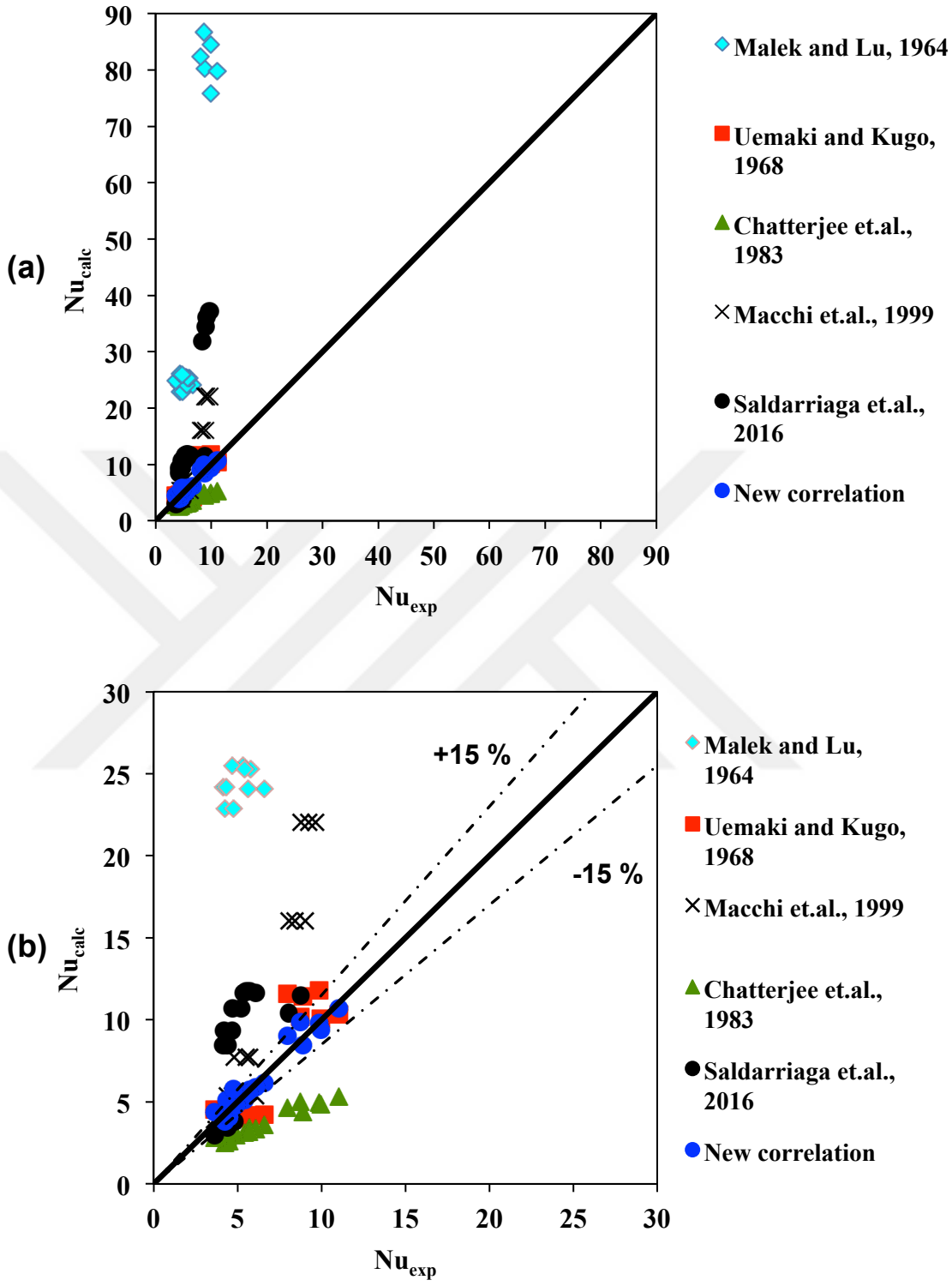

Figure 4.24 Comparison between experimental and calculated values of Nu (Correlations are given in Table 2.3, (a) axes range for Nu: 0-90 (b) magnified axes, Nu: 0-30)

CHAPTER 5

CONCLUSIONS

In this thesis, the radial and axial variation of the bed-to-surface heat transfer in conical spout and spout-fluid beds was experimentally investigated using high-density particles. A special heat transfer probe was designed, manufactured and tested for heat transfer measurements. The experiments were carried out in conical spouted and spout-fluid beds with 25 cm ID cylindrical section at two different conical angles (31° and 66°). In the experiments, the effects of bed design parameters (such as conical angle and inlet diameter of spouting gas entrance) and operating conditions (such as static bed height, particle size and density and spouting and fluidization gas flow rates) on the heat transfer characteristics were investigated in detail. An empirical heat transfer correlation for the average heat transfer coefficient in the annulus section for high-density particles ($2500 \leq \rho_p \leq 6000$ kg/m^3) was also proposed. The main conclusions and suggestions for future work are presented in the following sections.

5.1 Bed-to-Surface Heat Transfer

Local time-average heat transfer coefficients between the vertically placed heat transfer probe and the conical spouted bed were measured both in the annulus and spout regions. For all particles tested, the range of the heat transfer coefficients was found to be between 70 and 210 W/m^{2}K. The radial variation of the heat transfer coefficient shows a dependency on the conical angle; moving from wall to the spout axis, in 31° bed a peak value is observed at the spout-annulus interface whereas in 66° bed the heat transfer coefficient monotonically increases from the wall to the

spout axis. The gas inlet diameter does not play a significant role in the value of the heat transfer coefficient.

As far as the effects of the operational parameters are concerned, the results indicate that as the static bed height (H_b) is increased, the heat transfer coefficient also increases under the improved particle circulation rate and gas convection. The heat transfer coefficient increases with the spouting gas velocity up to 1.1 – 1.2 U_{ms}, beyond which no significant change is observed regardless of the particle type. Furthermore, the absolute values of the heat transfer coefficient depend on the particles density and size at the same $U_s/U_{ms,s}$. The denser and larger particles have higher minimum stable spouting velocities, which in turn lead to higher operational spouting velocities resulting in higher heat transfer coefficient values. The effect of particle diameter is more pronounced in the spout and spout-annulus interface whereas its effect diminishes in the annulus region. Overall, it can be proposed that the gas convection plays a major role in the heat transfer process.

The conical angle significantly affects the gas flow distribution and particle-probe contact dynamics in the bed and the results should be elaborated carefully with the required measurements (particle concentration, particle and gas velocities) to have more definitive conclusions. However, it is observed that the heat transfer values in the annulus decrease as the conical angle is widened due to lowered particle circulation. Moreover, placing the heater in the lower position produces higher heat transfer rates due to the increase in particle circulation, concentration and local gas velocities, presumably.

Results of spout-fluid operation shows that fluidizing gas provides a minor enhancement on the overall heat transfer rates. This behaviour can be explained by the jet penetration length of gas flow on the conical walls such that fluidizing gas does not penetrate sufficiently inside the bed to maintain an effective gas flow on the heat transfer surface. Therefore, from the heat transfer point of view, given the

required flow rates for spout-fluid bed operation, spout beds are more advantageous compared to spout-fluid beds.

In the light of the observed values of heat transfer coefficient inside the annulus and spout areas, the proper location of the cylindrical heater is just the surrounding space of the spout in the annulus region (spout-annulus interface). Hence, a spiral shape heat transfer surface around the spout can be a promising design fulfilling the duty of a draft-tube as well.

Since all bed-to-surface heat transfer correlations available in the literature for conical spouted beds were developed for relatively light particles ($\rho_p < 2600$ kg/m^3), they were not satisfactory enough to predict the experimental data produced in this work. Therefore, on the account of practical usage, the correlation of Uemaki and Kugo (1967) was modified for conical spouted beds operated with high density particles and the resulting new correlation was able to predict the average heat transfer coefficients inside the annulus region with reasonable accuracy (< 15% error).

5.2 Suggestions for Future Work

This study filled a significant gap in the literature and led to several ideas for future work. In the current study, the heat transfer measurements were only taken with the probe placed vertically since its effect on the gas-solid flow is minimal compared to horizontal case and it is easier to implement. However, the heat transfer coefficient certainly depends on the position of the heater with respect to gas-solid flow. Therefore, it is recommended that horizontal placement of the cylindrical heater as well as other various heater geometries (plate and sphere) are studied.

Lastly, the range of the particle size can be broadened. In this way, the effect of particle size can be studied in a wider range, such as between 0.5 mm to 3 mm. Particle diameter less than 1 mm may exhibit different trends in comparison larger particles.

REFERENCES

Bacelos, M.S., Camargo, C.F.S., Silveira, A.M., & Freire, J.T. (2011). Local heat-transfer coefficient of immersed cylindrical surface in fluidized and vibrated fluidized beds. Chem. Eng. Process Intensification, 50, 1152-1159.

Baskakov, A.P. (1964). The mechanism of heat transfer between a fluidized bed and a surface.Int. Chem. Eng., 4, 320–324.

Benjelloun, F.V.J. (1991). Determination des longueurs de jets de gaz horizontaux dans des lits fluidises, textes des communications presentees a l'occasion des 6emes journees europeenenes sur la fluidisation, Toulouse, Laguerie, C. G., P., Ed.

Berghel, J. (2007). The gas-to-particle heat transfer and hydrodynamics in spouted bed drying of sawdust. Drying Tech., 23, 1027-1041.

Botterill, J. S. M. (1986). Fluid bed heat transfer in Gas fluidization technology. New York: Wiley.

Brich, M.A., Ganzha, V.L., & Saxena, S.C. (1997). On the design of heat transfer probes. Int. C. Heat Mass Trans., 24, 151-159.

Chatterjee, A. (1970). Spout-fluid bed technique. Ind. Eng. Chem. Process Des. *Dev.*, *9* (2), 340–341.

Chatterjee, A. R. R., Adusumilli, S., & Deshmukh, A.V. (1983). Wall-to-bed heat transfer characteristics of spouted-fluid beds. Can. J. Chem. Eng., 61, 390–397.

Choi, M. & Meisen, A. (1992). Hydrodynamics of shallow, conical spouted beds. Can. J. Chem. Eng., 70, 916–924.

Churchill, S.W., & Bernstein, M. (1977). A correlating equation for forced convection from gases and liquids to a circular cylinder in crossflow. J. Heat Transf. (Trans. ASME), 99, 300–306.

Churchill, S. W., & Chu, H. H.-S., (1975). Correlating equations for laminar and turbulent free convection from a horizontal cylinder. International Journal of Heat and Mass Transfer, Vol. 18, 1049-1053.

Epstein, N., & Grace, J.R. (2011). Spouted and spout-fluid beds: Fundamentals and applications. New York: Cambridge University Press.

Epstein, N., & Mathur, K.B. (1971). Heat and mass transfer in spouted beds – a review. Can. J. Chem. Eng., 49, 467–476.

Fand, R. M. (1965). Heat Transfer by Forced convection from a cylinder to water in crossflow. International Journal of Heat and Mass Transfer, 8, 995-1010.

Fand, R., Morris, E., & Lum, M. (1977). Natural convection heat transfer from horizontal cylinders to air, water, and silicone oils for Rayleigh numbers between 3 × 102 and 2 × 107. Int J Heat Mass Transf 20, 1173–1184.

Fujii, T., Fujii, M., & Matsunaga, T. (1979). A numerical analysis of laminar free convection around an isothermal horizontal circular cylinder. Numer Heat Transf 2, 329–344.

Gloski, D., Glicksman, L., & Decker, N. (1983). Thermal resistance at a surface in contact with fluidized bed particles. Int. J. Heat Mass Transfer, 27, 599-610.

Grbavcic, Z.B., Vukovic, D.V., Zdanski, F.K., & Littman, H. (1976). Fluid flow pattern, minimum spouting velocity and pressure drop in spouted beds. Can. J. Chem. Eng., 54, 33-42.

He, Y-L., Jim, C., & Grace J.R. (2000). Pressure gradients, voidage and gas flow in the annulus of spouted bed. Can. J. Chem. Eng., 78, 161-167.

Kılkış, B., & Kakaç, S. (1991). Heat and mass transfer in spouted beds, in:Kakaç, S., Kilkis, B., Kulacki, F.A. (Eds.), Convective Heat and Mass Transfer in Porous Media, Kluwel Academic Publishers, 1031-1059.

Kim, S.W., & Kim, S.D. (2013). Heat transfer characteristics in a pressurized fluidized bed of fine particles with immersed horizontal tube bundle. Int. J. Heat Mass Transfer, 64, 269-277.

Klassen, J., & Gisher, P.E. (1958). Heat transfer from column wall to bed in spouted, fluidized and packed systems. Can. J. Chem. Eng., 36, 12-18.

Klimenko, Y.G., Karpenko, V.G., & Rabinovich, M.I. (1969). Heat exchange between the spouting bed and the surface of a spherical probe element. Heat Physics and Technology, 15, 81-84.

Kramers, H. (1946). Heat transfer from spheres to flowing media, Physica 12, 61–80.

Kuehn, T., & Goldstein, R. (1976). Correlating equations for natural convection heat transfer between horizontal circular cylinders. Int J Heat Mass Transf 19, 1127–1134.

Kucharski, J. & A. Kmiec. (1983). Hydrodynamics, Heat and MassTransfer During Coating of Tablets in a Spouted Bed. Can. J.Chem. Eng. 61, 435–439.

Kulah G., Sarı S., & Koksal M. (2016). Particle velocity, solids hold-up, and solids flux distribution in conical spouted beds operating with heavy particles. Ing. Eng. Chem. Res., 55, 3131-3138.

Kunii, D., & Levenspiel, O. (1991). Fluidization engineering, 2nd ed. New York: John Wiley and Sons.

Kunii, D., & Smith, J.M. (1960). Heat transfer characteristic of porous rocks. AIChE, 6, 71-78.

Lule, S.S., Colak, U., Koksal, M., & Kulah, G. (2015). CFD simulations of hydrodynamics of conical spouted bed nuclear fuel coaters. Chem. Vap. Deposition, 21, 122-132.

Lim, C.J., & Grace, J. (1987). Spouted bed hydrodynamics in a 0.91 m diameter vessel. Can. J. Chem. Eng., 65, 366-372.

Lopez, G., Olazar, M., Aguado, R., Elordi, G., Amutio, M., & Artetxe, M. (2010). Vacuumpyrolysis of waste tires by continuously feeding into a conical spouted bed reactor. Ind. Eng. Chem. Res. 49, 8990–8997.

Macchi, A., Bi, H.T., Legros, R., & Chaouki, J. (1999). An investigation of heat transfer from a vertical tube in a spouted bed. Can. J. Chem. Eng., 77, 45-53.

Makibar, J., Fernandez-Akarregi, A.R., Alava, I., Cueva, F., Lopez, G., & Olazar, M. (2011). Investigations on heat transfer and hydrodynamics under pyrolysis conditions of a pilot-plant draft tube conical spouted bed reactor. Chemical Engineering and Processing:Process Intensification, 50, 790-798.

Malek, M.A., & Lu, B.C.Y. (1964). Heat transfer in spouted beds. Can. J. Chem. Eng., 42, 14-20.

Mathur, K.B.,& Epstein, N. (1974). Spouted beds. New York: Academic Press.

Mickley, H.S., & Fairbanks, D.F. (1955). Mechanism of heat transfer to fluidized beds. AIChE, 1, 374-384.

Olazar, M.J., Jose, S., & Bilbao, J. (2011). Conical spouted beds, in: N. Epstein, J.R. Grace (Eds.), Spouted and Spout-fluid Beds: Fundamentals and Applications, Cambridge University Press, 82–104.

Olazar, M., San Jose, M.J., Aguayo, A.T., Arandes, J.M., & Bilbao, J. (1992). Stable operation conditions for gas-solid contact regimes in conical spouted beds. Ind. Eng. Chem. Res., 31, 1784–1791.

Ozkaynak, T.F., & Chen, J.C. (1980). Emulsion phase residence time and its heat transfer models in fluidized beds. AIChE, 26, 544-550.

Passos, M.L., Massarani, G., Freire, J.T., & Mujumdar, A.S. (1997). Drying of pastes in spouted beds of inert particles: design criteria and modelling, Dry. Technol. 15, 605–624.

Perkins, H. C., & Leppert, G. (1962). Forced Convection Heat Transfer From a Uniformly Heated Cylinder. J. Heat Transfer, Trans. ASME, Series C, 84, 257-263.

Pianarosa, L.D., Freitas, L.A.P., Lim C.J., & Grace, J.R. (2000). Voidage and particle profiles in a spout-fluid bed. Can. J. Chem. Eng., 78, 132-142.

Saldarriaga, J.F., Grace, J., Lim, C.J., Wang, Z., Xu, N., Atxutegi, A., Aguado, R., & Olazar, M. (2015). Bed-to-surface heat transfer in conical spouted beds of biomass-sand mixtures. Powder Technology, 283, 447-454.

San Jose, M. J., Olazar, M., Alvarez, S., Morales, A., & Bilbao, J. (2005a). Local porosity in conical spouted beds consisting of solids of varying density. Chem. Eng. Sci., 60, 2017-2025.

San Jose, M. J., Olazar, M., Alvarez, S., Morales, A., & Bilbao, J. (2005b). Spout and fountain geometry in conical spouted beds consisting of solids of varying density. Chem. Eng. Sci., 44, 193-200.

Sanitjai, S., & Goldstein, R.J. (2004). Forced convection heat transfer from a circular cylinder in crossflow to air and liquids. International Journal of Heat and Mass Transfer, 47, 4795-4805.

Sarı, S., Kulah, G., & Koksal, M. (2012). Characterization of gas solid flow in conical spouted beds operating with heavy particles. Experimental and Thermal Fluid Science, 40, 132-139.

Spreutels L., Haut B., Legros R., Bertrand F., & Chaouki J. (2015). Experimental investigation of solid particles flow in a conical spouted bed using radioactive particle tracking. AIChE, 62, 26-37.

Uemaki, O., & Kugo, M. (1967). Heat transfer in spouted beds. Kagaku Kogaku, 31, 348-353.

Vahlas, C., Juarez, F., Feurer, R., Serp, P., & Caussat, B. (2002). Fluidization, spouting, and metal–organic CVD of platinum group metals on powders, Chem. Vap. Depos., 8,
127–144.

Yagi, S., & Kunii, D. (1960). Studies on heat transfer near wall surface in packed beds. AIChE, 6, 97-103.

Yagi, S., & Wakao, N. (1959). Heat and mass transfer from wall to fluid in packed beds. AIChE, 79-85.

Yao, X., Zhang, Y., & Lu, C. (2014). Systematic study on heat transfer and surface hydrodynamics of a vertical heat tube in a fluidized bed of fcc paticles. AIChE, 61, 68-83.

Yates, J.G., Cobbinah, S.S., & Cheesman, D.J. (1991). Particle attrition in fluidized beds containing opposing jets. AIChE Symp. Series, 87, 13-19.

Wang, Z., Bi, H.T., & Lim, C.J. (2009). Measurements of local flow structures of conical spouted beds by optical fibre probes. Can. J. Chem. Eng., 87, 264-273.

Whitaker, S. (1972). Forced convection heat transfer correlations for flow in pipes, past flat plates, single cylinders, single spheres, and for flow in packed beds and tube bundles. AIChE J. 18, 361–371.

Zabrodsky, S.S.,& Mikhalik, V.D. (1967). The heat exchange of the spouting bed with a submerged heating surface. In Intensification of Transfer of Heat and Mass in Drying and Thermal Processes, Minsk, BSSR: Nauka i Technika, 130–137.

Zhang, D.,& Koksal, M. (2006). Heat transfer in a pulsed bubbling fluidized bed. Powder Technology, 168, 21-31.

Zukauskas, A.,& Ziugzda, J. (1985). Heat transfer of a cylinder in crossflow.Washington: Hemishere Pub.

APPENDICES

APPENDIX A

REPRODUCIBILITY AND UNCERTAINTY OF HEAT TRANSFER DATA

A.1 Reproducibility of Heat Transfer Measurements

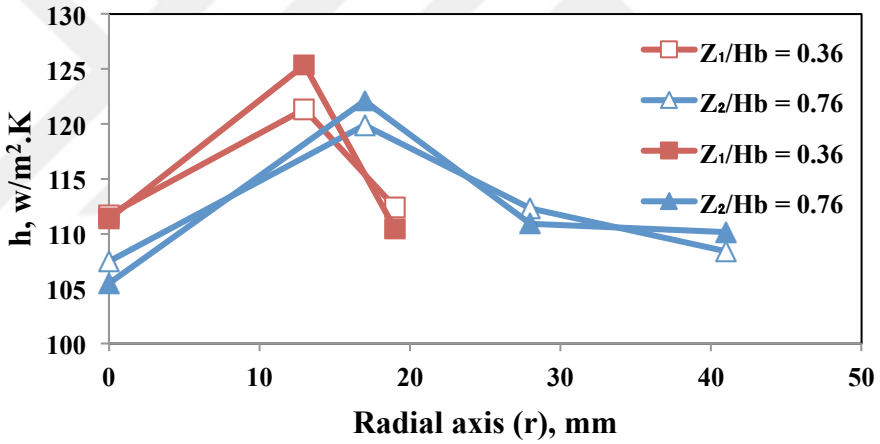

Figure A.1 Reproducibility of heat transfer profiles for glass beads (d_p = 1 mm, H_b = 168 mm, $U_s/U_{ms,s}$ = 1.1)

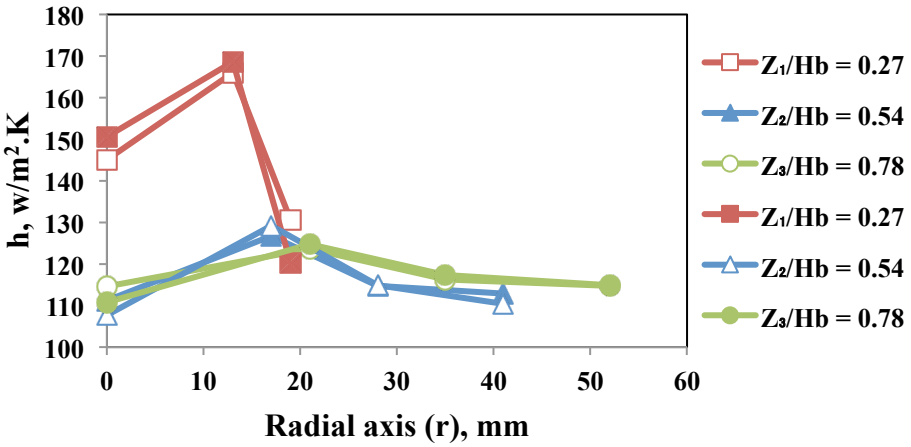

Figure A.2 Reproducibility of heat transfer profiles for glass beads (d_p = 1 mm, H_b = 235 mm, $U_s/U_{ms,s}$ = 1.1, γ = 31°)

A.2 Uncertainty of Heat Transfer Measurements

Table A.1 Uncertainty of heat transfer measurements taken from different days for glass beads (d_p = 2 mm, H_b = 168 mm, $U_s/U_{ms,s}$ = 1.1, γ = 31°, r/R = 0.5, Z_2/H_b = 0.76)

#	Date	h, W/m².K
1	**12/11/2016**	105.35
2	**28/12.2016**	105.65
3	**29/12/2016**	105.76
4	**30/12.2016**	106.91
5	**2/1/2017**	108.16
6	**4/1/2017**	106.14
7	**5/1/2017**	106.34
8	**6/1/2017**	105.72
9	**10/1/2017**	106.32
10	**15/1/2017**	105.31
	Average:	**106.17**
	Standard deviation:	**0.86**
	Relative uncertainty, %	**1.76**

Table A.2 Uncertainty of power supply (P)

P = VxI	
Amper, I	0.45 +/- 0.004 amper
Voltage, V	7.79 +/- 0.004 volts
Relative uncertainty, %	**0.9**

Table A.3 Uncertainty of surface area of the probe (A)

A = 2πrL	
Radius, r	7 +/- 0.1 mm
Length, L	26 +/- 0.1 mm
Relative uncertainty, %	**1.5**

Therefore, the total uncertainty of heat transfer measurements is about **2.5 %**.

APPENDIX B

HEAT LOSSES OF THE PROBE

B.1 Calculation of Heat Losses from Heat Transfer Probe

Heat loss of the probe was simply measured from the tip section as drawn in **Figure B.1**. During the measurement, supplied power (P) was **1.805 Watts**.

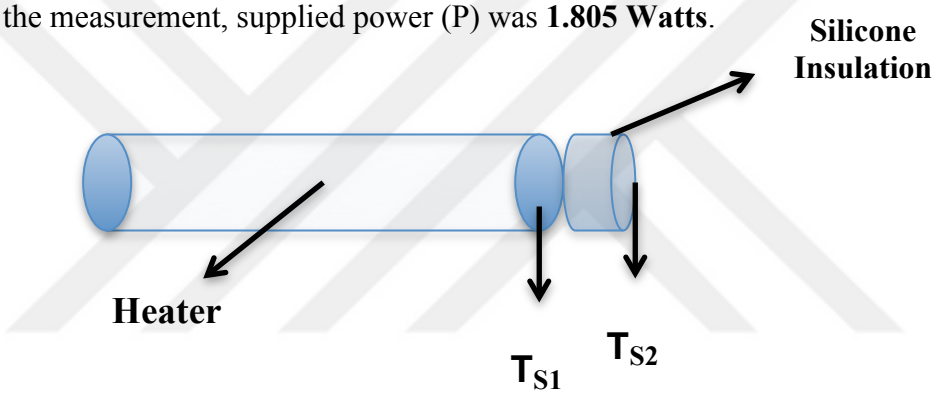

Figure B.1 Heat loss form the tip section of the probe

Since the thickness of silicone insulation is around 1 mm, temperature distribution inside the silicone material can be accepted as linear. Hence, heat losses can be calculated as;

$$\mathbf{Q} = \frac{\mathbf{kA}}{\mathbf{L}}\Delta\mathbf{T} \qquad \text{(B1)}$$

ΔT is the temperature difference between T_{S1} and T_{S2}. k is conductivity of silicone insulation material, L is the thickness of the silicone, and A is the surface area of the tip section.

Table B.1 Values of parameters in the calculation of heat loss

Parameters	Results
Conductivity of silicone, W/m.K	0.17
Surface area of the tip section, m^2	3.84×10^{-5}
Thickness of the silicone, m	0.001
T_{S1}, K	69.96
T_{S2}, K	97.48
Heat loss, W	0.18

As a result of measured heat loss from the tip section, total heat loss was calculated as about **10 %**based on the **Equation B1**.

APPENDIX C

HEAT TRANSFER PROFILES

C.1 Rest of the Heat Transfer Measurements

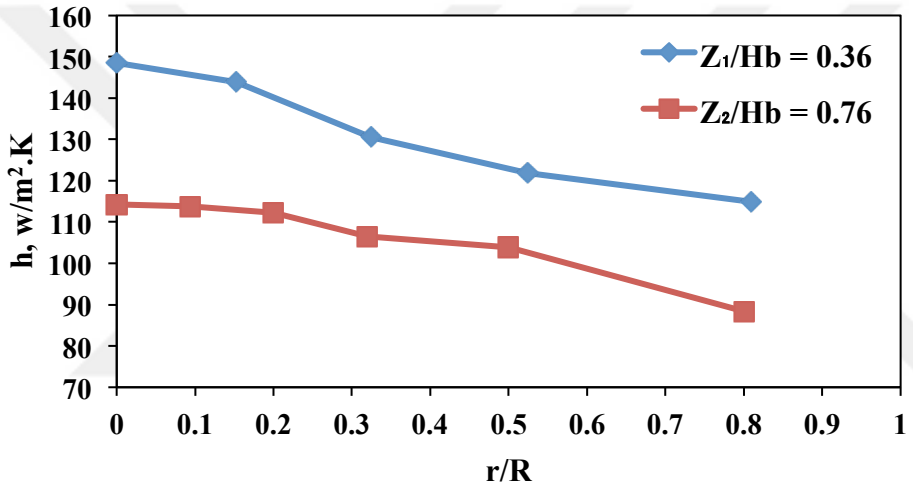

Figure C.1 Radial heat transfer profile for alumina particles (d_p = 1 mm, H_b = 144 mm, $U_s/U_{ms,s}$ = 1.1, D_o = 15 mm, γ = 66º)

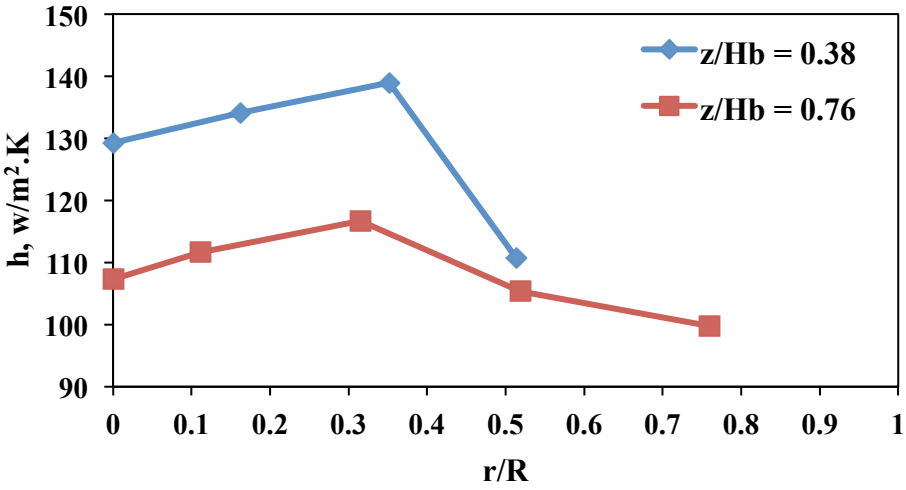

Figure C.2 Radial heat transfer profile for glass particles (d_p = 2 mm, H_b = 168 mm, $U_s/U_{ms,s}$ = 1.1, D_o = 15 mm, γ = 31°)

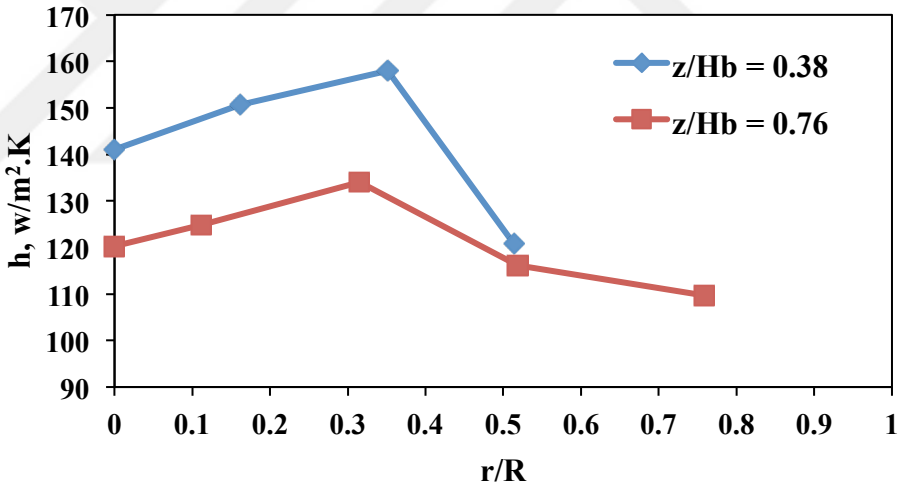

Figure C.3 Radial heat transfer profile for alumina particles (d_p = 2 mm, H_b = 168 mm, $U_s/U_{ms,s}$ = 1.1, D_o = 15 mm, γ = 31°)

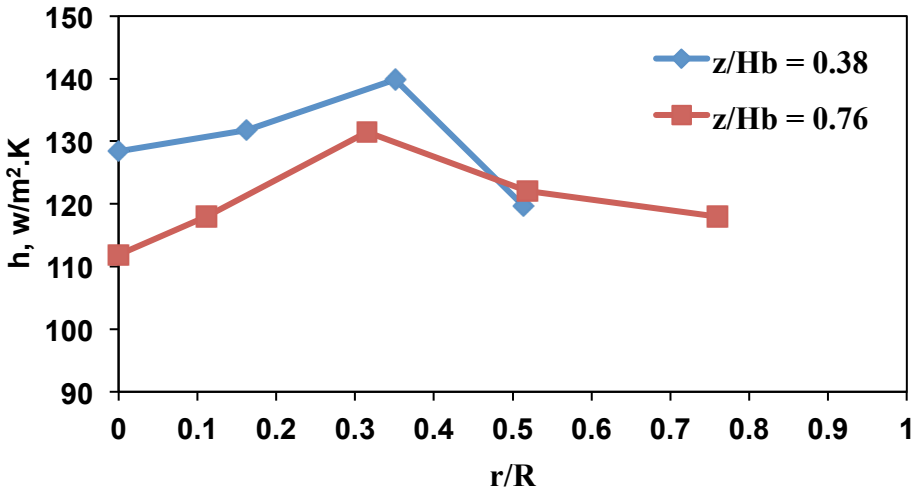

Figure C.4 Radial heat transfer profile for alumina particles (d_p = 1 mm, H_b = 168 mm, $U_s/U_{ms,s}$ = 1.1, D_o = 15 mm, γ = 31°)

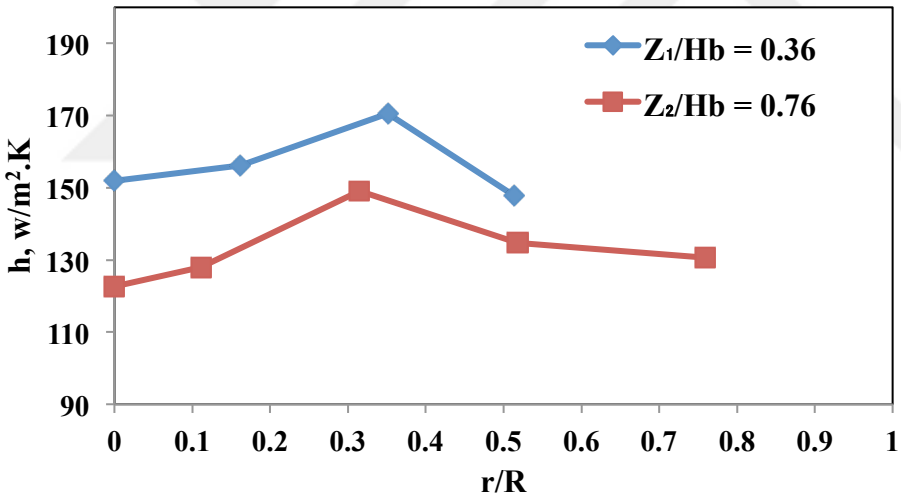

Figure C.5 Radial heat transfer profile for zirconia particles (d_p = 1 mm, H_b = 168 mm, $U_s/U_{ms,s}$ = 1.1, D_o = 15 mm, γ = 31°)

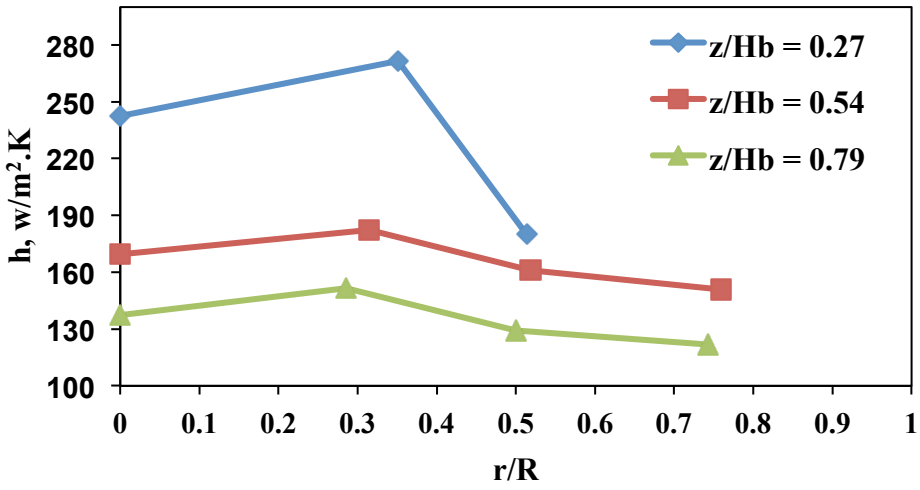

Figure C.6 Radial heat transfer profile for alumina particles (d_p = 1 mm, H_b = 235 mm, $U_s/U_{ms,s}$ = 1.25, D_o = 15 mm, γ = 31º)

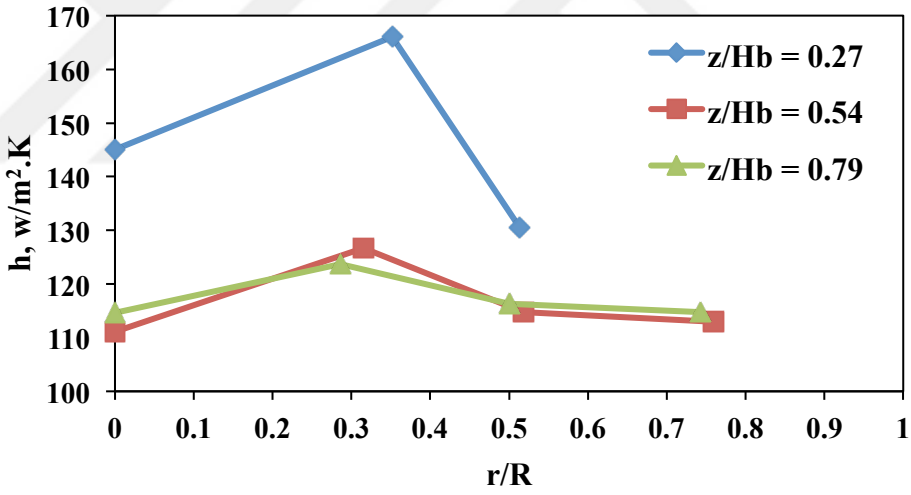

Figure C.7 Radial heat transfer profile for glass particles (d_p = 1 mm, H_b = 235 mm, $U_s/U_{ms,s}$ = 1.25, D_o = 15 mm, γ = 31º)

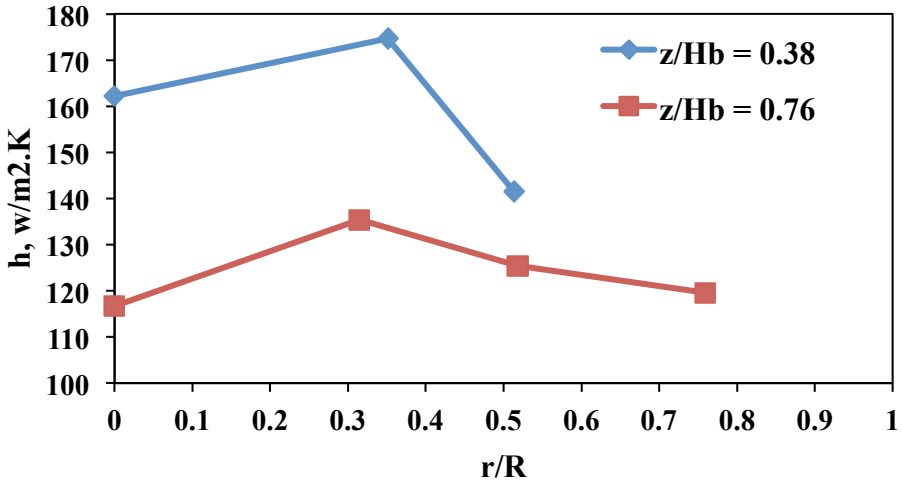

Figure C.8 Radial heat transfer profile for alumina particles (d_p = 1 mm, H_b = 168 mm, $U_s/U_{ms,s}$ = 1.25, D_o = 15 mm, γ = 31º)

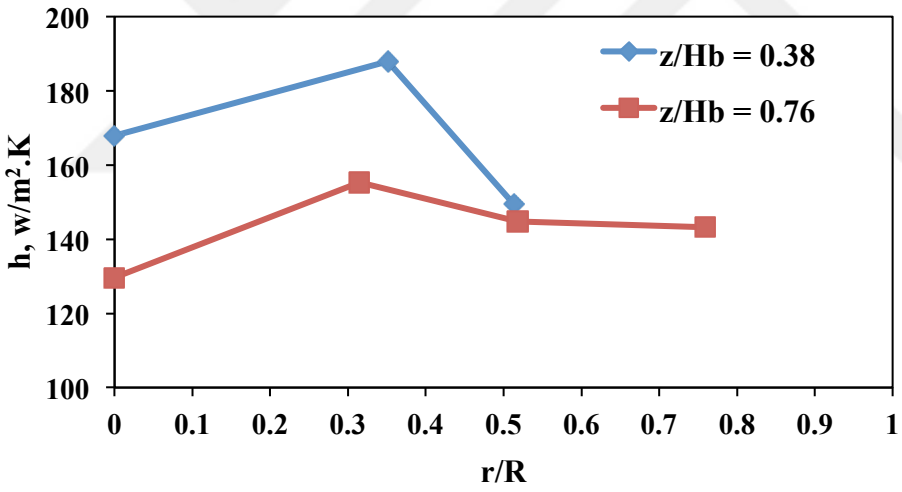

Figure C.9 Radial heat transfer profile for zirconia particles (d_p = 1 mm, H_b = 168 mm, $U_s/U_{ms,s}$ = 1.25, D_o = 15 mm, γ = 31º)

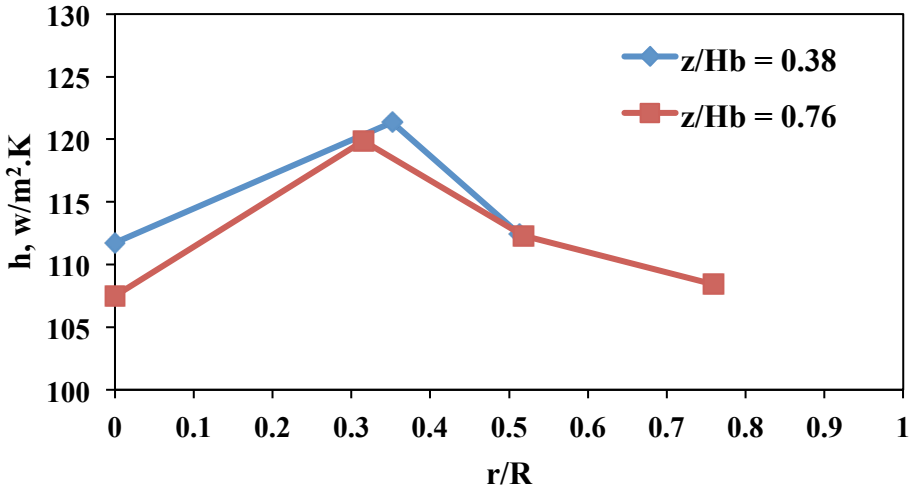

Figure C.10 Radial heat transfer profile for glass particles (d_p = 1 mm, H_b = 168 mm, $U_s/U_{ms,s}$ = 1.25, D_o = 15 mm, γ = 31°)

C.2 Empty Bed Heat Transfer Measurements

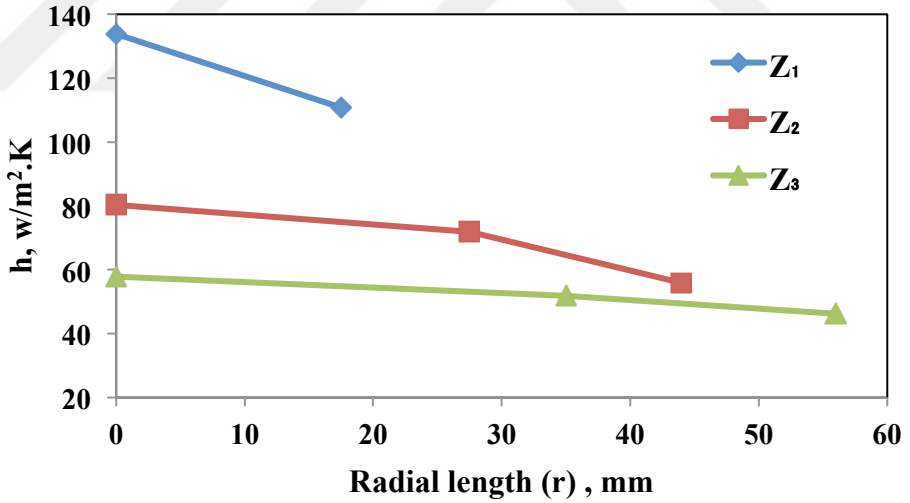

Figure C.11 Radial heat transfer profile for empty bed (D_o = 15 mm, γ = 31°, G_s = 0.375 m^3/min)

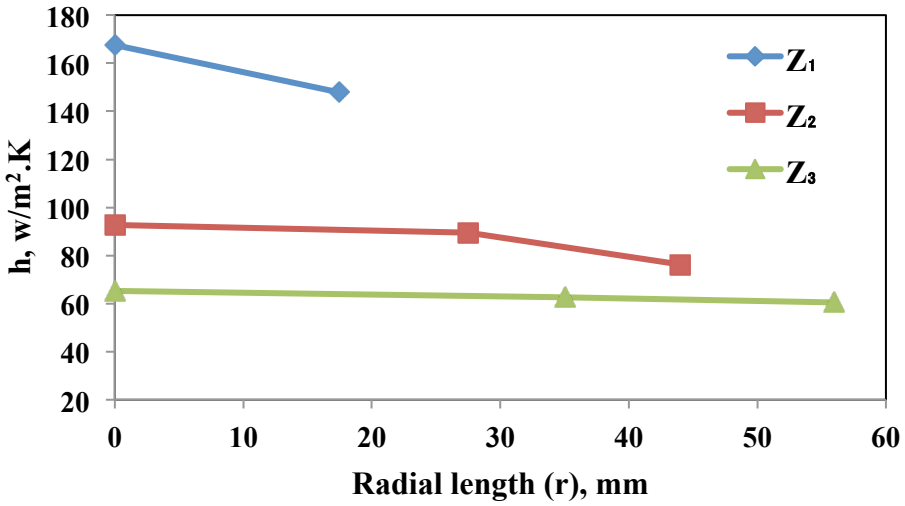

Figure C.12 Radial heat transfer profile for empty bed (D_o = 15 mm, γ = 31°, G_s = 0.544 m^3/min)

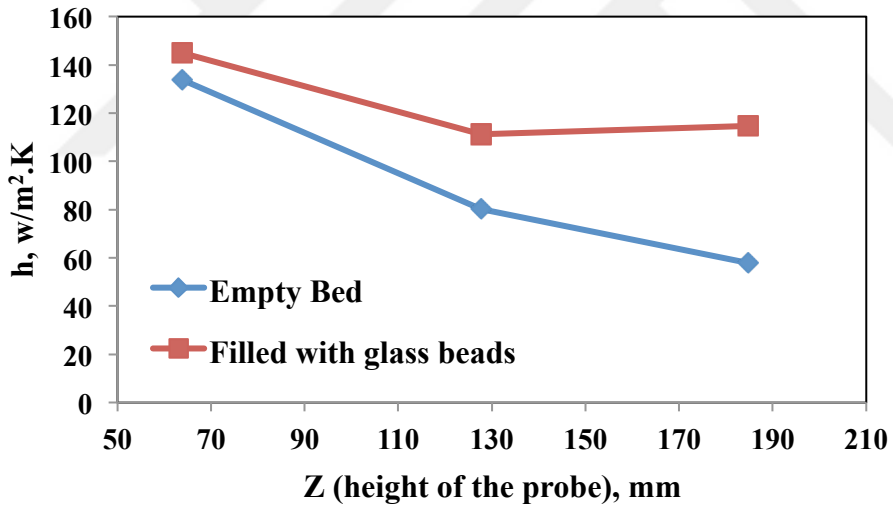

Figure C.13 Comparison of heat transfer profiles between empty and filled beds in the middle of spout section (D_o = 15 mm, r/R = 0, γ = 31°, G_s = 0.544 m^3/min, d_p = 1 mm (glass beads))

APPENDIX D

JET PENETRATION LENGTH

D.1 Calculation of Gas Jet Penetration Length

In order to understand the jet penetration behaviour of fluidizing gas during the spout-fluid bed operation, some correlations, given in **Table D.1**, were used.

Table D.1 Correlations for horizontal jet penetration length (L_j)

Author	Particles	Correlation
Benjolloun (1991)	**Catalyst, glass and sand**	$\frac{L_j}{d_o} = 5.52\left(\frac{\rho_o U_o^2}{(\rho_p - \rho_f) d_o g}\right)^{0.27}$
Yates et al. (1991)	**Calcinated alumina powder**	$\frac{L_j}{d_o} = 2.8\left(\frac{\rho_o U_o^2}{(\rho_p - \rho_f) d_o g}\right)^{0.4}$

Table D.2 Gas jet penetration lengths for different particles and bed angles (d_p = 1 mm, $H_{b,\,31^o}$ = 168 mm, $H_{b,\,66^o}$ = 144 mm)

	L_j (mm)					
Correlations	**Glass Beads (Y = 31º)**	**Alumina (Y = 31º)**	**Zirconia (Y = 31º)**	**Glass Beads (Y = 66º)**	**Alumina (Y = 66º)**	**Zirconia (Y = 66º)**
Benjelloun, (1991)	16.88	15.80	15.87	12.74	13.11	12.13
Yates, (1991)	14.66	13.30	13.39	9.67	10.09	8.99

Table D.3 Values of parameters in the gas jet penetration length correlations for different particles (d_p = 1 mm, $H_{b,\,31^o}$ = 168 mm, $H_{b,\,66^o}$ = 144 mm)

Parameters	**Glass Beads (Y = 31º)**	**Alumina (Y = 31º)**	**Zirconia (Y = 31º)**	**Glass Beads (Y = 66º)**	**Alumina (Y = 66º)**	**Zirconia (Y = 66º)**
Gas density at nozzle exit, kg/m^3	1.2	1.2	1.2	1.2	1.2	1.2
Gas velocity at the nozzle, m/s	35.82	38.58	49.54	21.28	27.32	30.13
Void fraction	0.35	0.39	0.37	0.35	0.39	0.37
Particle density, kg/m^3	2500	3700	6000	2500	3700	6000
Gravitational acceleration, kg/m^2.s	9.81	9.81	9.81	9.81	9.81	9.81
Particle diameter, m	0.001	0.001	0.001	0.001	0.001	0.001
Nozzle exit diameter, m	0.001	0.001	0.001	0.001	0.001	0.001
Gas density in the bed, kg/m^3	1.2	1.2	1.2	1.2	1.2	1.2
Fluidizing gas flow rate, m^3/s	0.00691	0.00745	0.00956	0.00745	0.00956	0.0105
Number of holes on the conical base	246	246	246	446	446	446
Static Bed Height, m	0.168	0.168	0.168	0.144	0.144	0.144
Area of a hole, m^2	7.85E-07	7.85E-07	7.85E-07	7.85E-07	7.85E-07	7.85E-07